ORNL/TM-2016/658

Transported Low Temperature Geothermal Energy for Thermal End Uses—Final Report

Zhiyao Yang
Xiaobing Liu
Kyle Gluesenkamp
Cary Smith
Jan-Mou Li
Ayyoub Momen

October 2016

OAK RIDGE NATIONAL LABORATORY
MANAGED BY UT-BATTELLE FOR THE US DEPARTMENT OF ENERGY

ORNL/TM-2016/658

Energy and Transportation Science Division

TRANSPORTED LOW TEMPERATURE GEOTHERMAL ENERGY FOR THERMAL END USES—FINAL REPORT

Zhiyao Yang
Xiaobing Liu
Kyle Gluesenkamp
Cary Smith
Jan-Mou Li
Ayyoub Momen

Date Published: October, 2016

Prepared by
OAK RIDGE NATIONAL LABORATORY
Oak Ridge, TN 37831-6283
managed by
UT-BATTELLE, LLC
for the
US DEPARTMENT OF ENERGY
under contract DE-AC05-00OR22725

CONTENTS

LIST OF FIGURES

LIST OF TABLES

NOMENCLATURE

ADS	adsorption
c	specific heat
C_f	flow coefficient
COP	coefficient of performance
CTSGA	crystal enhanced two-step geothermal absorption
DUH	direct-use heating
ED	energy density
FR	low ratio between solution and refrigerant
h_{fg}	enthalpy of evaporation of water
HTF	heat transfer fluid
IC	initial cost
LDD	liquid desiccant dehumidification
LCOSE	levelized cost of saved electricity
MRR	moisture removal rate
N	number of trucks
OPC	operating cost
q	heat
Re	Reynolds number
TSGA	two-step geothermal absorption
w	humidity ratio
ε	heat transfer effectiveness

Subscripts

db	dry bulb
fg	phase change between liquid and gas
ss	strong solution
wb	wet bulb
ws	weak solution

EXECUTIVE SUMMARY

The use of geothermal energy is an emerging area for improving the nation's energy resiliency. Conventionally, geothermal energy applications have focused on power generation using high temperature hydrothermal resources or enhanced geothermal systems. However, many low temperature (below 150°C/300°F) geothermal resources are also available but have not been fully utilized. For example, it is estimated that 25 billion barrels of geothermal fluid (mostly water and some dissolved solids) at 176°F to 302°F (80°C to 150°C) is coproduced annually at oil and gas wells in the United States (DOE 2015). The heat contained in coproduced geothermal fluid (also referred as "coproduced water") is typically wasted because the fluid is reinjected back into the ground without extracting the heat.

Hot water from low temperature geothermal reservoirs can be used to provide heat for industrial processes, agriculture and aquaculture, or to keep buildings warm. Such applications are usually called "direct use." Low temperature geothermal energy can also be used to provide space cooling and refrigeration through absorption or adsorption cooling technologies (Holdmann 2005, Lech 2009, Luo et al. 2010, Kreuter 2012, Wang et al. 2013). However, due to the low energy density of hot or chilled water and the high cost for developing pipelines over long distances, utilization of geothermal energy for space conditioning currently is limited to places where the geothermal resources are available at or very near the demand site, usually less than 2 miles away (OIT Geo-Heat Center 2005). This limitation has significantly hampered the widespread use of low temperature geothermal resources.

This study identified several potential technologies, including absorption, adsorption, ice storage, and desiccant dehumidification, that can utilize the low-temperature geothermal energy to provide space cooling and/or dehumidification for buildings. By splitting the charging and discharging process, and utilizing tractor-trailers to transport the energy storage media between the two processes, these technologies can be further developed to store and transport low-temperature geothermal energy and provide space cooling and/or dehumidification at buildings distant from the geothermal resources. This alternative geothermal cooling has potential to extend the utilization of the low temperature geothermal energy and displace electricity consumption for space cooling and/or dehumidification.

Among the technologies investigated in this study, the crystal-enhanced two-step geothermal absorption (CTSGA) system, which utilizes $LiBr\text{-}2H_2O$ crystals as energy storage media, can store and transport low temperature geothermal energy with the highest energy density (643 kJ/kg or 276 BTU/lb) for cooling applications. It is 4 times denser than conventional direct use for heating application and 28 times higher than direct use for cooling application. The energy density of CTSGA is also 1.6 times higher than the original two-step geothermal absorption (TSGA) system investigated by the authors previously (Liu et al. 2015). The liquid desiccant dehumidification (LDD) system utilizing $LiCl\text{-}H_2O$ crystals as energy storage media has a similar energy density (857 kJ/kg or 368 BTU/lb) as CTSGA, but its application is limited to dehumidification only. Ice storage has a similar energy density as the TSGA system, but it requires a higher heat source temperature (near 150°C/300°F) to operate. For space heating, all these technologies either cannot produce sufficiently hot water at the building site, or have similar energy density as conventional direct-use heating applications.

The conceptual system designs for applying each of the identified technologies are developed and computer models are programmed to predict their cost and performance. In addition to the energy density, these computer models also take into account many other factors, including distance between the geothermal resource and the building, electricity rate, building cooling load profile (i.e., peak and annual cooling load), efficiency of electric chillers replaced with the geothermal cooling, and the climate at both the geothermal site and the building site.

A software tool has been developed to analyze the economic viability of applying various geothermal cooling systems (including dehumidification) and the direct use heating system to meet a given building thermal demand with the available geothermal resources. This tool consists of a calculation engine for modeling various technologies, including the geothermal cooling, heating, or dehumidification systems, as well as the conventional electric chillers or natural-gas-fired boilers, and a user-friendly interface for accepting user inputs and displaying calculation results.

The economic viability of applying different geothermal cooling systems has been analyzed using the above developed software tool in two case studies: (1) using a hydrothermal resource near Santa Rosa, California, which has a 1,175 gpm (74 kg/s) flow rate and a bottom hole temperature of 138°C/280°F, to provide seasonal space cooling to office buildings in Santa Rosa; and (2) using coproduced water from an oil-field near Houston, Texas, which has a 2,020 gpm (127 kg/s) flow rate and a bottom hole temperature of above 100°C/212°F, to provide year-round base-load space cooling to a district cooling system. The economic viability is investigated under a range of conditions including various distances, electricity rates, and cooling load profiles. The results show that generally the payback of the geothermal cooling systems is shorter with closer distance, higher electricity rate, lower peak cooling load, or greater annual cooling demand. The shortest payback in both case studies is achieved by the CTSGA system, which yields a payback of less than 10 years for an 18-mile (29 km) distance at Houston, and a 50-mile (80 km) distance at Santa Rosa.

Based on available data of existing geothermal resources and cooling demands in the building sector, it is estimated that 0.17 Quad Btu (0.18 EJ) primary energy consumption for space cooling can be avoided each year in the United States by replacing conventional electric cooling with the geothermal cooling, which is a 3.5% reduction in the total primary energy consumption for space cooling in existing commercial and residential buildings in the United States.

Although the CTSGA system can store and transport low temperature geothermal energy with the highest energy density among all the investigated technologies, there are some significant technical challenges for applying this technology, including (1) dissolving crystals in time to increase the concentration of the weak solution at the building site; and (2) preventing crystals from entering and/or forming in the absorber. It is recommended an experimental study be conducted to characterize the process of crystal formation and dissolution. Furthermore, it is recommended that a prototype of the CTSGA system be developed to verify its performance through laboratory and field tests.

1. INTRODUCTION

The use of geothermal energy is an emerging area for improving the nation's energy resiliency. Conventionally, geothermal energy applications have focused on power generation using high temperature hydrothermal resources or enhanced geothermal systems. However, many low temperature (below 150°C) geothermal resources are also available but have not been fully utilized. For example, it is estimated that 25 billion barrels (3.97 million m^3) of geothermal fluid (mostly water and some dissolved solids) at 80°C to 150°C is coproduced annually at oil and gas wells in the United States (DOE 2015). The heat contained in coproduced geothermal fluid (also referred as "coproduced water") is typically wasted because the fluid is reinjected back into the ground without extracting the heat.

Hot water from low temperature geothermal reservoirs can be used to provide heat for industrial processes, agriculture and aquaculture, or to keep buildings warm. Such applications are usually called "direct use." In typical direct-use applications, a well is drilled into a geothermal reservoir, and a pumping system is used to extract a stream of hot water from the well. The hot water then delivers heat through a heat exchanger for its intended use. The cooled water is injected back underground or disposed of on the surface. Low temperature geothermal energy can also be used to provide space cooling and refrigeration through absorption or adsorption cooling technologies (Holdmann 2005, Lech 2009, Luo et al. 2010, Kreuter 2012, Wang et al. 2013).

However, due to the low energy density of hot or chilled water and the high cost of developing pipelines over long distances, utilization of geothermal energy for space conditioning currently is limited to places where the geothermal resources are available at or very near the demand site, usually less than 2 miles (3.2 km) away (OIT Geo-Heat Center 2005). Low energy density has significantly hampered the widespread use of low temperature geothermal resources.

In FY 2015, ORNL performed a feasibility analysis on an innovative two-step geothermal absorption (TSGA) system, which stores low temperature geothermal energy in liquid desiccant at ambient temperature and transports it over a long distance (e.g., 15 km) to buildings for space cooling via a split absorption cooling system (Liu et. al 2015). Figure 1 shows a diagram of the TGSA system, which decouples the production and regeneration of the conventional absorption cycle into a two-step process. The first step, regeneration, takes place near the geothermal resource. A weak aqueous solution of lithium bromide (LiBr) or another salt solution is heated using geothermal heat to drive off moisture from the solution. The concentrated solution is then allowed to cool to ambient temperature and is transported to commercial or industrial buildings by tractor-trailers (or other appropriate means, including, but not limited to, trains or ships). The second step is space conditioning at the building site, where liquid water is evaporated to provide cooling and the water vapor is absorbed at low pressure by the concentrated solution, which is kept near ambient temperature. The diluted solution is then transported back to the geothermal site to be regenerated (concentrated).

With this system, the low temperature geothermal energy is stored and transported at ambient temperature with an energy density of 349 kJ of cooling energy per kilogram of shipped $LiBr/H_2O$ solution, which is up to 5 times higher than transporting hot water for typical direct-use heating applications. A case study for applying the TSGA system at a large office building in Houston indicates that, for a 10 mile (16 km) distance from the geothermal site to the building, the simple payback of the TSGA system is 10.7 years compared with a conventional electric-driven vapor compression chiller.

There are a few technical challenges associated with the TSGA system, including (1) minimizing the required volume and the associated transportation cost of the working fluid; (2) maintaining appropriate vacuum levels at various components of the absorption cycle; (3) retaining good quality working fluid

during transportation and storage; and (4) harvesting heat from geothermal wells sparsely located and with varying production rates.

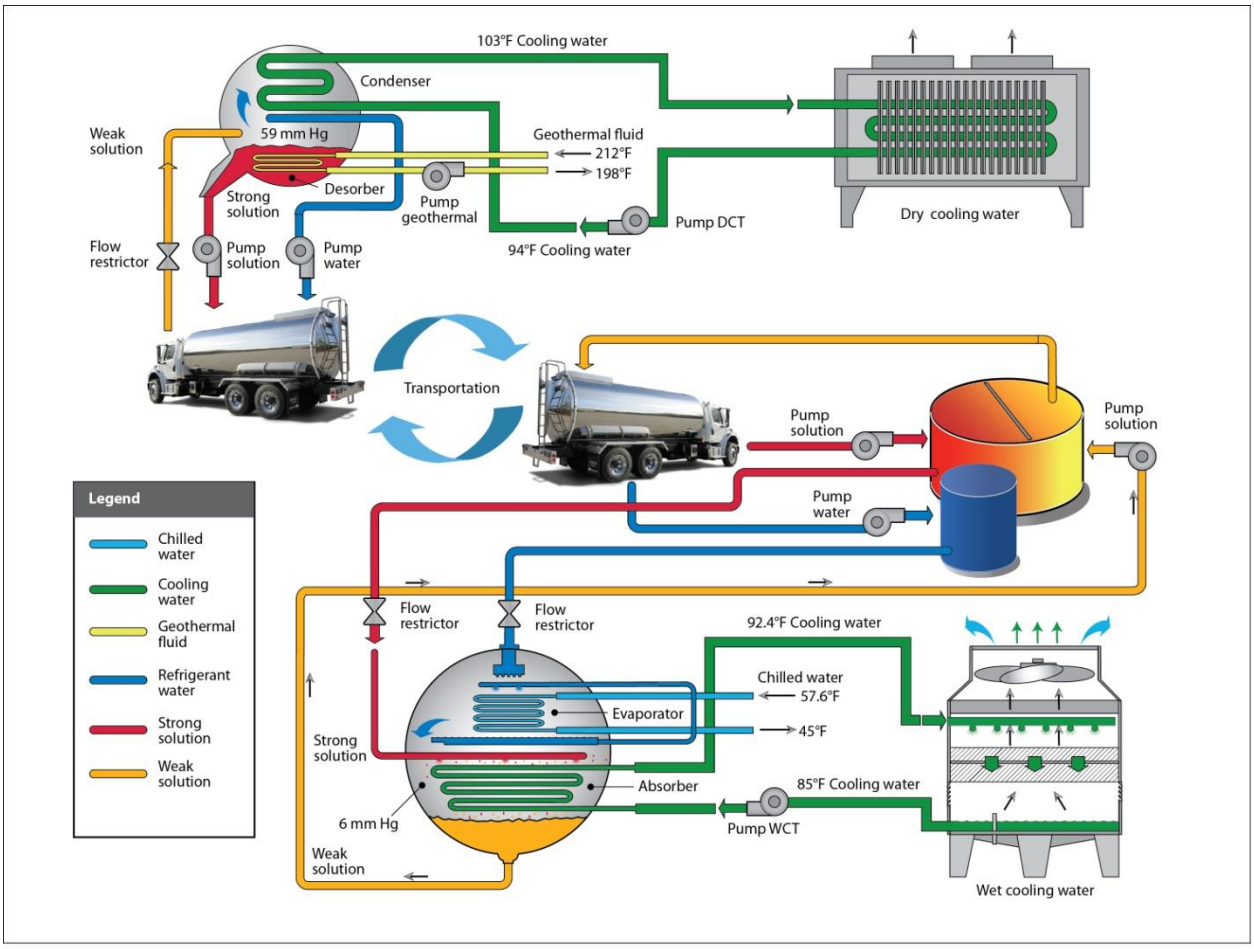

Fig. 1. Schematic of a two-step solution looping geothermal absorption cooling.

To improve the economics, the ORNL team in FY 2016 investigated possible enhancements of the two-step absorption system and explored other potential technologies for transporting the low temperature geothermal energy with higher energy density. The goal of this project is to address following questions:

- Can any other technologies store and transport low temperature geothermal energy with a higher energy density than that of TSGA?
- If so, how does the performance and cost of these technologies compare with conventional HVAC systems?
- What is the technical potential of these technologies? That is, how much energy could be saved and what would the annual reduction in carbon emissions be if these technologies were fully utilized in the United States?

2. PROJECT SCOPE AND APPROACH

This project identifies and evaluates technologies that have potential to store low temperature (below 150°C) geothermal energy and transport it at ambient temperature to buildings for thermal applications, including space cooling, dehumidification, or space/water heating. The transportation methods include tractor-trailer and pipeline (when applicable). Table 1 summarizes the scope of the potential technologies investigated.

Table 1. Scope of potential technologies

	Geothermal resources	End-use applications	Transportation	Equipment/technology
Included	<150°C coproduced, hydrothermal, or sedimentary	Space cooling Dedicated dehumidification Space heating	Truck Pipeline	Absorption Adsorption Liquid desiccant (for dehumidification only) Ice storage
Not included	>150°C	Industrial drying Desiccant-assisted cooling Refrigeration Other	Rail Ship	PCMs besides water Direct evaporative cooling Indirect evaporative cooling

This project develops (1) a systematic approach for evaluating the cost and benefits of potential technologies that utilize low temperature geothermal energy for thermal applications in buildings, (2) a set of algorithms and supporting data for modeling the performance of the potential technologies, (3) user-friendly software for assessing economic viability of the potential technologies, and (4) an assessment of the technical potential of potential technologies.

A comparison of various potential technologies is presented in Section 3. Based on this comparison, a few technologies that have potential to store and transport the low temperature geothermal energy with an energy density higher than, or similar to, that of TSGA or conventional direct-use heating (DUH) are identified. The conceptual system designs for applying each of the identified technologies are described in Section 4 along with the algorithms for modeling their cost and performance. An introduction is given in Section 5 to the software tool, which is developed for analyzing the economic viability of applying the potential technologies for a given building thermal application. The economic viability of the identified technologies is investigated through two case studies presented in Section 6, and the technical potential of applying these technologies is assessed in Section 7. Conclusions drawn from this study and the recommendations for future research and development are presented in Section 8.

3. COMPARION OF POTENTIAL TECHNOLOGIES

Through a comprehensive literature review, a few other technologies are found to have potential for utilizing low temperature geothermal energy for thermal applications. These technologies were originally developed for other purposes, such as industry waste heat recovery, compact thermal energy storage, and non-vapor compression cooling. The energy densities (i.e., the amount of heating/cooling energy provided by each unit of the transported energy storage media) of these technologies are compared in Table 2 (see next page) along with other characteristics, including transported media, underlying technology, and advantages and limitations. The energy densities are either obtained directly or calculated from information presented in published literature.

Based on this comparison, the following four technologies in addition to the TSGA system were selected (highlighted in Table 2) for further investigation in this study and included in the economic analysis tool. A brief description of each of the following technologies is given in Section 4.

- Adsorption (ADS) with solid desiccant
- Three-phase sorption (referred as crystal-enhanced TSGA or CTSGA henceforth)
- Liquid desiccant dehumidification (LDD)
- Ice storage (Ice)

Figure 2 is a graphical comparison of the investigated technologies. The triangles indicate cooling application and the circles indicate heating application. The size of these symbols indicates relative system complexity or uncertainty. The color of a symbol indicates a particular technology. The value of each data point indicates the energy density of the transported energy media.

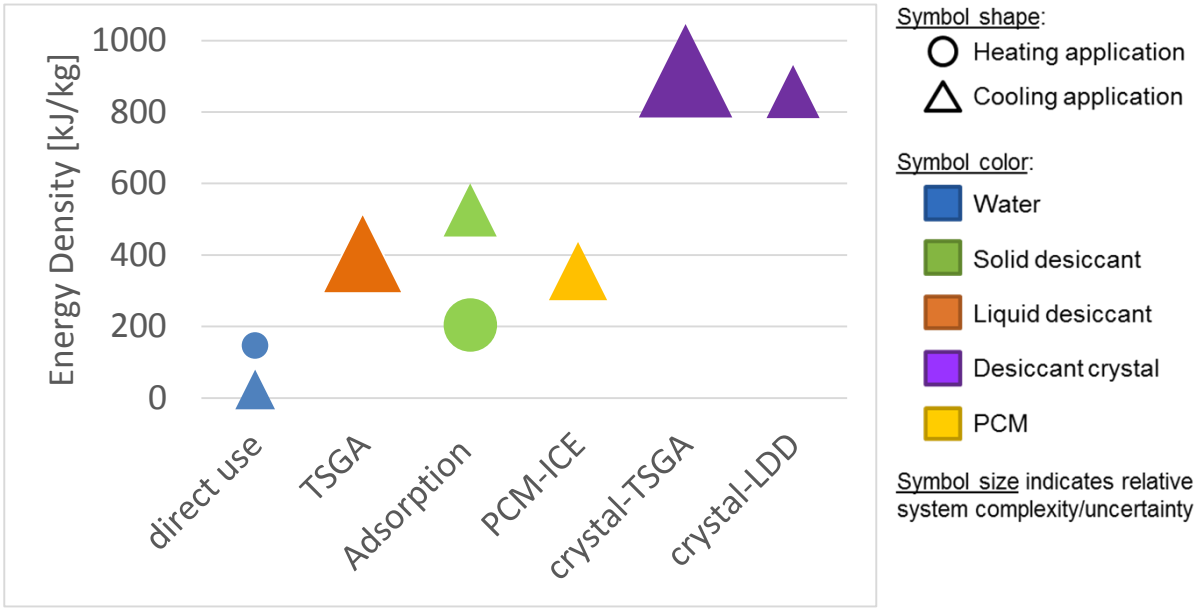

Fig. 2. Comparison of energy densities of potential technologies.

As shown in Fig. 2, all these technologies can provide space cooling but with different energy densities. TSGA, ADS, and Ice have similar energy density for cooling application, which is more than 15 times higher than direct-use cooling, which produces chilled water at the geothermal site and transports it to buildings, and more than double the energy density of DUH. The energy density is nearly further doubled with CTSGA and LDD. However, only ADS can produce needed hot water for heating application and its

energy density in heating is only slightly higher than that of DUH. As a result, only the cooling application of these potential technologies is investigated in this study.

Table 2. Technologies for utilizing low temperature geothermal energy for thermal applications

Transported medium	Application technology	Energy density		Advantages	Limitations
		Heating (kJ_{th}/kg)	Cooling (kJ_{clg}/kg)		
Water	Direct use	146[1]	23[2]	Simplest technology	Only feasible for short distance
	Absorption heat transformer	272[3]	-	Higher energy density than direct use	Limited hot water supply temperature and additional cost
Solid desiccant	Adsorption	202[4]	526[5]	High energy density	Need high charging temperature, slow charging/discharging, varying outputs
Salt solution	Absorption with TSGA	-[6]	405[7]	High energy density	Technical challenges to maintain vacuum at components and prevent air infiltration, need prevent crystallization
	Three-phase sorption (crystal enhanced)[8]	-[7]	915	High energy density	New tech. and need to be customized for geothermal applications
	Liquid desiccant dehumidification	-[7]	857	Higher energy density, ambient pressure operation, lower initial cost	Only deals with latent cooling load, performance dependent on climate
Phase change material (PCM)	PCM chemicals	265[9]	165[10]		Lower energy density, long charge/discharge time
	Ice (with absorption chiller using ammonia/water)	-	355[11]	Mature tech. with lower initial cost	Need heavy insulation when transporting ice in summer, varying charge/discharge rate

[1] Operation temperatures are 95°C /60°C (ANSI/ARI 2000).
[2] With 6.7°C chilled water generated at the geothermal site and a return chilled temperature at the building of 12.2°C (ANSI/ARI 2000).
[3] Based on system introduced by Jiang et al. (2015).
[4] Zeolite 5A charged with 150°C heat source to produce 55°C hot water and absorbing heat from 10°C ambient.
[5] AQSOA Z02 charged with 150°C heat source to produce 6.7°C chilled water with cooling water temperature at 30°C.
[6] These technologies are not able to produce 55°C hot water while absorbing heat from 10°C ambient.
[7] Using 100°C heat input and 34°C/29°C cooling input, concentrations of the strong and weak solutions of the $LiBr/H_2O$ working fluid pairs are 61.9% and 53.1%, respectively (Liu et al. 2015).
[8] Concepts introduced by Yu et al. (2014).
[9] Using $Ba(OH)_2$-$8H_2O$ with melting point at 78°C (Abhat 1983).
[10] Using C14 paraffin with melting point at 5°C (Demirbas 2006).
[11] Melting 0°C ice to 5°C water, fusion heat of ice is 334 kJ/kg.

4. SYSTEM DESIGN AND PERFORMANCE MODELING

The methodologies for performance modeling and economic analysis of the TSGA system have been described in detail by Liu et al. (2015). In order to apply the same analysis to all the new technologies in this study, the modeling procedure has been generalized so that the analysis can be easily carried out and programmed by plugging different technology and transportation modules into the procedure. In this section, the system design and modeling procedures for each potential technology are introduced.

4.1 GENERAL MODELING PROCEDURE

The general procedure for evaluating the cost and performance of the potential technologies is depicted in Fig. 3. For a given thermal application and load profile, the evaluation is performed in following steps:

- Calculate the initial and operating costs of a baseline cooling system (i.e., electric chiller).
- Size equipment and predict performance of alternative cooling systems, and calculate their initial and operating costs.
- Calculate transportation-related initial and operating costs based on the characteristics of the alternative systems (e.g., energy density, charging/discharging rate) and the distance between the building and the geothermal site.
- Evaluate the economic, energy, and environmental impacts of each alternative system by comparing the performance of the alternative system against the baseline system.

While other technologies are analyzed on an annual basis, the LDD system is analyzed on a monthly basis since its performance is more dependent on outdoor air humidity than other technologies. A detailed description of the modeling algorithm for LDD is given in Appendix D. Since the DUH and TSGA systems use liquid as energy storage media, they can use both tractor-trailer and pipeline as the means of transportation. But tractor-trailer is the only option for the other technologies, which use solid energy storage materials (e.g., solid desiccants, crystals of salt hydrate, or ice).

Several performance metrics are used to evaluate various technologies, including simple payback period, levelized cost of saved electricity (LCOSE), primary energy saving, and carbon emission reductions. The simple payback period (SP) is perhaps the most direct index for evaluating the economic performance of a technology, which is calculated with Eq. (1):

$$SP = \frac{IC_{tech} + IC_{trans} + IC_{wells} - IC_{baseline}}{OPC_{baseline} - OPC_{tech} - OPC_{trans} - OPC_{wells}} \quad (1)$$

where IC stands for initial cost and OPC stands for operating cost. The subscript “tech” refers to the technology being evaluated, subscript “trans” refers to transportation method, subscript “baseline” refers to the baseline system to ne compared with, and subscript “wells” refers to the geothermal wells.

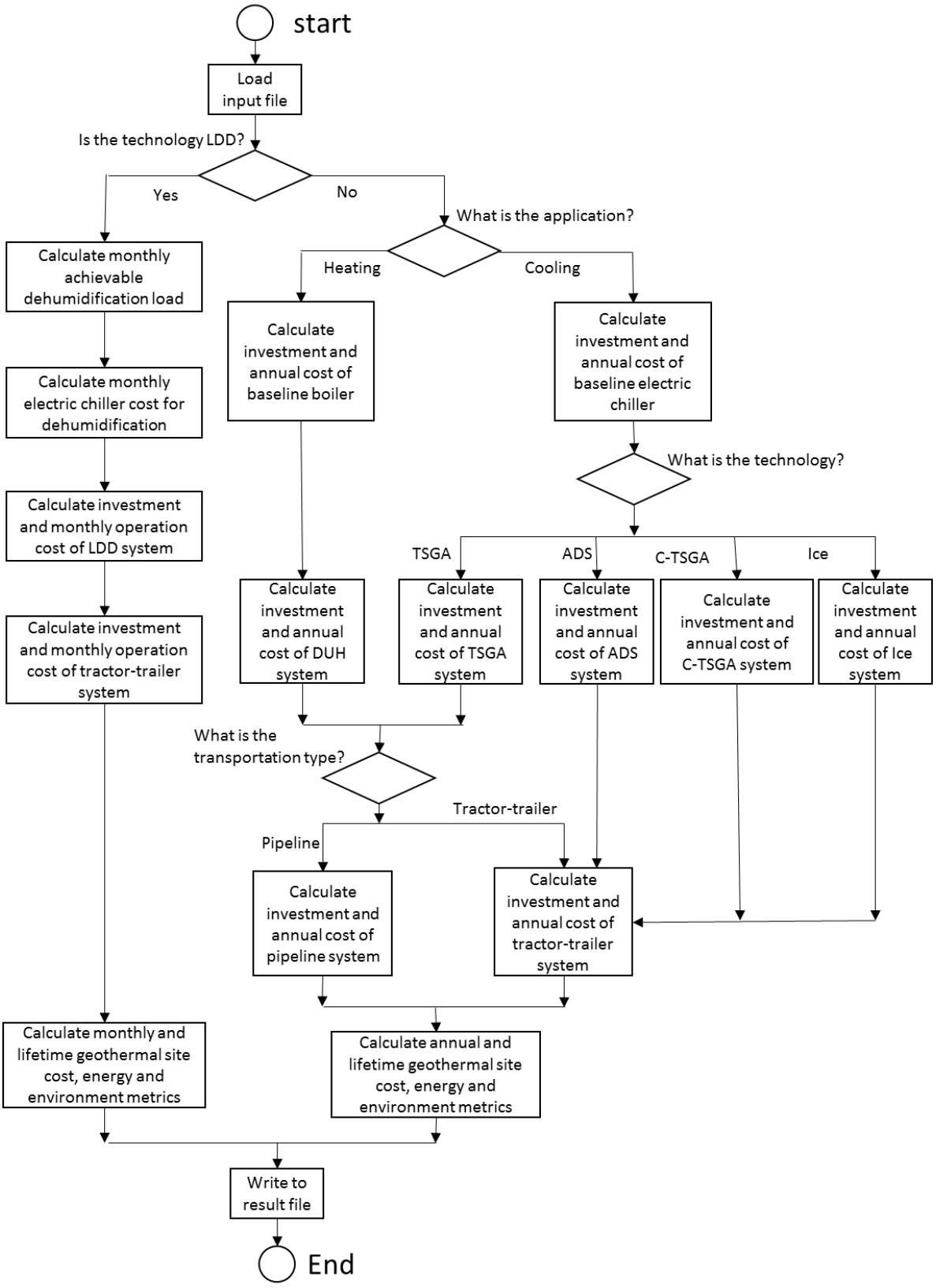

Fig. 3. Flow chart depicting the general modeling procedure.

LCOSE is calculated as the ratio of all the investments needed to save electricity, which includes the initial cost premium and the cumulative operating cost of an alternative system over a given time period (e.g., the lifespan of the system), to the cumulative electricity savings over the same time period:

$$LCOSE = \frac{Investment}{Electricity\ Saved} = \frac{(IC_{tech}+IC_{trans}-IC_{baseline})+\sum_{k=1}^{n}[(OPC_{tech}+OPC_{trans})/(1+DR)^k]}{\sum_{k=1}^{n}[(Ele_{baseline}-Ele_{tech})/(1+DR)^k]} \quad (2)$$

where *n* is the lifetime of the system and DR is the annual discount rate.

The primary energy and carbon emission calculations are carried out for consumption of all forms of energy (electricity, diesel fuel, natural gas, etc.) of both the baseline system and the alternative system using conversion factors from Deru and Torcellini (2007).

4.2 BASELINE COOLING SYSTEM

The baseline cooling system includes an electric chiller, a cooling tower, and a pump to circulate cooling water between the chiller and the cooling tower. The initial cost ($IC_{eleChiller}$) and operating cost ($OPC_{eleChiller}$) of the baseline system are calculated on the basis of the size and the electricity consumption of its components, as expressed with Eqs. (3) and (4), respectively.

$$IC_{eleChiller} = IC_{chiller}(peakload) + IC_{CT}\left(peakLoad * \left(1+\frac{1}{COP_d}\right)\right) + IC_{pump}(peakLoad * (1+\frac{1}{COP_d})) \quad (3)$$

where COP_d is the cooling efficiency of the electric chiller (represented as the coefficient of performance or COP) at the design condition and $peakload$ is the capacity of the electric chiller. The correlations between the equipment cost and capacity are derived based on the 2011 RSMeans mechanical cost data (Mossman 2010).

$$OPC_{eleChiller} = ElePrice * \frac{totalLoad}{COP_a} * (1 + PowerRatio_{CT} + PowerRatio_{pump}) \quad (4)$$

where COP_a is the annual average operational efficiency of the electric chiller; $totalLoad$ is the annual total cooling load; $PowerRatio_{CT}$ and $PowerRatio_{pump}$ are the ratio of the electricity consumptions of the cooling tower and the pump to the chiller, respectively; and $ElePrice$ is the local electricity rate.

4.3 TSGA

The generalized equations for calculating the initial cost, annual operating cost, and energy density of the transported energy storage media of the TSGA system are given below. More details of the algorithms used for modeling the TSGA system are given in a previous report (Liu et al. 2015) and Appendix B.

The initial cost of the TSGA system (IC_{TSGA}) is calculated with Eq. (5), which includes the costs of the absorption chiller ($IC_{Abs\_chiller}$), cooling towers (IC_{Abs_CT}), and the circulation pumps (IC_{Abs_pump}).

$$IC_{TSGA} = IC_{Abs_{chiller}}\left(\frac{peakLoad}{CF_{Cap}}\right) + IC_{Abs_{CT}}\left(peakLoad * \left(1+\frac{1}{COP_d}\right)\right) + IC_{Abs\_pump}(peakLoad * (1+\frac{1}{COP_d})) \quad (5)$$

The individual component cost is determined as a function of its nominal size/capacity. The nominal size of the absorption chiller is determined based on the peak cooling demand and the actual (non-nominal) operating condition of the chiller (i.e., the heat source temperature and the ambient web bulb temperature). Due to lack of published performance data of absorption (and adsorption) chillers at non-nominal conditions, the cooling capacity and thermal efficiency of the TSGA system at various operating conditions are determined using computer simulations of a single-effect absorption chiller, which is developed with SorpSim by Liu et al. (2015). The modeled absorption chiller is driven by hot water to produce 7.2°C chilled water. The simulation-predicted capacities and COPs are then correlated to the heat source temperature and the ambient web-bulb temperature. The nominal (rating) conditions for TSGA, CTSGA, Ice and ADS systems are listed in Appendix B and a brief introduction of the SorpSim simulations for the TSGA and CTSGA systems is presented in Appendix C.

A correction factor (CF_Cap), which is the ratio of the chiller's capacity at a given operating condition to that at the standard rating condition, assuming constant solution flow rate, is used to determine the nominal capacity of the absorption chiller. The correction factors are shown in Fig. 4. Each curve in this figure represents a certain heat source temperature. The correction factor at the rating condition (100°C heat source temperature and 23.8°C ambient wet-bulb temperature) is 1. With lower heat source temperature and higher wet-bulb temperature, the correction factor is smaller, which means a chiller with a larger nominal size is needed to provide the needed cooling capacity at the actual operating condition.

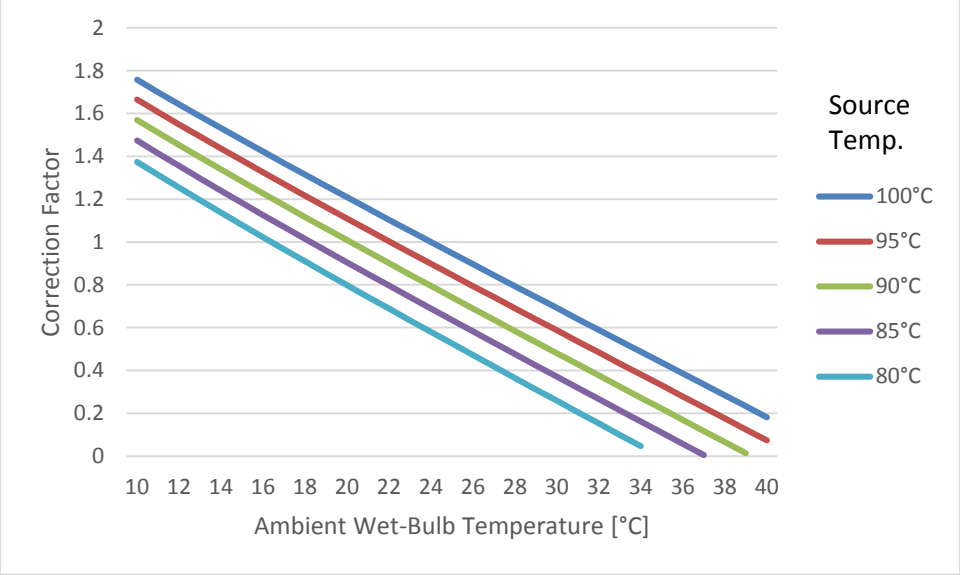

Fig. 4. Capacity correction factor of TSGA system at various heat source and ambient wet-bulb temperatures.

The capacities of the cooling towers and circulation pumps are determined based on $peakLoad$ and the design thermal efficiency (COP_d) of the absorption chiller. For a single effect absorption chiller, the typical value of COP_d is 0.7 (Herold et al. 2016).

The operating cost of the TSGA system (OPC_{TSGA}) is calculated with Eq. (6), which includes the costs of electricity consumption of the cooling towers and circulation pumps. These electricity consumptions are calculated based on the electricity consumptions of the cooling towers and circulation pumps of the baseline cooling system, and adjusted according to the ratio of the heat rejection load of the TSGA system to that of the baseline cooling system.

$$OPC_{TSGA} = ElePrice * \frac{totalLoad}{COP_{a_{baseline}}} * (PowerRatio_{CT} + PowerRatio_{pump}) * \frac{1+\frac{1}{COP_{a_{absChiller}}}}{1+\frac{1}{COP_{a_{baseline}}}} \quad (6)$$

where $COP_{a_{absChiller}}$ is the annual average operational thermal COP (the ratio of total cooling output to the total heat input) of the absorption chiller and $COP_{a_{baseline}}$ is the annual average operational electric COP of a baseline electric chiller. $COP_{a_{absChiller}}$ at various annual average operating conditions is determined with the SorpSim model and is shown in Fig. 5.

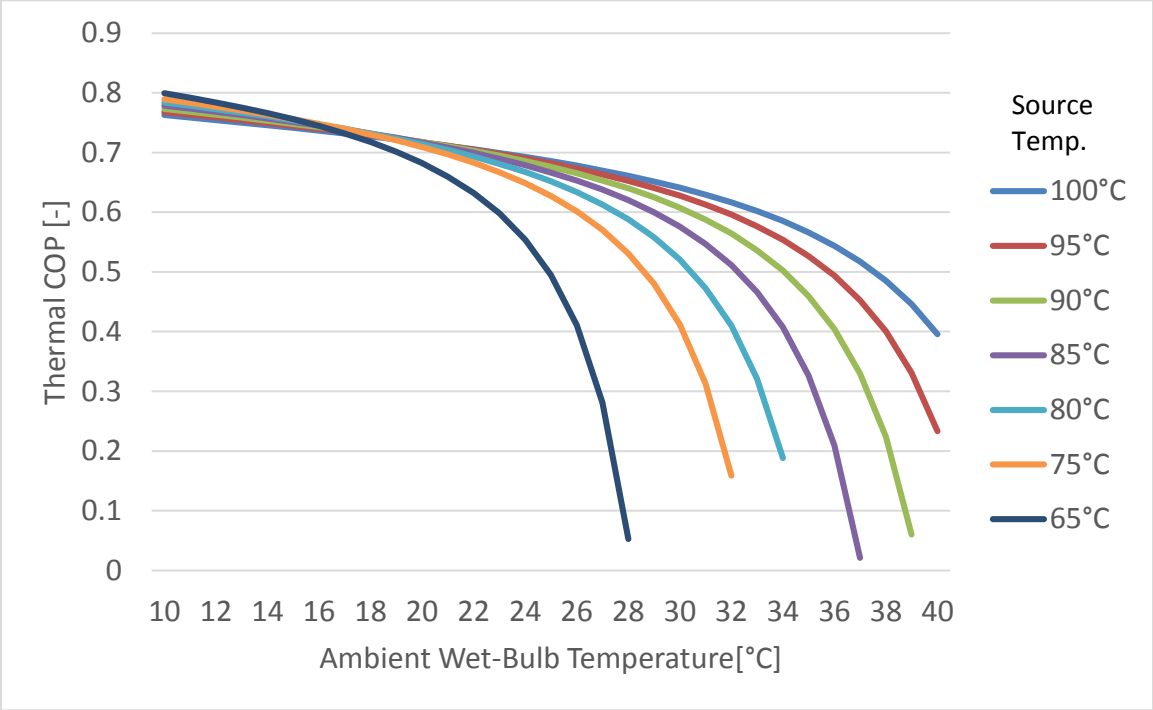

Fig. 5. Thermal COP of TSGA at various heat source and ambient wet-bulb temperatures.

As shown in Fig. 5, $COP_{a_{absChiller}}$ is affected by both the heat source temperature and the ambient wet-bulb temperature. It is around 0.7 at the standard rating condition. With lower source temperature and higher wet-bulb temperature, $COP_{a_{absChiller}}$ declines quickly. Note that when the source temperature is above 85°C and wet-bulb temperature is below 30°C, the curves are quite linear.

In the TSGA system, LiBr/H_2O solution is used as the energy storage media. The energy density of the solution is determined by the LiBr concentration in the strong solution and the weak solution. The concentrations of the solution are calculated using correlations derived from the simulation results with the SorpSim model at various operating conditions. Figure 6 shows the strong solution concentration (C_{ss}) and weak solution concentration (C_{ws}) at various operating conditions. The strong solution concentration is determined by both the heat source temperature and the wet-bulb temperature. It increases when the heat source temperature becomes higher or the wet-bulb temperature goes down, and vice versa. Since the chilled water temperature is fixed at 7.2°C, and the effect of strong solution concentration on the weak solution concentration can be neglected (since the desorber and the absorber are not directly connected in the TSGA system), the weak solution concentration is affected only by the wet-bulb temperature—it increases with the increase of wet-bulb temperature.

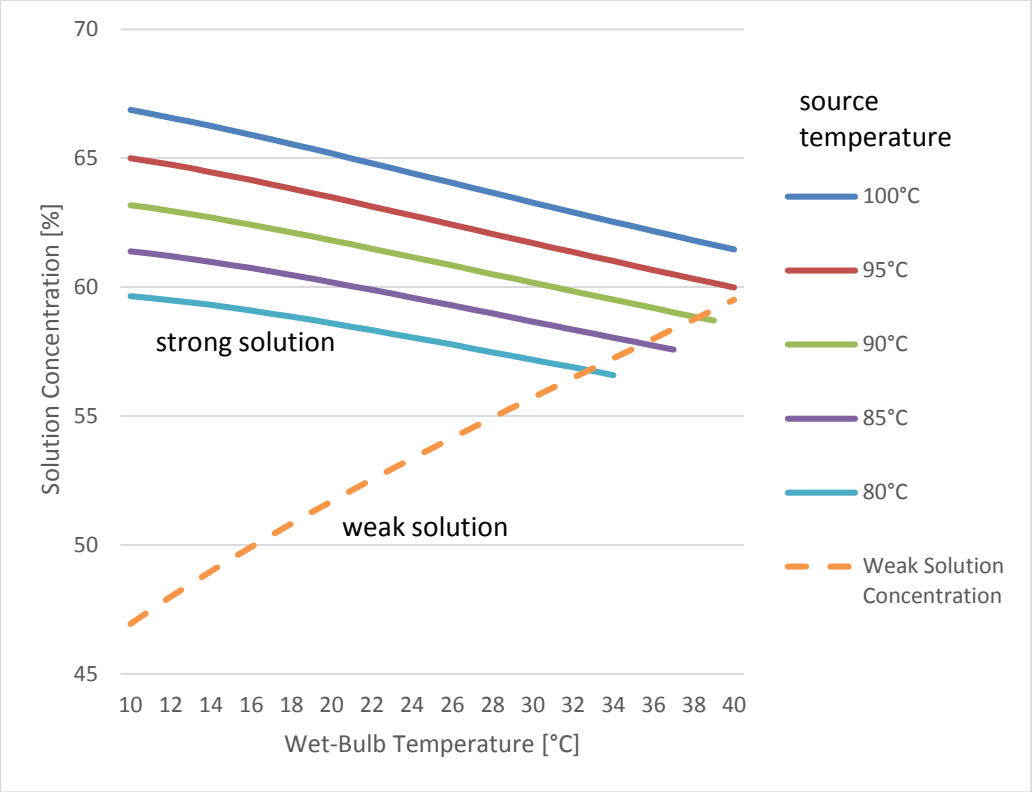

Fig. 6. Concentration of LiBr/H_2O solution at various heat source and ambient web bulb temperatures.

The energy density of the TSGA system (ED_{TSGA}, evaluated based on the mass of the transported weak solution) is calculated based on the solution concentrations and the evaporation heat of water (h_{fg}), as expressed in Eq. (7).

$$ED_{TSGA} = \left(1 - \frac{C_{ws}}{C_{ss}}\right) * h_{fg} \tag{7}$$

4.4 CTSGA

The most important difference between the CTSGA and TSGA systems is that CTSGA uses crystals of salt hydrate as the energy storage media to achieve a higher energy density. A concept design of the CTSGA system is shown in Fig. 7. As shown in this figure, the desorber at the geothermal site generates strong solution using hot geothermal fluid. This strong solution is then cooled in a tank (i.e., the trailer) until it crystallizes into salt hydrate. Since the mass fraction of salt in the crystals is higher than the strong solution, more energy is stored in the crystals. The remaining solution in the tank is recirculated into the desorber to drive off enough water content so that it can crystallize in the tank. At the building site, weak solution leaving from the absorber goes into the tank filled with the mixture of crystals and saturated solution. After dissolving some crystals, the weak solution becomes strong again, and then flows back into the absorber to generate more chilled water.

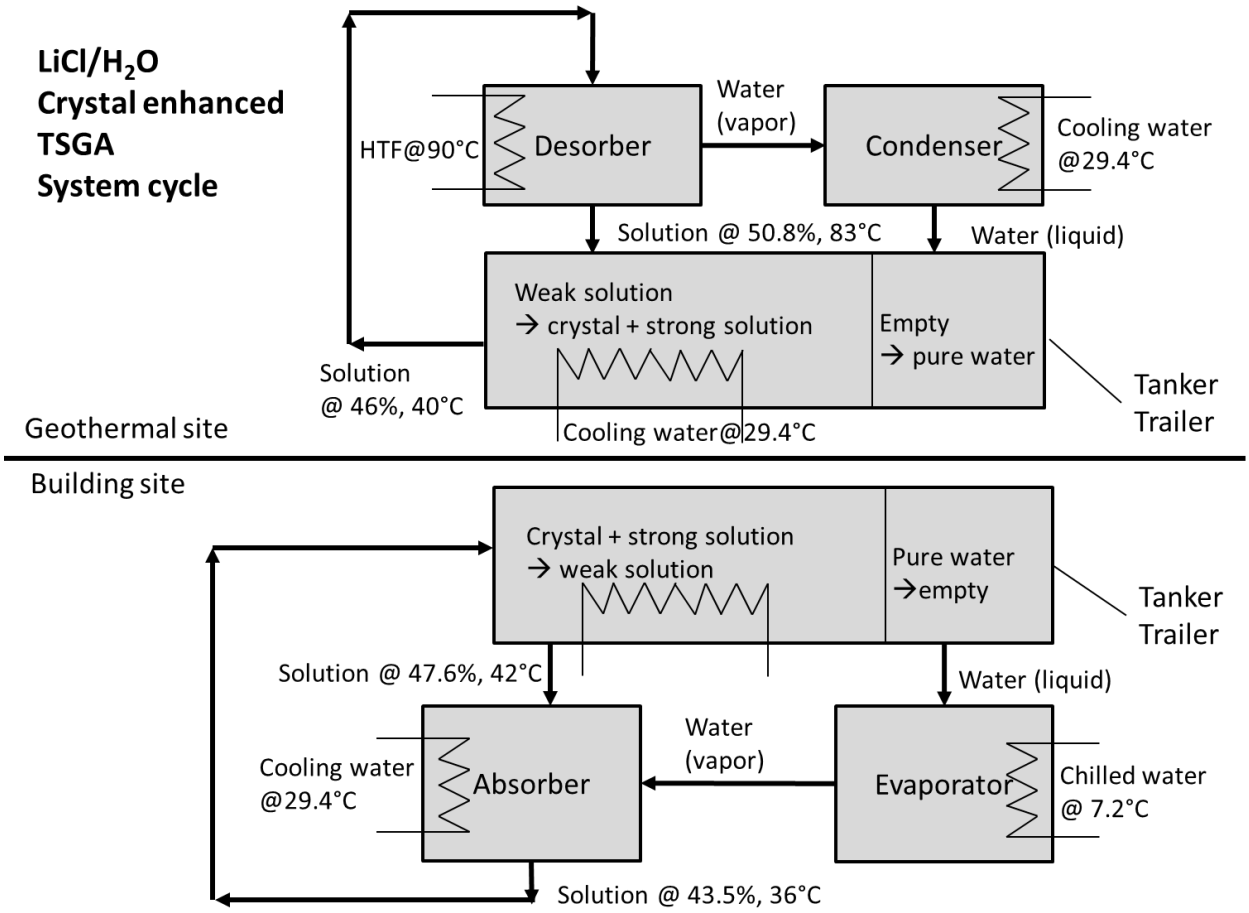

Fig. 7. Crystal-enhanced TSGA system operation cycle.

The initial and operating costs of the CTSGA system are calculated with equations similar to those for the TSGA system but with a different capacity correction factor (Fig. 8) and thermal COP (Fig. 9), which are determined with SorpSim simulations for the CTSGA system. Within the typical range of low temperature geothermal resources (<120°C) and the ambient wet-bulb temperature, only $LiBr{\cdot}2H_2O$ can be produced at the geothermal site. Since both the concentration of the strong solution at the building site and the chilled water temperature are fixed, CTSGA system's cooling capacity is affected only by the ambient wet-bulb temperature. However, the thermal COP of CTSGA system is affected by both the heat source and wet-bulb temperatures. The cooling capacity and thermal COP decrease with higher wet-bulb temperature, but a higher heat source temperature could increase the thermal COP when the wet-bulb temperature is higher than 20°C. As can be seen in Fig. 9, when the wet-bulb temperature is lower than 20°C, increase source temperature will reduce the thermal COP. It is because the increase of the heating input to warm up the solution, which is at the ambient temperature when entering the desorber, is bigger than the increase of the cooling output when the ambient temperature is low.

The concentration of the strong solution leaving the desorber is affected by both the heat source temperature and the wet-bulb temperature. Figure 10 shows that the strong solution concentration increases with higher heat source temperature or lower wet-bulb temperature. Same as the TSGA system, the regeneration and dilution of the solution is split into two independent processes. Therefore, the weak solution concentration is affected only by the wet-bulb temperature for producing the 7.2°C chilled water and it is calculated using the same correlations for the TSGA system as shown in Fig. 6.

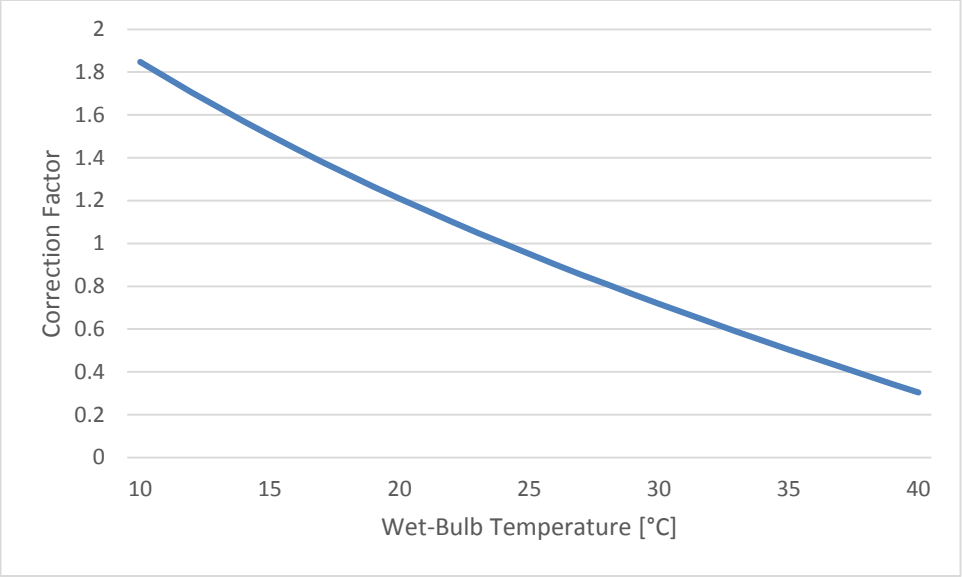

Fig. 8. Capacity correction factor of CTSGA system at various heat source and ambient wet-bulb temperatures.

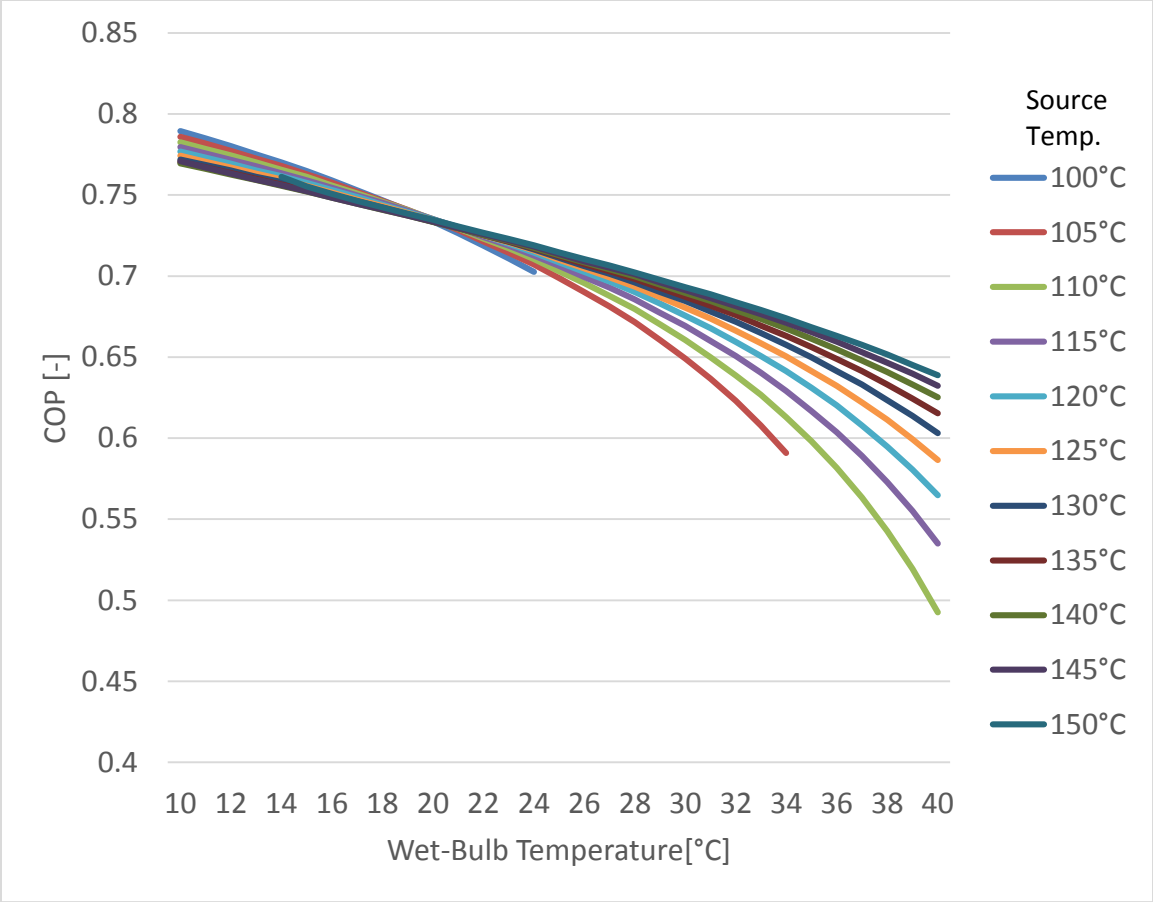

Fig. 9. Thermal COP of CTSGA system at various heat source and ambient wet-bulb temperatures.

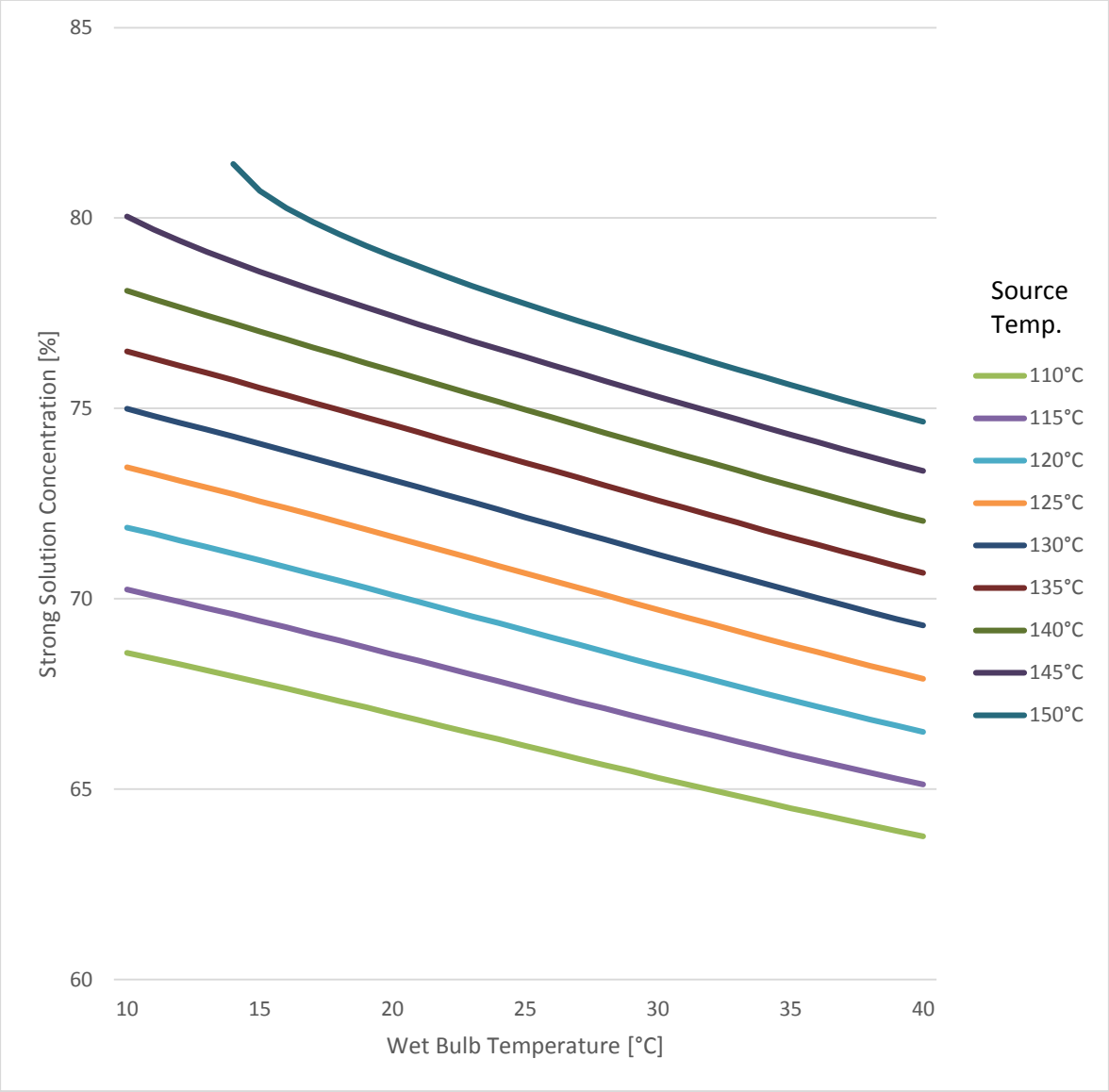

Fig. 10. Strong solution concentration leaving desorber of CTSGA system.

A parameter indicating the mass ratio of crystals ($crystalRatio$) in the storage tank is introduced, and the equivalent concentration of the mixture of crystals and saturated solution in the storage tank is calculated as expressed with Eq. (8):

$$C_{ss_{eq}} = C_{crystal} * crystalRatio + C_{ss} * (1 - crystalRatio) \quad (8)$$

where $C_{crystal}$ is the mass fraction of LiBr in the crystal (i.e., 70% for LiBr-2H_2O).

The energy density of CTSGA (ED_{CTSGA}), which is the energy transported by a CTSGA system based on the mass of weak solution, is calculated with Eq. (9):

$$ED_{CTSGA} = \left(1 - \frac{C_{ws}}{C_{ss_{eq}}}\right) * h_{fg} \quad (9)$$

4.5 ADS

In the adsorption (ADS) system, the adsorber/desorber containing both the solid desiccant and the heat exchanger embedded in the desiccant is transported between the geothermal site and the building site. Figure 11 shows the concept design of the adsorption system. At the geothermal site, hot fluid flows through the heat exchanger embedded in the solid desiccant to drive off water until it is thoroughly dry. The water vapor is then condensed in the condenser and collected into a separate chamber in the container. At the building site, the dry desiccant maintains a low vapor pressure in the evaporator by constantly adsorbing water vapor. With water constantly evaporating in the evaporator, chilled water at the desired temperature is produced.

Several commonly used solid desiccants (silica gel, zeolites) and a high-performance material (AQSOA-Z02) were investigated as the transported energy media. The performance of solid desiccants is assessed based on their water loading factors (i.e., water content mass per unit dry desiccant mass). A larger difference in the loading factors between discharging (cooling and/or heating) and the regeneration process indicates higher energy density. The loading performance data of Zeolite 13X, 5A, and silica gel are derived from correlations developed by Wang and LeVan (2009). The loading performance data of AQSOA-Z02 is from Mitsubishi (2016). The loading factors of various solid desiccants in different applications with 100°C and 150°C geothermal source temperatures are presented in Appendix A. Figure 12 shows the loading factors with a 150°C geothermal source temperature. In this figure, the high end of each bar indicates the maximum water loading corresponding to discharging operation at the building site, and the low end of each bar indicates the minimum water loading corresponding to charging (regeneration) operation at the geothermal site.

As can be seen in Fig. 12, AQSOA-Z02 has the best water loading performance in cooling applications, and it yields an energy density (with 150°C geothermal source temperature) 30% higher than that of the original LiBr/H_2O-solution-based TSGA. However, the other inexpensive industrially prevalent solid desiccants have much lower energy densities than that of TSGA. For space heating, Zeolite 5A with a 150°C geothermal source temperature demonstrates the highest energy density, but it only exceeds that of transporting hot water (i.e., the conventional direct use of low temperature geothermal energy) by 8%. Besides, the simultaneous heating and cooling operation does not offer any higher energy density than transporting hot water. Therefore, only the ADS cooling system with AQSOA Z02 is included in this study as a competitive alternative to the original TSGA system. The high-performance AQSOA Z02 has not been massively manufactured yet and has a higher material cost than LiBr/H_2O solution. The price of the solid desiccant is included as a variable in the economic analysis.

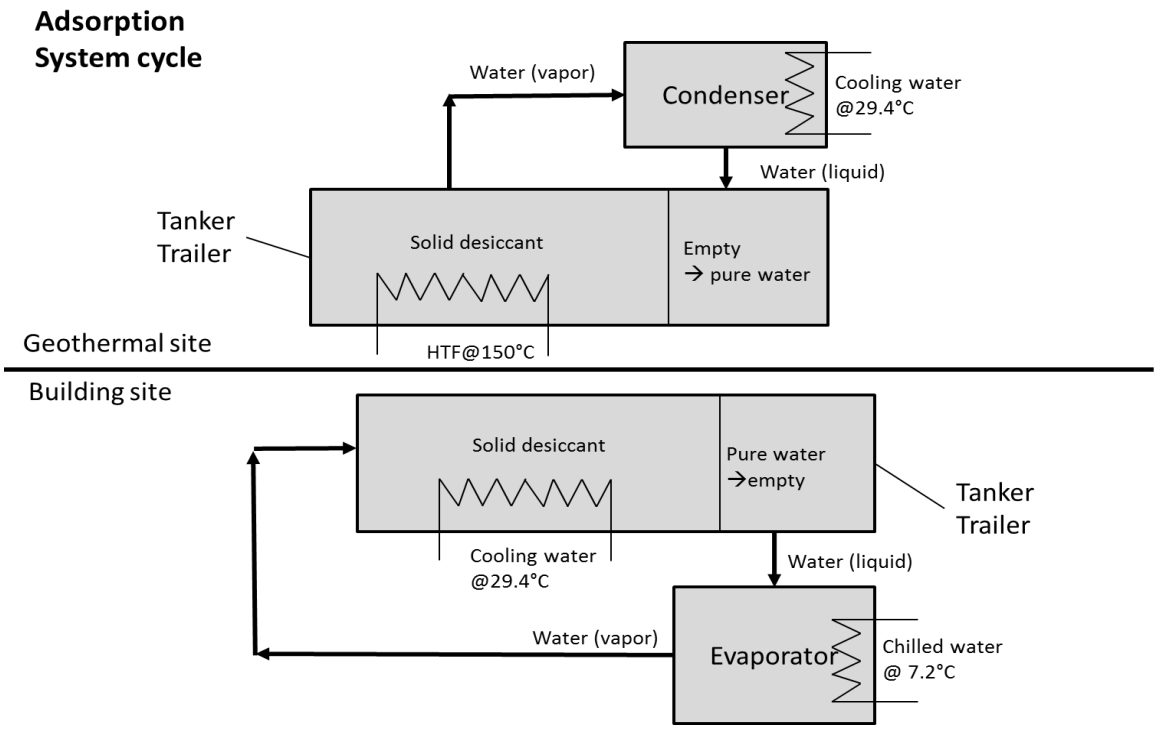

Fig. 11. Adsorption system operation cycle.

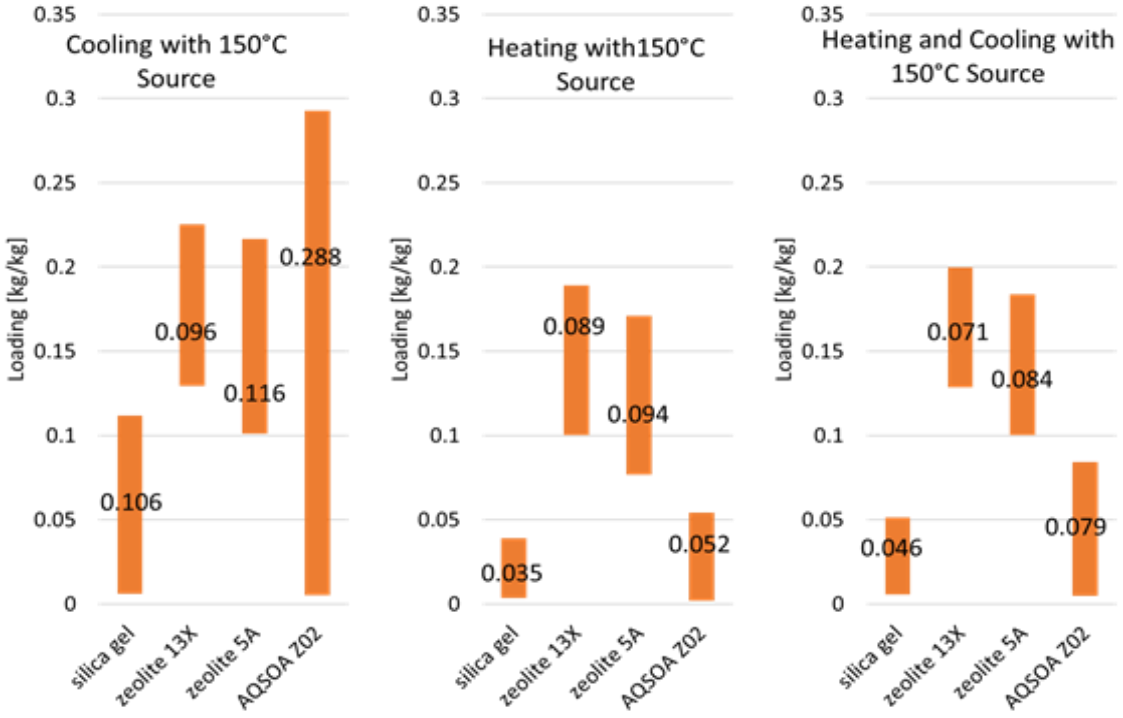

Fig. 12. Water loading performance of various solid desiccants in different thermal applications (cooling only, heating only, and simultaneous heating and cooling) with a 150°C geothermal source temperature.

Given the similarity between ADS and TSGA, the initial and operating costs of the ADS system are calculated using the same equations and correlations as the TSGA system. The only difference is that the COP of the ADS system is 0.6, which is about the upper bound of the thermal efficiency of adsorption cooling systems operating with higher than 85°C heat source temperature and sufficient charging/discharging time (Wang et al. 2014).

The ADS chiller is sized with the same approach as that for sizing the TSGA system. Since no standard rating condition exists for the absorption system, a 150°C heat source temperature is assumed as the nominal condition since adsorption cooling systems usually require a higher heat source temperature to operate. The equilibrium water loading of the charging (q_{reg}) and discharging (q_{ads}) process at various operating conditions are calculated with the property data of AQSOA Z02 and shown in Fig. 13. Since the discharging process (absorbing water vapor) is tied to the 7.2°C chilled water production at the evaporator, the water loading of the discharging process is only affected by the wet-bulb temperature. On the other hand, the water loading of the charging process is affected by both the heat source temperature and the web bulb temperature. The solid desiccant becomes drier (with more capacity to absorb water vapor during the discharging process) with higher heat source temperature or lower wet-bulb temperature.

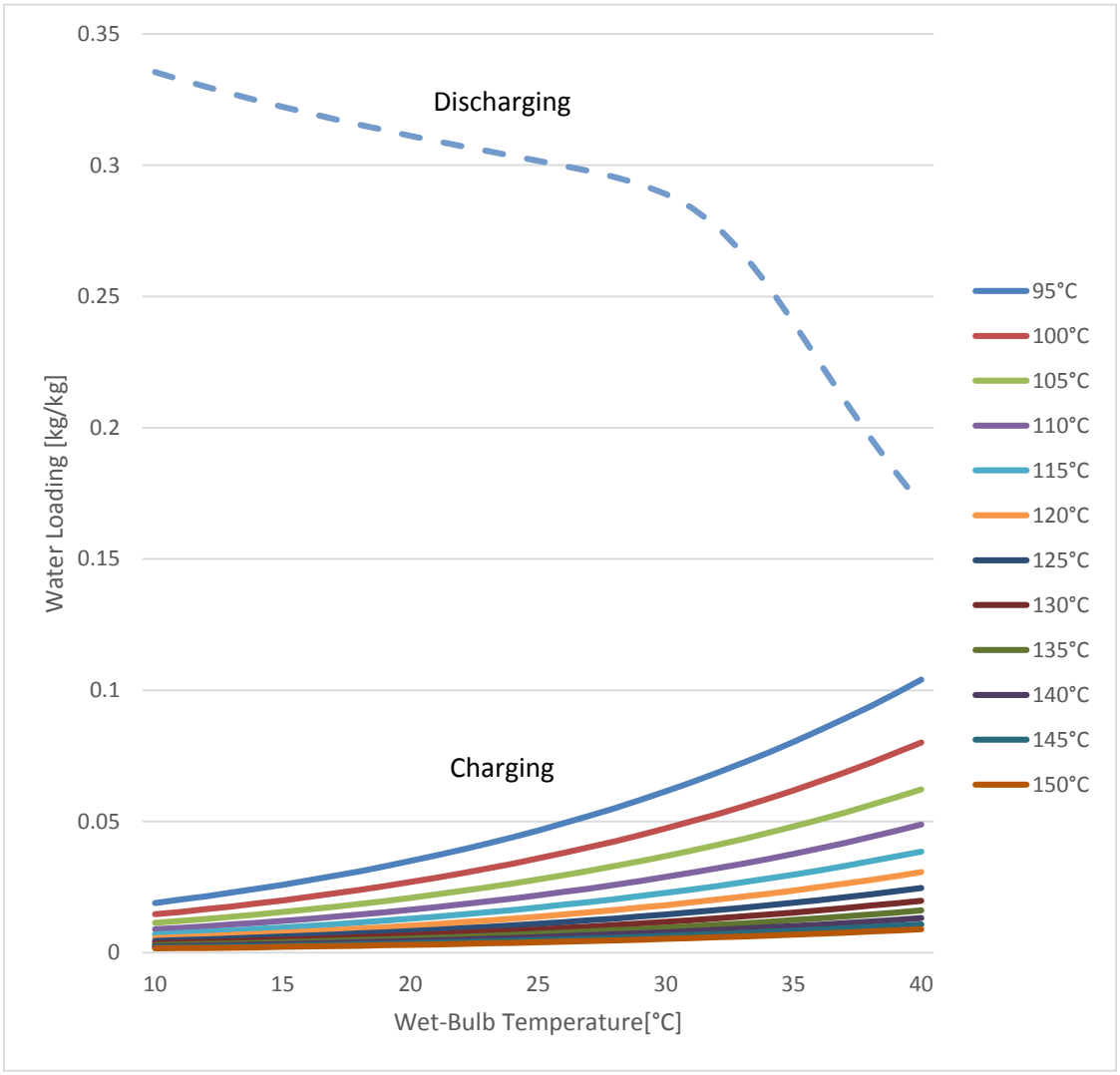

Fig. 13. Water loading of AQSOA Z02 at various heat source and ambient web bulb temperatures.

Due to limited charging/discharging time in practice, only partial equilibrium can be reached. Moreover, because heat exchangers are embedded within the solid desiccant, only part of the tanker is filled with the solid desiccant. To represent these non-ideal situations, a parameter called loading percentage ($loadingPercentage$), which is determined by the charging/discharging time and the heat exchanger design, is introduced to calculate the energy density of a ADS system (ED_{ADS}) as expressed with Eq. (10). ED_{ADS} is the energy that can be transported by each unit mass of wet (discharged) desiccant.

$$ED_{ADS} = \frac{1}{1+q_{ads}} * \left(q_{ads} - q_{reg}\right) * loadingPercentage * h_{fg} \quad (10)$$

4.6 ICE

The ice storage system generates ice using an ammonia absorption system at the geothermal site. The ice is then transported in a large tanker trailer to the building to generate chilled water for space cooling. The tanker consists of an insulated cylindrical enclosure with spiral polyethylene coils inside. Heat transfer fluid (HTF) flows inside the coil, and water/ice is kept in the tanker outside the coil. The ammonia/water absorption system is able to generate cooling at below freezing temperatures. Therefore, heat transfer fluid (e.g., aqueous glycol solution) can be cooled to sub-zero temperatures and used to freeze the water in the tanker trailer as shown in Fig. 14. However, the ammonia/water absorption system requires a higher heat source temperature, typically above 130°C, for operation.

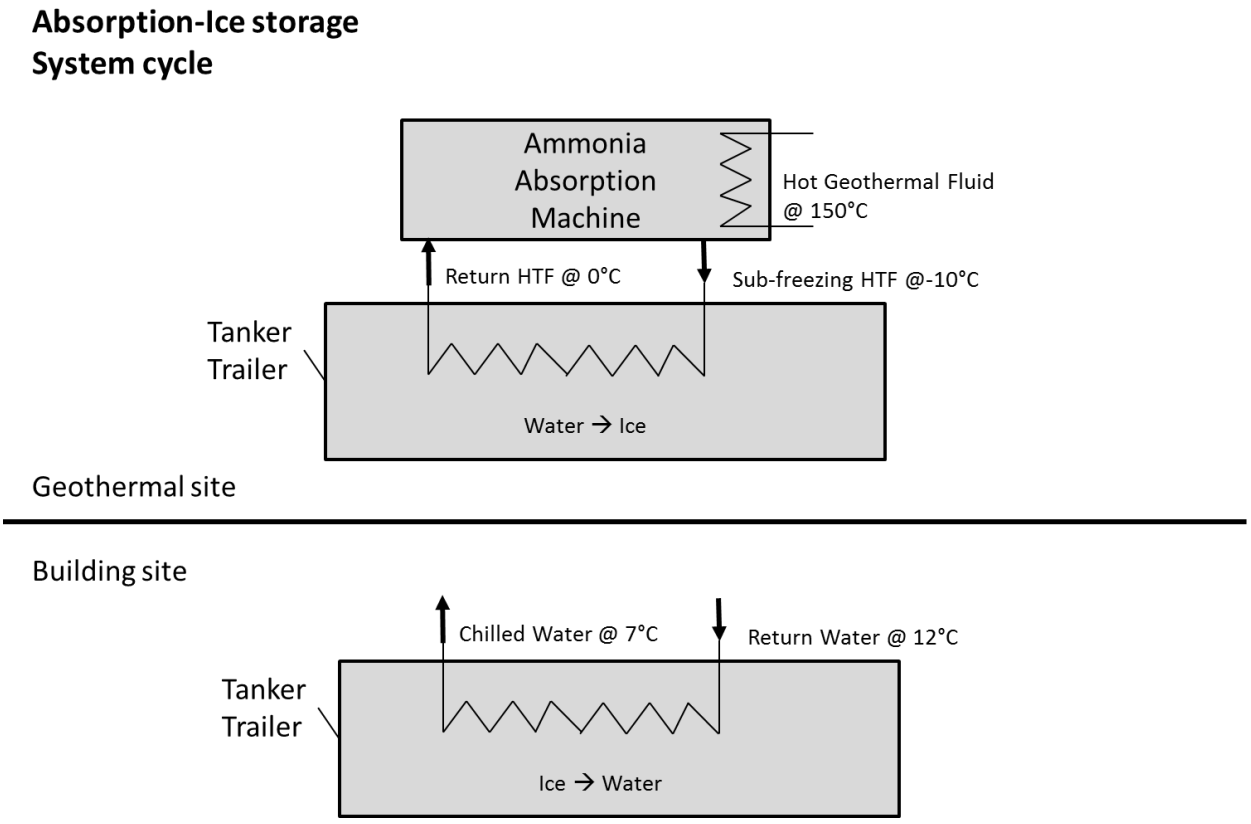

Fig. 14. Ice storage system operation cycle.

The capacity and charging/discharging rate of the ice-on-coil storage tanker trailer depend on the size of the tanker and the design of the coils. In the current study, they are calculated based on the experimental result reported by Drees and Braun (1995) on a stationary ice storage system. It is assumed that multiple coils, which are the same as that used in the experimental study, are installed in the tanker; therefore, the

tanker storage capacity and charging/discharging rate are directly proportional to the size of the tanker (i.e., the number of coils that can fit into the tank). For the maximum tanker capacity of about 27 tons, the total cooling energy stored is 2524 kWh_{clg}, the average charging (ice-making) rate is 196 kW, and the average discharging (ice-melting) rate is 687 kW. The ice system has two unique characteristics: (1) cost-free heat storage media (i.e., water) and (2) lower energy density (355 kJ_{clg}/kg) and longer charging/discharging time than that of the TSGA system[12], which means smaller discharge (cooling) rate from each tanker at the building site compared with the TSGA system. To ensure the ice system can satisfy the peak cooling demand of the building, multiple tankers are needed to discharge in parallel.

The initial and operating costs of the ice storage system are calculated with the same equations as for the TSGA system but with different equipment size. Based on the charging and discharging time of the ice storage tank studied by Drees and Braun (1995), it is calculated that the needed capacity of the ammonia absorption chiller is only 2/7 of the peak cooling load when the heat source temperature is 150°C. Subsequently, the cooling tower and circulation pumps associated with the absorption chiller also have smaller sizes than their counterparts in the electric chiller system.

The energy density of the ice storage system is directly calculated as the heat needed to melt a unit mass of ice and raise the melted ice's temperature from 0°C to 5°C. The calculated energy density is 355 kJ/kg (of ice).

4.7 TRANSPORTATION SYSTEMS

Two transportation systems are available to move the energy storage media of each technology between the geothermal site and the building that needs cooling or heating. First, the tractor-trailer system, which uses heavy-duty semi-tractors dragging tanker trailers, can transport the energy storage media on highways and public truck routes. The tractor-trailer system can transport both liquid (e.g., water and salty solution) and solid (e.g., solid desiccant) materials, so it can work with all the potential technologies. Second, the pipeline system consists of a two-way, fully filled pipeline and associated pumps. The transported material can only be liquid, so only the TSGA and DUH systems can use pipeline.

The costs of transportation are calculated after the energy density associated with each of the potential technologies is evaluated. Based on the energy density and other transportation-related information (e.g., building heating/cooling loads, distances, trailer size, etc.), the initial and operating costs of transportation are determined.

4.7.1 Tractor-Trailer

For tractor-trailer transportation, it is assumed that tractor-trailers are rented from contractors/operators on an hourly basis to transport energy storage media back and forth between the geothermal resource and the building. According to the federal regulation (National Research Council (US) 2010), the maximum allowed gross vehicle weight in the United States is 80,000 lbm, which includes around 20,000 lbm of empty vehicle weight, so at most 60,000 lbm (27,215 kg) of energy storage media can be transported. To ensure continuous heating and cooling operation in the building, additional tanker trailers are needed to provide temporary storage, and the required number of the additional tanker trailers depends on the applied technologies, as listed in Table 3.

Table 3. Number of additional tankers needed for each technology

Technology	TSGA	CTSGA	ADS	Ice	DUH
Additional tanker needed	3	1	1	*	2

[12] 3.6 hours to fully melt the ice, and 12.8 hours to freeze an entire tanker of water (Drees and Braun 1995).

* For the Ice system, the number of additional trailers ($N_{addTrailer}$) is determined by the number of tankers needed to operate in parallel to meet the peak cooling load. Thus it is calculated as expressed with Eq. (11).

$$N_{addTrailer} = \frac{peakLoad}{refCoolingPower * \frac{tankerSize}{refSize}} \quad (11)$$

where $refCoolingPower$ is the cooling output power of the reference ice storage system, $refSize$ is the capacity of the reference ice storage system, and $tankerSize$ is the capacity of the tanker trailer.

Since the tractor-trailers are rented (assuming each tractor comes with a tank trailer), it only contributes to the operating cost and does not require any upfront investment. Therefore, the initial cost of tractor-trailer transportation includes only the cost for purchasing the additional tanker trailers and the cost for purchasing the energy storage media to fill all these tanker trailers.
The number of tractors is calculated with the peak hourly heating/cooling demand and the transportation cycle time, as expressed in Eq. (12):

$$N_{tractor} = Ceiling(\frac{peakLoad * cycleTime}{tankerSize * ED}) \quad (12)$$

where ED is the energy density of a particular technology, $cycleTime$ is the minimum time for a round trip between the geothermal resource and the building site.

Once the numbers of tractors and additional trailers are determined, the initial cost of the tractor-trailer system is calculated as expressed in Eq. (13):

$$IC_{tractorTrailer} = trailerPrice * N_{addTrailer} + materialPrice * (N_{addTrailer} + N_{tractor}) * m_{Trailer} \quad (13)$$

where $trailerPrice$ is the price of a trailer, $materialPrice$ is the price of the energy storage media per unit of mass, and $m_{Trailer}$ is the weight of the energy storage media that can be shipped with a trailer.

There is a trade-off between (1) using large tankers and more energy storage media to minimize frequency of transportations and associated cost, and (2) using small tankers so that less energy storage media is needed, but more frequent transportation to ensure continuous operation of the heating or cooling systems in the building. The trade-off can be analyzed with the economic analysis tool developed through this project (Section 5 and Appendix E).

The operating cost of a tractor-trailer is calculated based on the number of deliveries and the cost per delivery. The cost for each delivery (a complete cycle between the geothermal site and the building) is calculated using the national average hourly trucking cost (Fender and Pierce 2013) adjusted with the transportation distance and the cycle time, as expressed in Eq. (14).

$$OPC_{tractorTrailer} = \left(Rate_{fix} + \frac{Rate_{mile}}{40} * \frac{2 * distance}{cycleTime}\right) * cycleTime * \frac{totalLoad}{tankerSize * ED} \quad (14)$$

In this equation, the hourly rate of leasing a tractor-trailer is divided into two parts: fixed rate ($Rate_{fix}$), which includes costs that are not related to the transportation distance, such as driver wages; and mileage-related rate ($Rate_{mile}$), which includes distance-sensitive costs such as fuel cost, maintenance cost, and

toll fees. The original rate is based on a 40 mile-per-hour scenario, and the total hourly rate used in this calculation is adjusted according to the actual distance traveled in an hour.

4.7.2 Pipeline

A two-way pipeline can be used to transport liquid energy storage media (working fluid) between the geothermal resource and the building. Since the transported working fluid is at ambient temperature (excluding DUH), insulation is not needed for the pipeline. To prevent air infiltration, the entire pipeline is pressurized and fully filled with the working fluid, which is transported with multiple variable-speed pumps installed along the pipeline. It is assumed that the pumps are controlled to supply the needed amount of working fluid to maintain continuous operation of the heating/cooling system in the building.

The design flow rate of the circulation pump (FR) is determined based on the peak load and the energy density of the transported working fluid, as expressed in Eq. (15).

$$FR = \frac{peakLoad}{ED} \tag{15}$$

The pipe size is determined based on the calculated design flow rate following the recommendation of minimum pipe size for given flow rate given by Kevin Rafferty (2001) and listed in Table 4.

Table 4. Flowrate and minimum pipe diameter

Flowrate, FR (gpm)	Flowrate, FR (l/s)	Minimum pipe diameter (in.)
2	0.13	0.5
4	0.25	0.75
8	0.50	1
12	0.76	1.25
22	1.39	1.5
40	2.52	2
70	4.41	2.5
120	7.56	3
260	16.38	4
550	34.65	6

The pressure drop across one leg of the two-way pipeline is calculated with Eq. (16):

$$\Delta P = C_f * \frac{distance * density * \frac{velocity^2}{2}}{d_n} \tag{16}$$

where C_f is the friction coefficient of the pipeline, which is calculated using Eq. (17), $density$ is the fluid density, $Velocity$ is the flow rate, and d_n is the diameter of the pipe.

$$\frac{1}{C_f^{\frac{1}{2}}} = -2 * \log[\frac{2.51}{Re * C_f^{\frac{1}{2}}} + \frac{\frac{k}{d_n}}{3.72}] \tag{17}$$

where Re is the Reynolds number of the flow, and k is the roughness of the pipe's interior surface.

The pipeline transportation initial cost includes the cost of the piping materials and their installation, the cost of liquid energy storage media to fully fill the pipes, as well as the cost associated with the circulations pumps:

$$IC_{pipeline} = IC_{pipe}(diameter, distance) + IC_{pump}(FR) + IC_{fluid}(diameter, distance) \quad (18)$$

In the above equation, IC_{pipe} is calculated using the diameter and length of the pipeline, and the material and installation costs of the pipes are extracted from RSMeans (Mossman 2010). IC_{fluid} is calculated by multiplying the needed mass to fill the two-way pipeline with the price of the working fluid per unit of mass. The price of each circulation pump is calculated based on the previously calculated mass flow rate, and the number of pumps is calculated using the total pressure drop along the entire pipeline and the pressure rating of the pipe. For high density polyethylene (HDPE) pipe with a diameter to thickness ratio of 11, the pressure rating is 125 psi at 38°C, which means that for each 125 psi pressure drop, there needs to be a pump for each direction of pipeline flow. The HDPE pipe is the most inexpensive material available in the RSMeans (Mossman 2010) category, and it is resistant to the corrosion effect of LiBr/H_2O solution. Other corrosion-resistant materials such as stainless steel are much more expensive than the HDPE pipe and thus not considered in this study.

The operating cost of pipeline transportation includes the electricity cost for pumping and the right-of-way (ROW) cost for constructing the pipeline across public or private lands, as expressed with Eq. (19).

$$OPC_{pipeline} = OPC_{pumping}(FR, \Delta P) + ROW(distance) \quad (19)$$

The operating cost of pumping can be calculated as expressed with Eq. (20)

$$OPC_{pumping} = ElePrice * \frac{totalLoad}{peakLoad} * \frac{FR * \Delta P * density}{\eta} \quad (20)$$

where η is the total efficiency of the pump.

The right-of-way is usually a per-year-per-length lease fee that is highly case-specific. It is a user input in the economic analysis tool developed through this project.

4.8 GEOTHERMAL RESOURCE RELATED COSTS

Geothermal energy is renewable, but using it may involve some costs. If there are no existing geothermal wells or oil/gas wells that can produce hot geothermal fluid, an initial cost (IC_{wells}) will be needed for drilling the well. Once the system is set up, there may also be costs during operation of the site (OPC_{wells}), such as contracting with the oil/gas owners for using their established wells, or fees paid to the land owners that allow a geothermal well to be drilled and operated on their land.

In this study, we assume both the initial and operating costs of a single well, be there any, is given. Also provided is the average mass flow rate of the geothermal fluid from each well. With this mass flow rate (FR_{well}), as well as the source temperature (T_{src}) and the minimum temperature to drive a certain technology (T_{min}), the heat flux that can be extracted from each well (q_{well}) is calculated as expressed with Eq. (21)

$$q_{well} = FR_{well} * (T_{src} - T_{min}) * C_{p_w} \quad (21)$$

where C_{p_w} is the specific heat of the geothermal fluid, which is approximated using the specific heat of water.

With the operational thermal COP of the selected technology (COP_{th_a}) and the peak cooling load of the target building, the total number of wells required to supply enough heat for the building load can be calculated with Eq. (22)

$$N_{wells} = \frac{peakLoad}{COP_{th\_a} * q_{well}} \tag{22}$$

Then the geothermal resource related costs can be determined with Eqs. (23) and (24), respectively:

$$IC_{wells} = IC_{perWell} * N_{wells} \tag{23}$$

$$OPC_{wells} = OPC_{perWell} * N_{wells} \tag{24}$$

5. DEVELOPMENT OF AN ECONOMIC ANALYSIS TOOL

The economic analysis tool is designed for evaluating various potential technologies that utilize low temperature geothermal resources for thermal applications (i.e., space/water heating, space cooling, or dehumidification). With this tool, a user can compare the cost and performance of candidate technologies and hence make an informed decision on which technology is most cost effective for utilizing the low temperature geothermal resource at the given conditions.

5.1 SOFTWARE STRUCTURE

This economic analysis tool is composed of a calculation engine, which predicts performance and cost of the technologies described in previous section, and a web interface for accepting user inputs and displaying calculation results. The web interface allows the tool to be accessed by potential users worldwide via the Internet. The structure of the calculation engine and its connection with the interface is illustrated in Fig. 15.

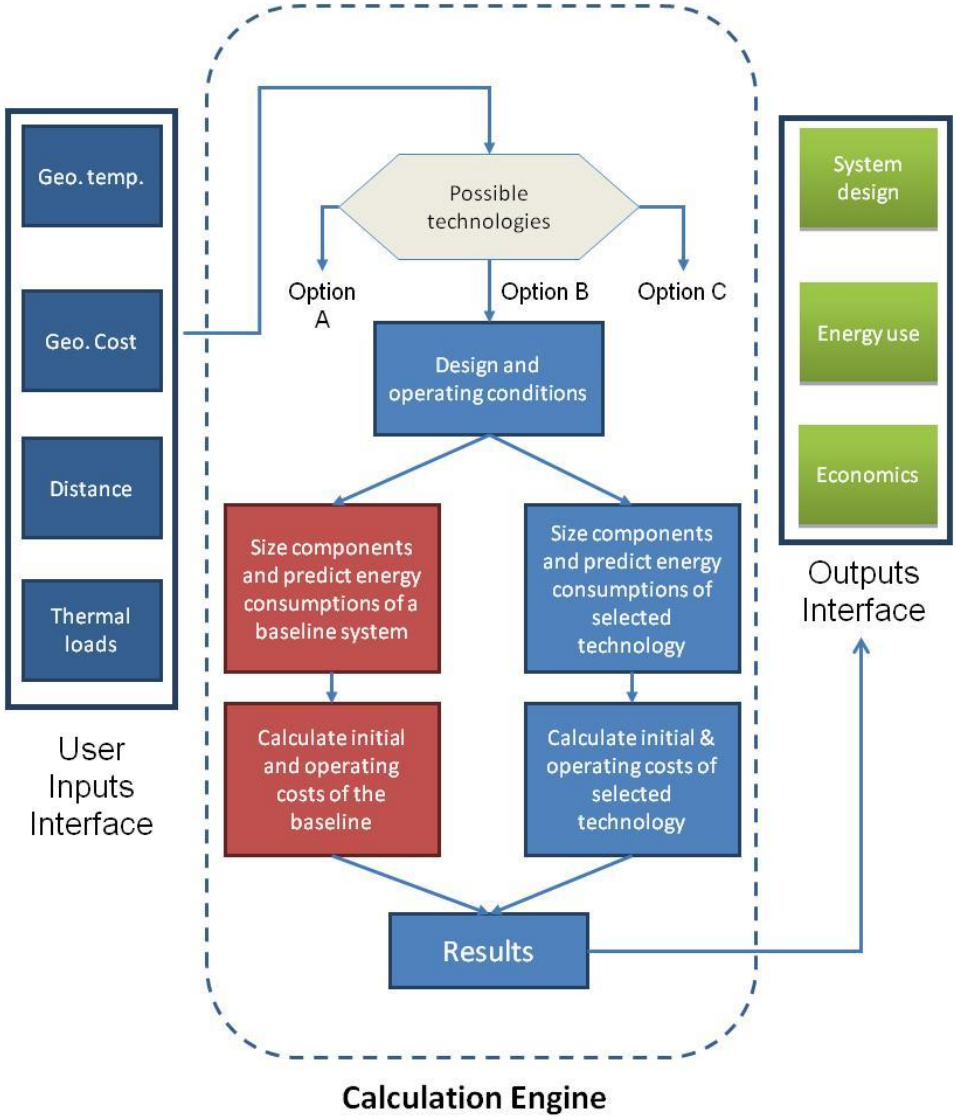

Fig. 15. Structure of the economic analysis tool.

Based on the user-specified geothermal source temperature, operating conditions (e.g., weather conditions), and expected end-use application (e.g., heating or cooling), the tool will show the available technologies that can meet those user-defined constraints. It will then calculate their performance and cost, along with that of a comparable baseline system. The specific technologies that fit each user-defined scenario are determined by use of a decision tree as shown in Fig. 16.

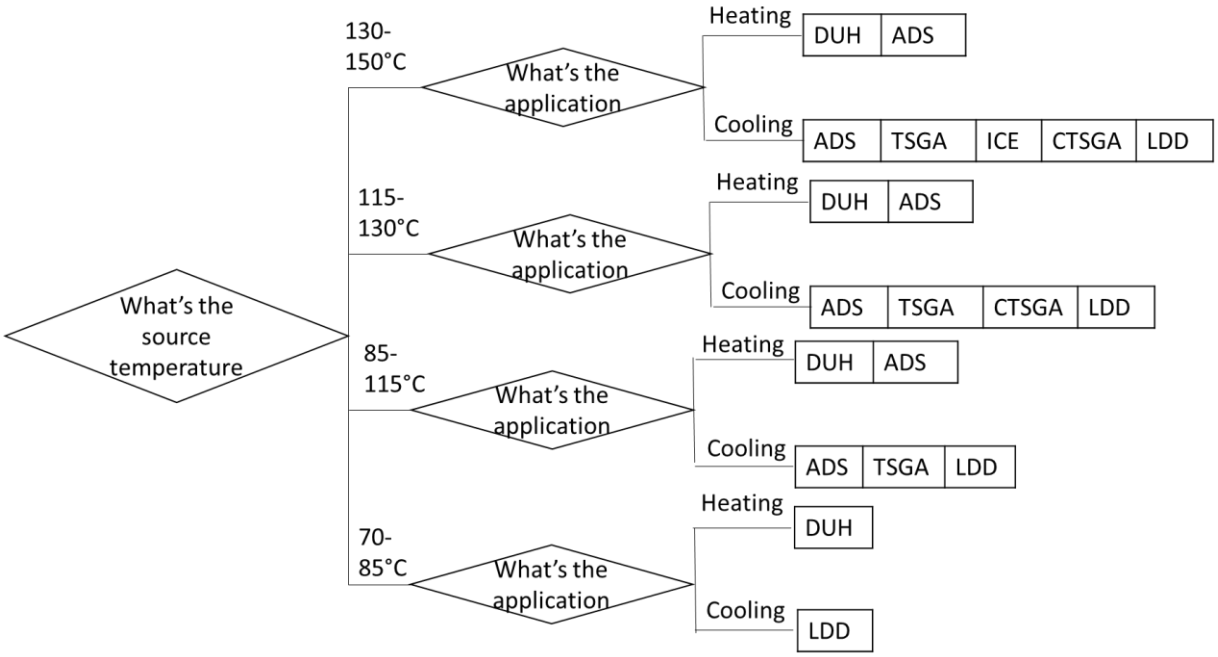

Fig. 16. Decision tree for selecting suitable technologies for analysis.

5.2 CALCULATION ENGINE

The calculation engine includes a series of computation modules for each of the potential technologies. With these modules and a few user inputs (i.e., temperature of the available geothermal resource, thermal loads, and distance between the geothermal site and the thermal loads), this tool will size needed equipment and calculate the energy consumptions of each selected technology. Based on the equipment size and the predicted energy consumption, this tool will calculate both the initial and operating costs of the selected technology using standard cost data (e.g., RSMeans cost data for mechanical equipment/system and the national average carrier cost of motorized vehicles). To determine energy savings and simple payback of the selected technology, the energy consumptions and costs of a baseline system (i.e., an electric-driven vapor compression chiller for cooling load and a natural-gas-fired boiler for heating load) for satisfying the same thermal loads will also be calculated with the tool. At the end, this tool will report key performance metrics of the selected technology, including system design parameters, annual energy savings and associated emission reductions, and economics (e.g., simply payback and levelized cost) of the selected technology. The calculation sequence is illustrated in Fig. 17. The calculation engine reads the user input from a text data file generated by the web interface, and then performs needed calculations to predict the performance and cost of both the baseline system and the selected technologies for providing the same heating/cooling service. The energy consumptions of both systems are calculated based on the heating/cooling loads; their operating costs, including the transportation cost, are calculated as well. The comparison module in the calculation engine finally gathers and compares the results of both systems to evaluate the economic, energy, and environmental impact of using the selected technologies to replace the baseline system. All the results are written into another text data file for the web interface to read and display to the user.

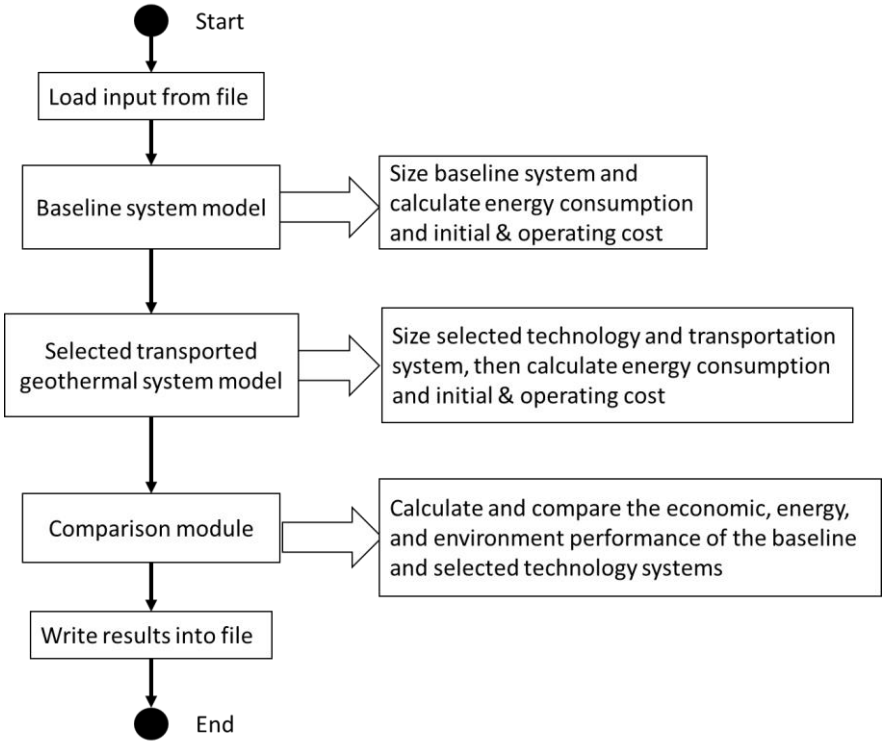

Fig. 17. Calculation sequence of the calculation engine.

5.3 INTERFACE

The web interface operates in a linear sequence: after the welcome page, six consecutive input pages allow user to define an application scenario, and after calculation, a series of output pages display the calculation results in tabular and graphical forms. Figure 18 shows a screenshot of the web interface. The webpages are developed using PHP[13] and HTML language, and the result display webpages use a free service, Google Charts, to generate various charts illustrating the calculation results. A user manual of the economic analysis tool, which includes a step-by-step introduction, is given in Appendix C.

[13] The recursive acronym for PHP is Hypertext Preprocessor. PHP is a widely used open-source general-purpose scripting language that is especially suited for web development and can be embedded into an HTML webpage.

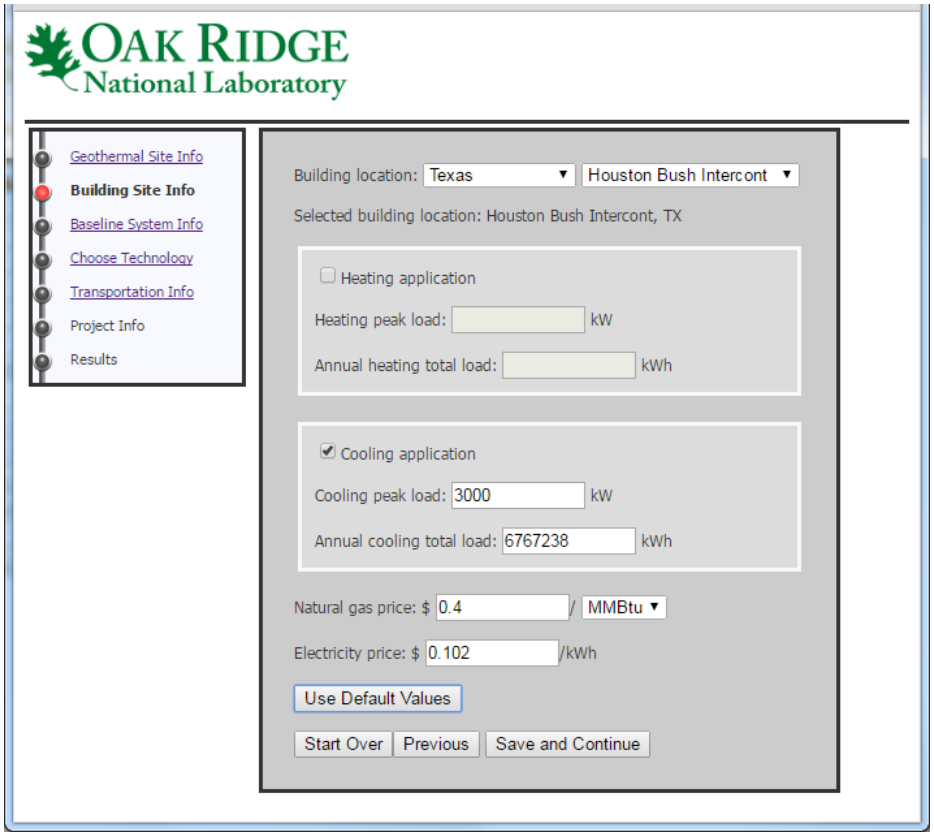

Fig. 18. A screenshot of the web interface.

6. CASE STUDIES

To evaluate the economics of applying the alternative cooling systems that utilize low temperature geothermal energy, two sites are identified for case studies:

- a district cooling system in downtown Houston, Texas, which is close to a large oil field; and
- an office building in Santa Rosa, California, which is close to a low temperature hydrothermal resource.

These two sites are identified based on the following criteria:

- moderate proximity to low-cost geothermal resources
- significant cooling demands
- existing infrastructure for transporting geothermal energy

Information and case study results of the two sites are presented in Sections 6.1 and 6.2, respectively.

6.1 DISTRICT COOLING SYSTEM AT HOUSTON, TX

6.1.1 Geothermal Resource

The Hastings oilfield is located 18 miles south of Houston on the Brazorian–Galveston county line. It is approximately 5 miles long and 4 miles wide. It was discovered on December 23, 1934, and divided into Hastings East and Hastings West in 1958. The Hastings field is in an advanced stage of primary depletion, and artificial lift systems are needed to produce oil from the wells. A total of 297 wells existed in 1985.[14] Table 5 lists the oil production of Hastings East and Hastings West in 2015.

Table 5. Oil production of the Hastings East and Hastings West in 2015[15]

Oil field	Production in 2015 (bbl)
Hastings, West	2,476,928
Hastings, East	81,649

The average water–oil ratio (WOR) of oil fields in Texas is reported around 14 (Welch and Rychel 2004) to 21 (Clark and Veil 2009), which means for every barrel (bbl) of crude oil, 14–21 barrels of hot water is produced from the oil well. According to the oil/gas well data shown in NREL's geothermal prospector,[16] the wells in the vicinity of the Hastings oil field have a bottom hole temperature of above 100°C. Conservatively assuming the WOR of the oil wells in the Hastings field is 10, the total annual coproduced water is 25,585,770 bbl (4.07 million m^3) combining both west and east fields, which is equivalent to 2020 GPM (gallon per minute) or 7,620 L/m assuming year-round continuous operation of the oil wells.

6.1.2 Thermal Demand

Downtown Houston has a district cooling system[17] currently serving 24 buildings containing approximately 550,000 m^2 of building floor space, including offices, church, hotels, apartments, and

[14] https://tshaonline.org/handbook/online/articles/doh01
[15] Texas Railroad Commission online system, http://www.rrc.state.tx.us/oil-gas/research-and-statistics/production-data/monthly-crude-oil-production-by-district-and-field/
[16] https://maps.nrel.gov/geothermal-prospector/
[17] http://www.enwaveusa.com/Houston

restaurants. The district cooling system has a capacity of 102,515 kW_{clg}, which is provided by eight electric-driven chillers. The district system has 8.8 km of chilled-water piping in place, which has a capacity to deliver 280,000 kW_{clg} of cooling to allow future expansion.

6.1.3 Transportation

Three available truck routes connecting the Hastings oilfield and downtown Houston are shown in Fig. 19. The blue route on the map has the shortest travel distance 33.5 km. Assuming 64.4 kmh speed and 10 minute loading time at both the geothermal site and the building, it takes 1.34 hours for a tractor-trailer to deliver the energy storage media to the building and ship it back to the geothermal site. The cost per delivery is calculated with a generic truck transportation cost model described by Liu et al. (2015) as $76.3 based on the traveling time and distance.

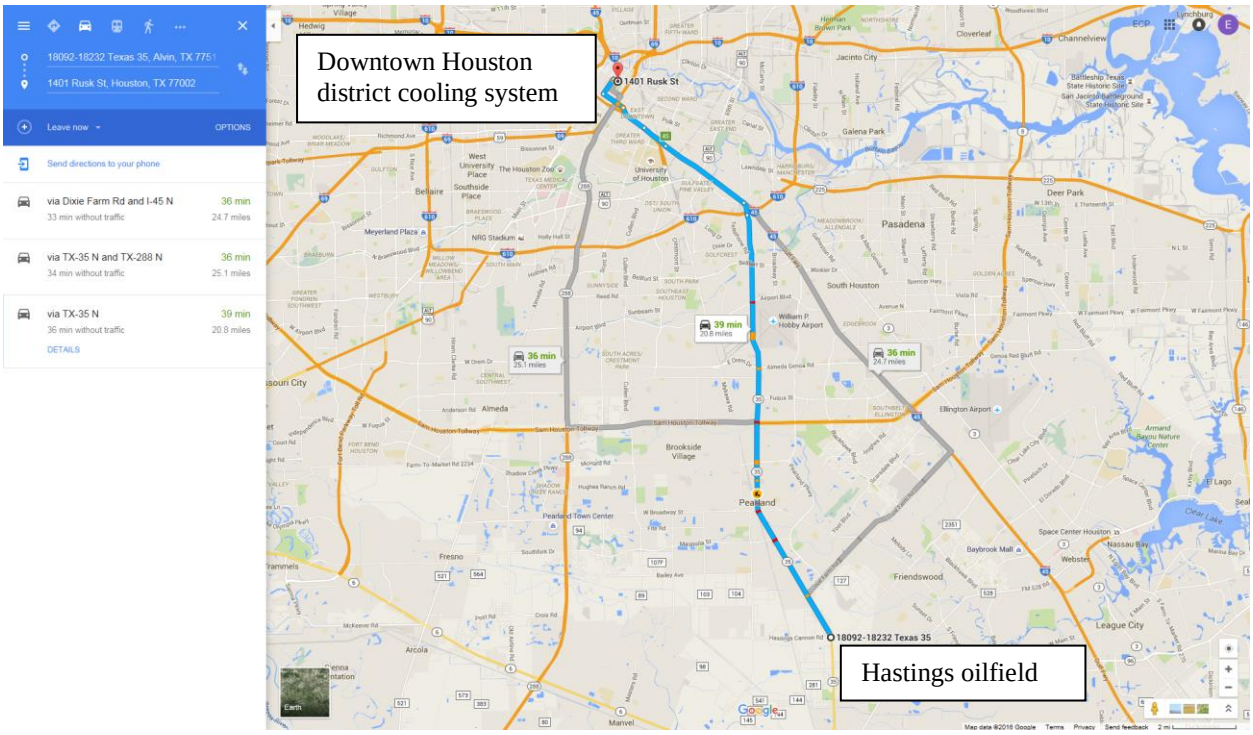

Fig. 19. Existing truck routes in Houston, Texas (Map data: Google).

A segment of rail tracks about 30.6 km long connects the Hastings oilfield and downtown Houston. However, a railway transportation analysis indicates that the cost of shipping the solution over the 33.5 km distance by rail is higher than transporting it by tractor-trailers.

6.1.4 Application of Alternative Cooling Systems

If the coproduced water temperature is 115°C, which is high enough to drive the alternative cooling systems that utilize TSGA, CTSGA, or ADS technology, the heat released from the 25,585,770 bbl of annually coproduced water with a temperature drop of 10°C could produce 31,193,318 kWh of cooling, which is equivalent to running a 3,500 kW_{clg} alternative cooling system all year long (e.g., to satisfy the base load of the district cooling system). It is assumed that the coproduced water is used free of charge.

In this case, the baseline cooling system is a 1000 ton water-cooled centrifugal chiller, which has an electrical COP of 6 (the minimum allowed efficiency according to ASHRAE Standard 90.1-2013). The

initial and operating costs of both the baseline cooling system and the alternative cooling systems are calculated with the economic analysis tool introduced in Section 5.

6.1.5 Economic Analysis

The economic analysis results indicate that the three alternative cooling systems can result in 50–61% source energy savings and 53–62% carbon emission reduction as shown in Fig. 20. The calculations of source energy and carbon emission account for both the electricity savings and fuel consumption for the transportation. However, with the 20 mile (32 km) distance and the current $0.102/kWh electricity rate,[18] CTSGA is the only technology that can achieve any lifetime cost saving after 20 years of operation due to its higher energy density and the resulting lower transportation cost. The simple payback of the CTSGA system is 14 years. If the distance becomes shorter or the electricity rate increases, the other technologies can also offer lifetime cost savings. The maximum break-even distance for applying the TSGA and ADS technologies with the current electricity rate is about 9 miles. If the electricity rate is higher than $0.203/kWh, both the TSGA and ADS can result in lifetime cost savings with the 33.5 km distance.

A series of parametric studies has been carried out to investigate the impact of distance and electricity rate on CTSGA system's payback. Figure 21 shows the simple payback of the CTSGA system resulting from various combinations of distance and electricity rate. The distance ranges from 5 to 20 miles (8 - 32 km) and the electricity rate ranges from 0.102 to 0.124 $/kWh. The area colors in Fig. 21 indicate different simple payback periods. With shorter distance and higher electricity rate, the payback period declines quickly as shown in the figure. For the same distance, the payback can be reduced to within 10 years if the electricity rate increases only by 6% to $0.108/kWh. On the other hand, with the current $0.102/kWh electricity rate, the investment of a similar CTSGA application can be paid back within 10 years if the distance is shortened to 18 miles (29 km).

[18] The average electricity energy price in Houston in 2016 plus estimated transmission and distribution cost.

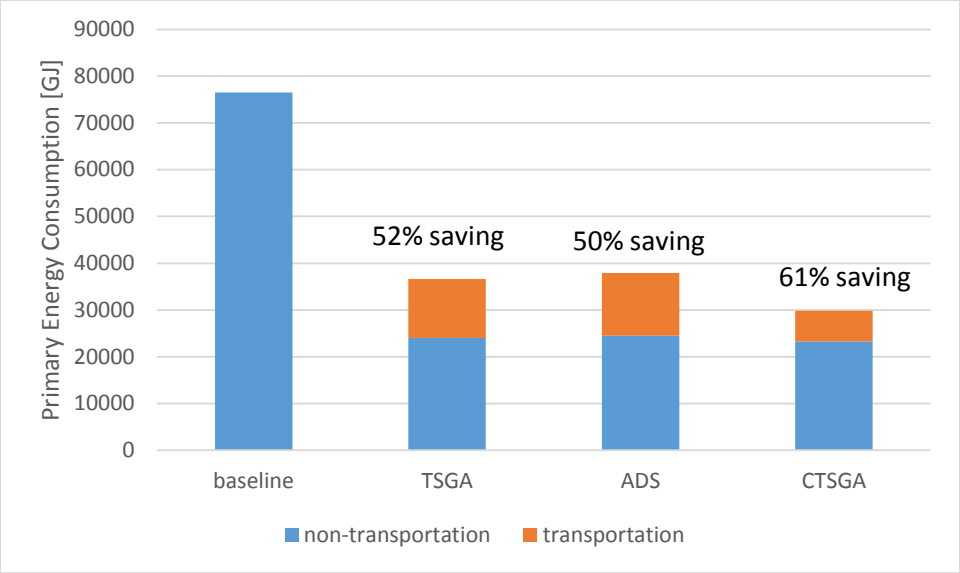

(a)

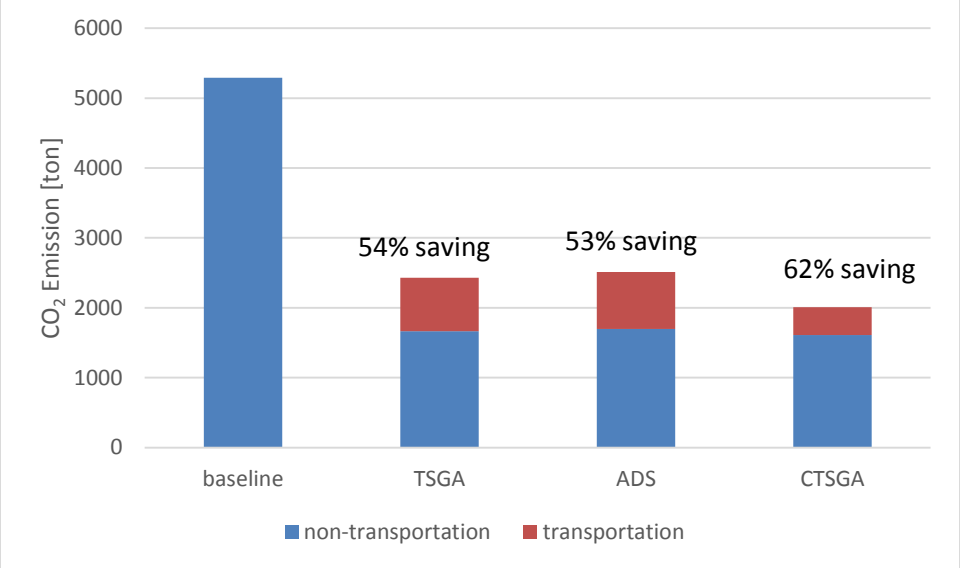

(b)

Fig. 20. Performance comparison between geothermal cooling systems and the baseline electric cooling: (a) primary energy consumptions and (b) carbon emissions at Houston, Texas.

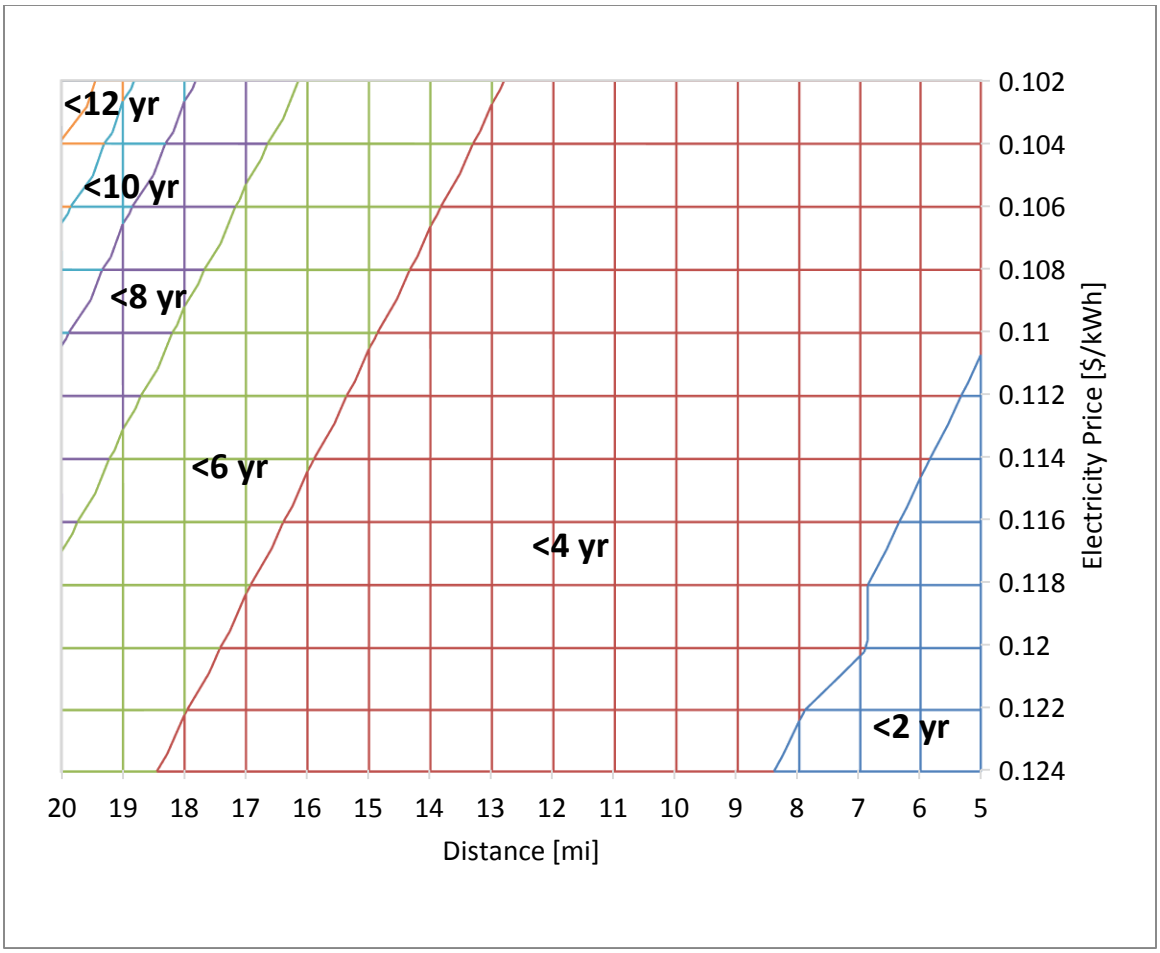

Fig. 21. Simple payback of CTSGA system resulting from various combinations of distance and electricity rate.

6.2 OFFICE BUILDINGS IN SANTA ROSA, CALIFORNIA

6.2.1 Geothermal Source

Calistoga, California, has 35 geothermal wells (Mullane et al. 2016). These geothermal wells are only 738 ft (244 m) deep, and the geothermal fluid temperature is 280°F (138°C). The total flow rate of the geothermal fluid is 1,175 GPM (4,447 L/m). Calistoga is a small town and had a population of only 5,155 during the 2010 census. Population density in the area surrounding Calistoga is very low (<1,000 people per square mile)[19] except at Santa Rosa, which is about 20 miles southwest of Calistoga. Santa Rosa is the county seat of Sonoma County, California. Its estimated 2014 population was 174,170.

6.2.2 Thermal Demand

The targeted thermal demand is the space cooling loads of medium-sized office buildings in Santa Rosa. Given the mild weather there, air-cooled chillers are commonly used to produce chilled water for space cooling. The DOE commercial reference building model (Deru et al. 2011) is used to estimate the peak and annual cooling loads of a medium-sized office building in Santa Rosa. The estimated peak cooling

[19] http://www.city-data.com/city/Santa-Rosa-California.html

load is 350 kW, and the total annual cooling load is 268,800 kWh. According to EIA,[20] the average electricity rate in California is $0.18/kWh for commercial customers.

6.2.3 Transportation

The shortest truck route connecting the geothermal resources at Calistoga and the office building at Santa Rosa is shown in Fig. 22. The length of this route is about 75.6 km (one way). It should be noticed that the route through Petrified Forest Road (about 27 km) across a mountain is not a designated truck route and therefore not being considered in this case study. No information has been found with regard to other transportation options (e.g., existing pipelines or railway).

With the 75.6 km distance and assuming a 10-minute loading time at both the geothermal site and the building, it takes the tractor-trailer 2.69 hours to complete a round trip between the geothermal site and the building. The cost per delivery is calculated as $164.4 based on the traveling time and distance with a generic truck transportation cost model described by Liu et al. (2015).

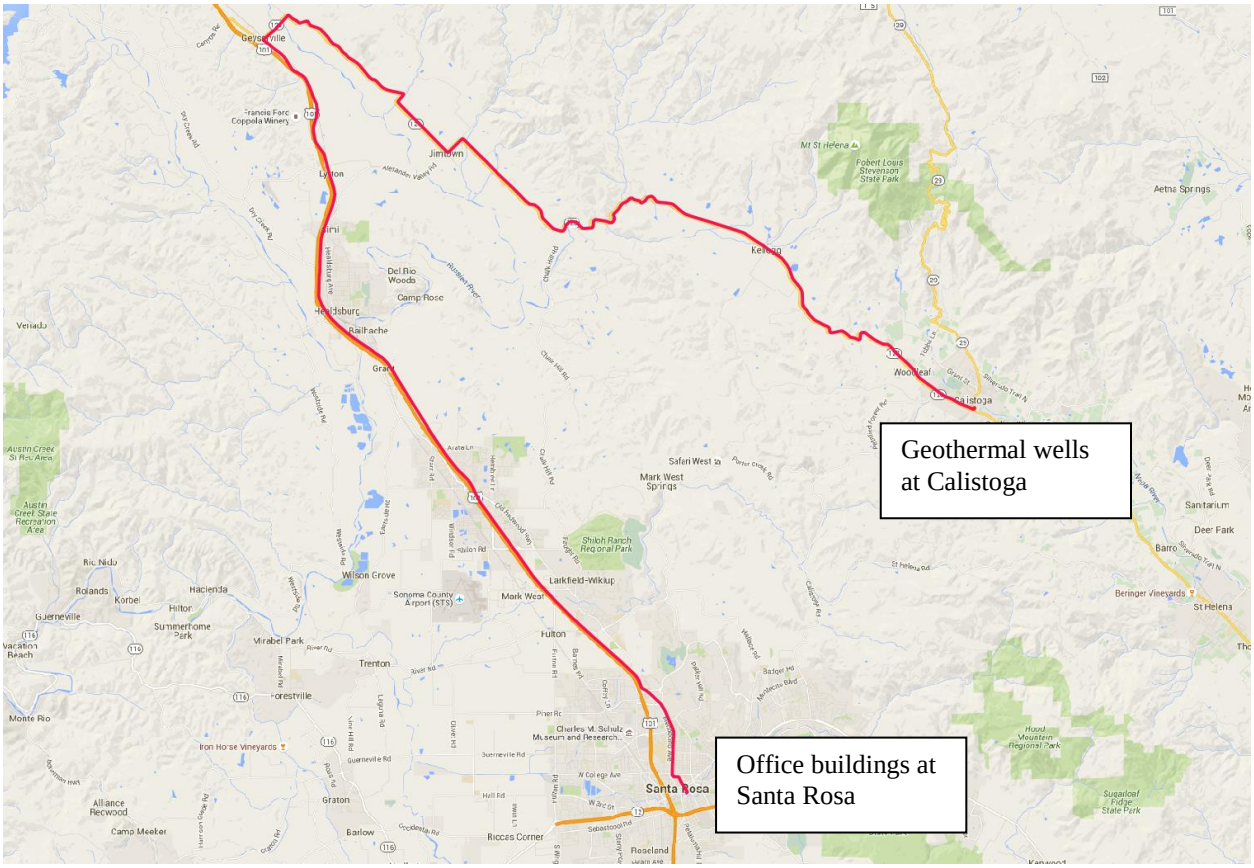

Fig. 22. Truck route in California connecting the geothermal resources at Calistoga and the office building in Santa Rosa (Map data: Google).

[20] https://www.eia.gov/electricity/monthly/epm_table_grapher.cfm?t=epmt_5_6_a

6.2.4 Application of Alternative Cooling Systems

The 138°C geothermal fluid produced at the geothermal wells in Calistoga, California, can drive alternative cooling systems that utilize TSGA, CTSGA, or ADS technology. Assuming a 15°C temperature difference when extracting heat from the geothermal fluid and a 0.6 thermal COP of the alternative cooling system, the maximum cooling capacity that the 1,175 GPM/4,447 L/m geothermal fluid can support is around 850 tons (2,975 kWh_{clg}). It is assumed that the geothermal fluid is utilized in a cascaded approach—first, to regenerate desiccants used in the alternative cooling system with a 15°C temperature difference, and then to utilize the cooler geothermal fluid (but still higher than 100°C) to provide heating for industrial processes or agriculture productions. In this case, the cost of using the geothermal fluid for the alternative cooling may be shared with the other uses of the same geothermal resource, or probably even be waived. The cost of using the geothermal fluid is included as a variable in this case study.

The baseline cooling system to be compared with the alternative cooling is a packaged electric chiller with integral air-cooled condenser. According to California title 24,[21] the minimum allowed electrical COP is 2.8 for air-cooled chillers with larger than 220 kW cooling capacity. The air-cooled chiller does not need a cooling tower and the associated cooling water circulation pump. It is commonly used in California, given the mild weather and the shortage of water. To have a fair comparison, all the alternative cooling systems use dry coolers, which do not consume any water. The initial and operating costs of both the baseline and the alternative cooling systems are calculated with the economic analysis tool introduced in Section 5.

6.2.5 Economic Analysis

The economic analysis results indicate that the three alternative cooling systems can result in 46–61% source energy savings and 24–51% carbon emission reduction compared with the baseline cooling system, as shown in Fig. 23. The calculations of source energy and carbon emission account for both the electricity savings and the fuel consumed in transportation. However, it is found that the economics of the alternative cooling systems are poor if the systems are used to provide space cooling to only one medium-sized office building, even without accounting for the cost associated with using geothermal fluid. This result occurs because the transportation cost and the material cost of the desiccants are more than the monetary value of the saved electricity.

[21] http://www.energy.ca.gov/2015publications/CEC-400-2015-037/CEC-400-2015-037-CMF.pdf

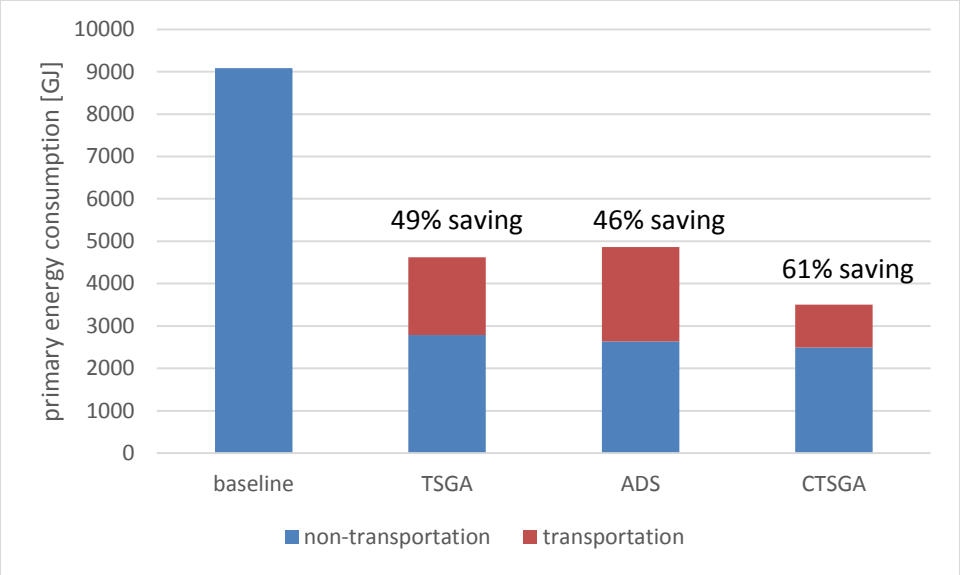

(a)

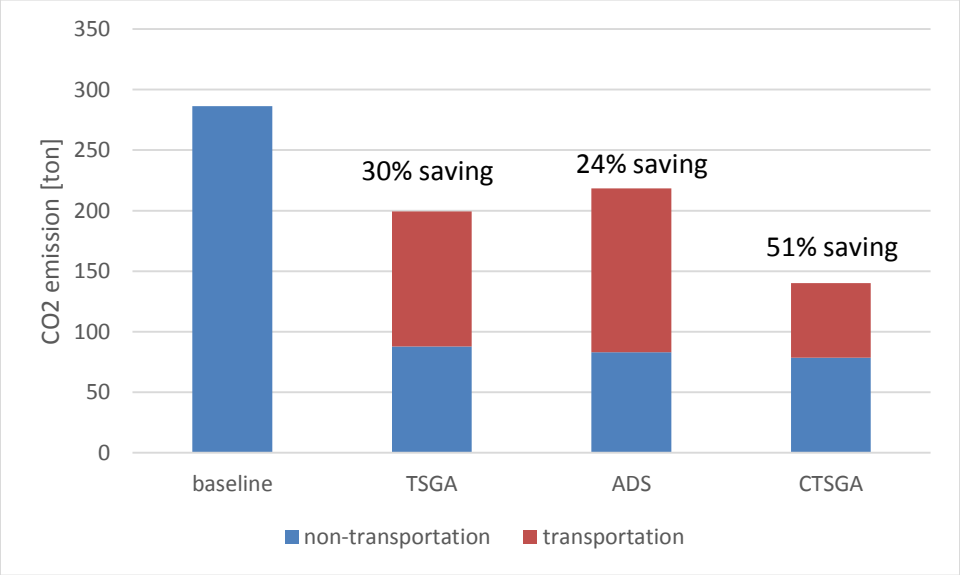

(b)

Fig. 23. Performance comparison between geothermal cooling systems and the baseline electric cooling: (a) primary energy consumptions and (b) carbon emissions at Santa Rosa, California.

Since the cooling demand of the building determines the amount of energy storage media needed and the transportation frequency, the impact of building peak cooling load is investigated for a range of distances. The simple paybacks of applying the CTSGA system in buildings with various peak cooling load (assuming the annual total cooling load is proportional to the peak cooling load) and at various distances away from the geothermal resource are calculated with the economic analysis tool, and the results are shown in Fig. 24. The X-axis of this figure is the peak cooling load ranging from 100 to 850 ton (350 kW to 2,975 kW). The Y-axis is the distance between the geothermal resource and the building, which ranges from 5 to 75 miles (8-121 km). The various colors in this figure indicate different simple payback periods. Figure 24 shows that, for the same distance, the payback declines with increase in building peak cooling load. For a distance less than 40 miles, the shortest payback comes from the largest possible peak cooling

load (850 ton/2,975 kW). Once the distance is longer than 40 miles (64 km), the shortest payback for each distance is achieved by applying the CTSGA system at buildings with a peak cooling load less than 850 tons/2,975 kW. This result occurs because additional trailers filled with charged desiccants are needed to ensure continuous operation of the CTSGA system at buildings with 850-ton/2,975-kW peak cooling load and more than 40 miles away from the geothermal resource.

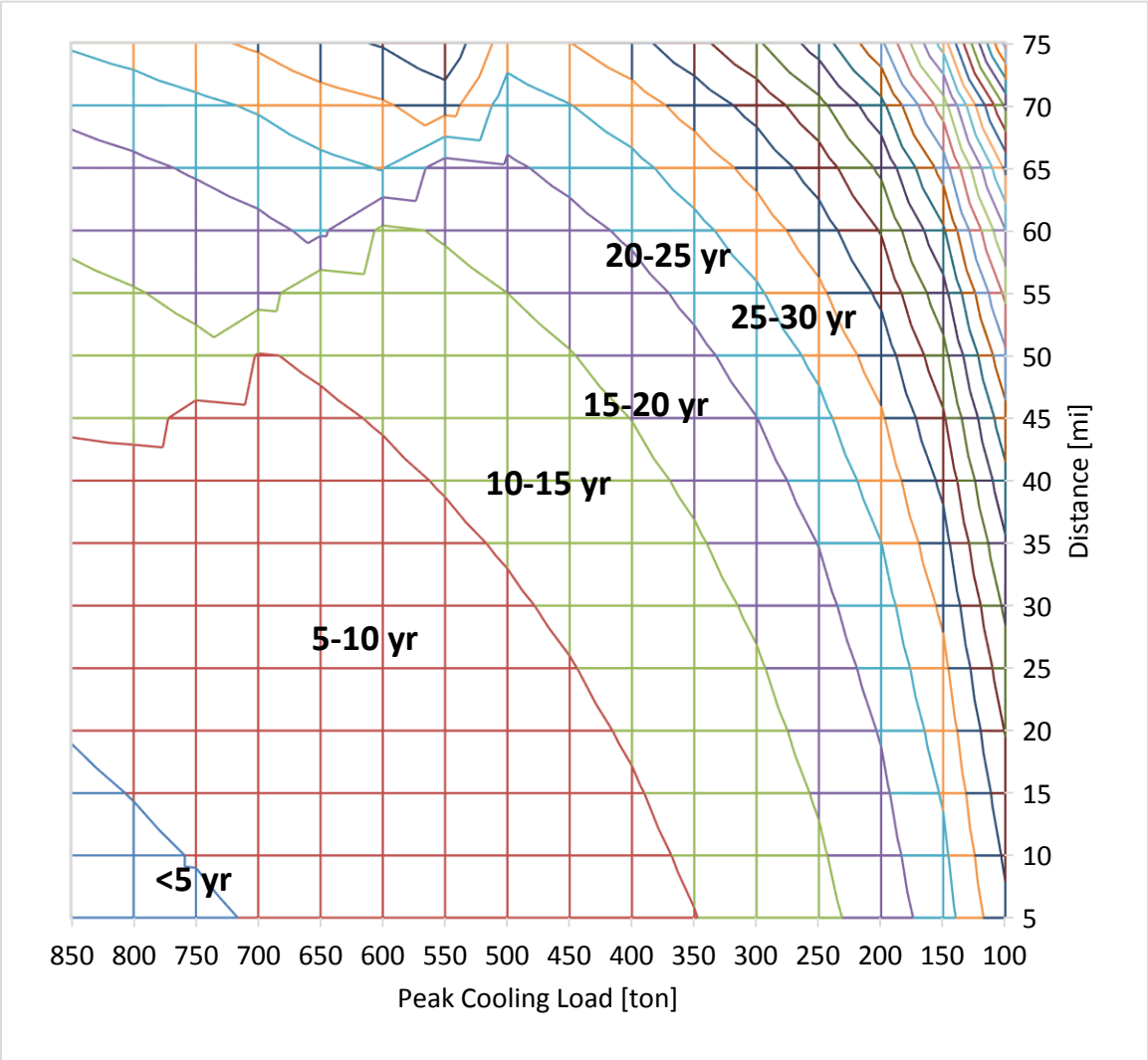

Fig. 24. Simple paybacks of the CTSGA system serving buildings with various cooling loads and at various distances from the geothermal resource.

The shortest paybacks and the corresponding peak cooling load at distances ranging from 5 to 75 miles (8 – 121 km) are listed in Table 6. With the current electricity rate, the CTSGA system is economically viable only if applied to buildings that are closer to the geothermal resource and have a peak cooling load closer to the distance-specific optimum listed in this table.

A series of parametric studies has been carried out to investigate the impact of distance and electricity rate on the payback of the CTSGA system. Figure 25 shows the simple payback of the CTSGA system resulting from various combinations of distance and electricity rate. The distance ranges from 5 to 75 miles (8 – 121 km) and the electricity rate ranges from 0.15 to 0.215 $/kWh (about ±20% from $0.18/kWh). The different colors in Fig. 25 indicate different simple payback periods. Generally, with

shorter distance and higher electricity rate, the payback is lower. The increase of electricity price helps to stretch the economically feasible distance for applying the CTSGA system—the longest distance for a payback less than 10 years is 50 miles/80.5 km with a $0.18/kWh electric rate, and it is extended to over 60 miles/90.6 km when the electricity rate increases by 20% to $0.215/kWh. An increase in the electricity rate could result in a shorter payback period. For example, while applying an 850-ton CTSGA system to a building 30 miles/48 km away from the geothermal site takes more than 5 years to achieve payback with the current electricity rate, it takes less than 5 years when the rate increases above $0.2/kWh.

For the 47-mile/75.6 km case, 750 ton/2,625 kW is the optimum capacity and the corresponding payback is 8.6 years. If there is expense to operate the geothermal site based on the amount of hot water used, in order to achieve lifetime cost saving within 20 years, the maximum annual geothermal site operating cost should be less than $32,800.

Table 6. Distance-specific optimum cooling loads for applying the CTSGA systems in California

Distance (miles)	Distance (km)	Capacity (tons)	Capacity (kW)	Payback (years)
<45	<72	850	2,975	4.3–6.8
45	72	750	2,625	8.3
50	80	700	2,450	9.8
55	88	650	2,275	11.6
60	96	600	2,100	14.1
65	105	550	1,925	17.8
70	113	500	1,750	22.6
75	121	500	1,750	27.2

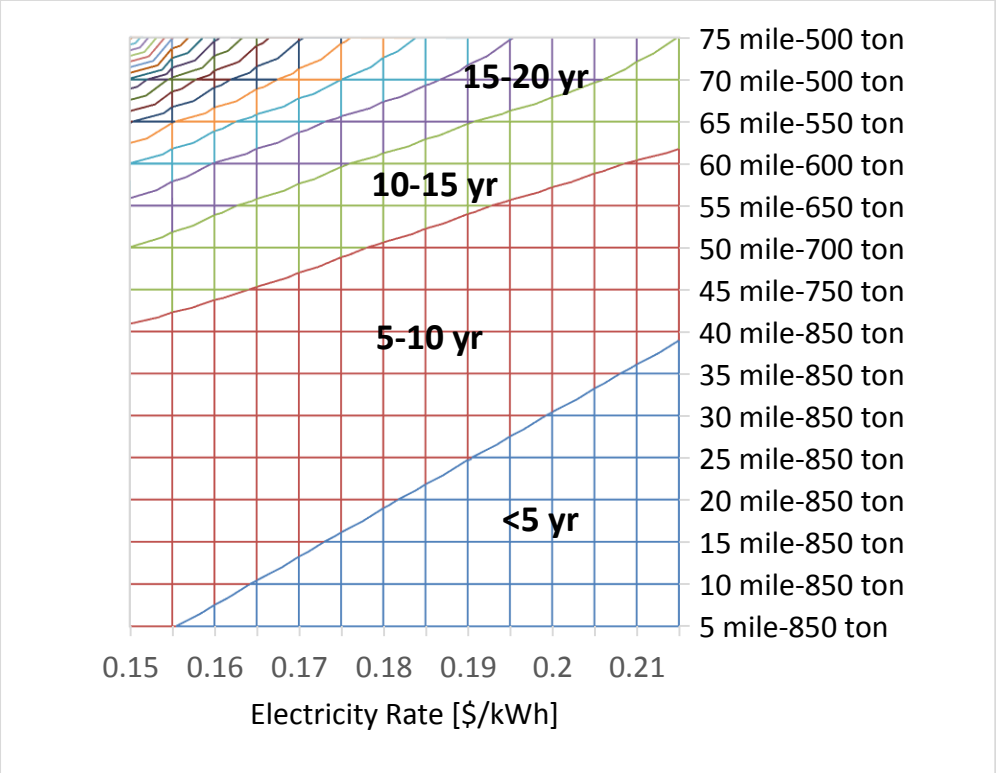

Fig. 25. Simple paybacks of the CTSGA system serving buildings at various distances from the geothermal resource and with various electricity rates.

7. ASSESSMENT OF TECHNICAL POTENTIAL

The technical potential of utilizing low temperature geothermal energy for providing space cooling in residential and commercial buildings in the United States is assessed. The technical potential is the maximum cooling demand that can be met with low temperature geothermal energy by using the technologies investigated in this study, as well as the resulting impacts in primary energy consumptions and carbon emissions.

Given that the economic viability of the alternative cooling systems are very sensitive to distance, as demonstrated with the case studies in Section 6, the technical potential is assessed on the county level, which is the finest resolution of publically available data on the thermal demands in the building sector (McCabe et al. 2016). It is assumed that there is no economic constraint for utilizing geothermal energy for space cooling in each county. The maximum deliverable cooling energy in a county (Max_CL_i) is estimated as the smaller value between the maximum cooling energy that can be produced with all the existing low temperature geothermal resources (hydrothermal and coproduced water) in the county, and the total cooling demand of all the existing residential and commercial buildings in the same county, as expressed with Eq. (25).

$$Max\_CL_i = Min\left(LTG_i * COP_{avg\_alt\_th} \middle| SECL_i * COP_{avg\_elec}\right) \quad (25)$$

where LTG_i is the annual beneficial heat of the available geothermal resources in the ith county; $COP_{avg\_alt\_th}$ is the average thermal COP of the alternative cooling systems; $SECL_i$ is the total annual site energy consumption by existing cooling systems in all residential and commercial buildings in the ith

county; and COP_{avg_elec} is the average electrical COP of conventional space cooling systems, of which 99% are electric-driven chillers/air conditioners/heat pumps.

Several databases are used in calculating Max_CL_i, including:

1. County-level data of discovered hydrothermal resources (Mullane et al. 2016). The beneficial heat of geothermal resources usable for alternative cooling (i.e., has a temperature higher than 90°C) is corrected by adjusting the reference temperature from 25°C to 80°C, which is the minimum temperature of geothermal fluid leaving from the alternative cooling systems.
2. County-level data of existing coproduced water (SMU 2016). The beneficial heat of coproduced water usable for alternative cooling (i.e., has a temperature higher than 90°C) is calculated based on the average oil production rate (150 GPM or 951 L/m per well) with a water–oil ratio of 10 and a reference temperature of 80°C.
3. County-level data of site energy consumption for space cooling in existing residential buildings (McCabe el al. 2016).
4. County-level data of site energy consumption for space cooling in existing commercial buildings (McCabe el al. 2016).

A parametric study is performed to predict the thermal COPs of the various alternative cooling systems at all climate zones of the continental United States and compared with typical water-cooled and air-cooled conventional cooling systems. Based on the results of this parametric study, it is estimated that COP_{avg_alt} of the CTSGA system is 0.7. Based on the minimum allowed efficiencies of conventional cooling equipment specified in ASHRAE Standard 90.1-2013, it is estimated that COP_{avg_elec} is 3.

The national primary energy savings (PES) and carbon emission reductions (CER) resulting from replacing conventional electric cooling with alternative geothermal cooling are calculated with Eqs. (26) and (27), respectively.

$$PES = \sum_i^n Max\_CL_i * [CF_{PE\,elec}/(COP_{avg\_alt\_el} - COP_{avg\_elec}) - R\_Fuel * CF_{PE\,fuel}] \quad (26)$$

$$CER = \sum_i^n Max\_CL_i * [* CF_{CE\,elec}/(COP_{avg\_alt\_el} - COP_{avg\_elec}) - R\_Fuel * CF_{CE\,fuel}] \quad (27)$$

where $CF_{PE\,elec}$ and $CF_{PE\,fuel}$ are the primary energy conversion factor for electricity and transportation fuel, respectively; $COP_{avg\_alt\_el}$ is the electrical COP of the alternative geothermal cooling, which is the ratio of cooling output to electricity consumption at pumps and cooling towers; R_Fuel is the ratio of transportation fuel consumption to the cooling energy provided by alternative geothermal cooling; and $CF_{CE\,elec}$ and $CF_{CE\,fuel}$ are the carbon emissions factors for electricity and transportation fuel, respectively.

R_Fuel is determined by the energy density of the transported energy storage media and the distance between the geothermal resource and the building. For a 20 mile (32 km) distance, R_Fuel is 0.01 gal/kWh for the CTSGA system. $COP_{avg\_alt\_el}$ is determined by the thermal COP of the alternative geothermal cooling and the efficiency of the cooling towers and pumps. It is around 11 for the CTSGA system. The primary energy conversion factors and the carbon emission factors are the national average given in Deru and Torcellini (2007).

Figure 26 is a color-coded national map showing the primary energy saving potential in each county.

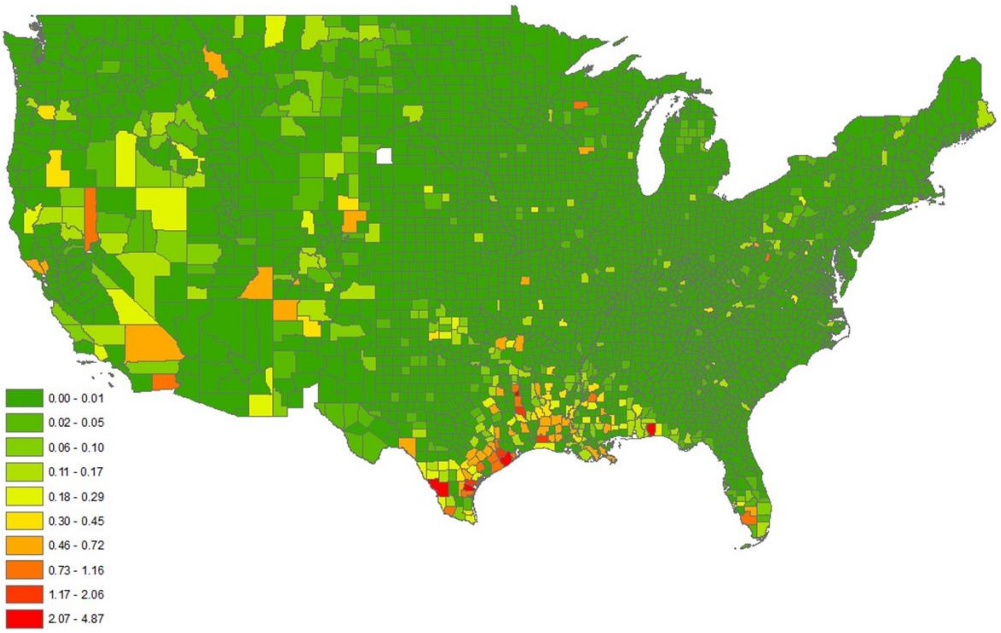

Fig. 26. Color-coded national map visualizing the primary energy saving potential (in trillion BTU) in each county by replacing the existing electric cooling with the alternative geothermal cooling.

The calculation results indicate that 0.17 Quad BTU or 0.18 EJ primary energy for space cooling can be avoided each year in the United States by replacing conventional electric cooling with the alternative geothermal cooling, which reduces by 3.5% the total primary energy consumption for space cooling in existing commercial and residential buildings in the United States.

8. CONCLUSIONS AND RECOMMDENDATIONS

8.1 CONCLUSIONS

This study identified several potential technologies, including absorption, adsorption, ice storage, and desiccant dehumidification, that can utilize the low-temperature geothermal energy to provide space cooling and/or dehumidification for buildings. By splitting the charging and discharging process, and utilizing tractor-trailers to transport the energy storage media between the two processes, these technologies can be further developed to store and transport low-temperature geothermal energy and provide space cooling and/or dehumidification at buildings distant from the geothermal resources. This alternative geothermal cooling has potential to extend the utilization of the low temperature geothermal energy and displace electricity consumptions for space cooling and/or dehumidification.

Among the technologies investigated in this study, the crystal-enhanced two-step geothermal absorption (CTSGA) system, which utilizes LiBr-2H_2O crystals as energy storage media, can store and transport the low temperature geothermal energy with the highest energy density (643 kJ/kg or 276 BTU/lb) for cooling application. It is 4 times higher than conventional direct use for heating application and 28 times higher than direct use for cooling application. The energy density of CTSGA is also 1.6 times higher than the original two-step geothermal absorption (TSGA) system investigated by the authors previously (Liu et al. 2015). The liquid desiccant dehumidification (LDD) system utilizing LiCl-H_2O crystals as energy storage media has a similar energy density (857 kJ/kg or 368 BTU/lb) as CTSGA, but its application is limited to dehumidification only. Ice storage has a similar energy density as the TSGA system, but it requires a higher heat source temperature (near 150°C/300°F) to operate. All these technologies either

cannot produce sufficiently hot water at the building site for space heating, or have similar energy density as the conventional direct-use heating applications.

The conceptual system designs for applying each of the identified technologies are developed and computer models are programmed to predict their cost and performance. In addition to the energy density, these computer models also take into account many other factors, including distance between the geothermal resource and the building, electricity rate, building cooling load profile (i.e., peak and annual cooling load), efficiency of electric chillers replaced with the geothermal cooling, and the climate at both the geothermal site and the building site.

A software tool has been developed to analyze the economic viability of applying various geothermal cooling systems (including dehumidification) and the direct use heating system to meet a given building thermal demand with the available geothermal resources. This tool consists of a calculation engine for modeling various technologies, including the geothermal cooling, heating, or dehumidification systems, as well as the conventional electric chillers or natural-gas-fired boilers, and a user-friendly interface for accepting user inputs and displaying calculation results.

The economic viability of applying different geothermal cooling systems has been analyzed using the above developed software tool in two case studies: (1) using a hydrothermal resource near Santa Rosa, California, which has a 1,175 gpm (74 kg/s) flow rate and a bottom hole temperature of 138°C/280°F, to provide seasonal space cooling to office buildings in Santa Rosa; and (2) using coproduced water from an oil-field near Houston, Texas, which has a 2,020 gpm (127 kg/s) flow rate and a bottom hole temperature of above 100°C/212°F, to provide year-round base-load space cooling to a district cooling system. The economic viability is investigated under a range of conditions including various distances, electricity rates, and cooling load profiles. The results show that generally the payback of the geothermal cooling systems is shorter with closer distance, higher electricity rate, lower peak cooling load, or greater annual cooling demand. The shortest payback in both case studies is achieved by the CTSGA system, which yields a payback of less than 10 years for an 18-mile (29 km) distance at Houston, and a 50-mile (80 km) distance at Santa Rosa.

Based on available data of existing geothermal resources and cooling demands in the building sector, it is estimated that 0.17 Quad BTU (0.18 EJ) primary energy for space cooling can be avoided each year in the United States by replacing conventional electric cooling with the geothermal cooling, which is a 3.5% reduction in the total primary energy consumption for space cooling in existing commercial and residential buildings in the United States.

8.2 RECOMMENDATION FOR FUTURE RESEARCH AND DEVELOPMENT

Although the CTSGA system can store and transport the low temperature geothermal energy with the highest energy density among all the investigated technologies, there are some significant technical challenges for applying this technology, including (1) dissolving crystals in time to increase the concentration of the weak solution at the building site; and (2) preventing crystals from entering and/or forming in the absorber. It is recommended an experimental study be conducted to characterize the process of crystal formation and dissolution. Furthermore, it is recommended that a prototype of the CTSGA system be developed to verify its performance through laboratory and field tests.

9. REFERENCES

Abhat, A. 1983. Low temperature latent heat thermal energy storage: heat storage materials, *Solar Energy* **30**(4): 313–332.

ANSI/ARI. 2000. Standard 560, *Absorption Water Chilling and Water Heating Packages.*

ASHRAE. 2013. Standard 90.1-2013, *Energy Standard for Buildings Except Low-Rise Residential Buildings*

Clark, C. E., J. A. Veil. 2009. *Produced Water Volumes and Management Practices in the United States,* ANL/EVS/R-09-1, Argonne National Laboratory.

Conde, Manuel R. 2004. "Properties of aqueous solutions of lithium and calcium chlorides: formulations for use in air conditioning equipment design," *International Journal of Thermal Sciences* **43**(4): 367–382.

Demirbas, M. Fatih. 2006. "Thermal energy storage and phase change materials: an overview," *Energy Sources, Part B: Economics, Planning, and Policy* **1**(1): 85–95.

Deru, M. P., P. A. Torcellini. 007. *Source Energy and Emission Factors for Energy Use in Buildings,* National Renewable Energy Laboratory, Golden, CO.

Dieckmann, J., K. Roth, J. Brodrick. 2008. "Liquid desiccant air conditioners," *Ashrae Journal* **50**(10): 90–94.

DOE. 2015. "Direct Use of Geothermal Energy." Available at http://energy.gov/eere/geothermal/direct-use-geothermal-energy.

Deru, M., Field, K., Studer, D., Benne, K., Griffith, B., Torcellini, P., & Yazdanian, M. (2011). US Department of Energy commercial reference building models of the national building stock.

Drees, K. H., J. E. Braun. 1995. Modeling of area-constrained ice storage tanks, *HVAC&R Research* **1**(2): 143–158.

Fender, Katherine J., and Pierce, David A. 2013. An analysis of the operational costs of trucking: a 2013 update. American Transportation Research Institute.

OIT Geo-Heat Center. Geothermal Direct-Use Case Studies. *Website: http://geoheat.oit.edu/casestudies.htm. Accessed: June* 23 (2005):

Mitsubishi. 2016. Physical property data of AQSOA Z02 (not in public domain)

Grossman, G., & Zaltash, A. (2001). ABSIM—modular simulation of advanced absorption systems. International Journal of Refrigeration, 24(6), 531-543.

Herold, K. E., R. Radermacher, S. A. Klein. 2016. *Absorption Chillers and Heat Pumps,* CRC Press.

Holdmann G. 2005. "Geothermal Powered Absorption Chiller." Presented at the 2005 Rural Energy Conference, Valdez, Alaska, September 20, 2005.

Jiang et al. 2015. "Absorption heat exchangers for long distance heat transportation," ICR 2015.

Kreuter H. 2012. "Geothermal Applications: Geothermal Cooling." Proceedings of the Renewable Energy Training Program, 10 July 2012, ESMAP – IFC, Washington, DC.

Lech, P. 2009. *A New Geothermal Cooling – Heating System for Buildings*. Master's Thesis. University of Iceland and the University of Akureyri.

Liu, X., Z. Yang, K. Gluesenkamp, A. Momen. 2015. *A Technical and Economic Analysis of an Innovative Two-Step Absorption System for Utilizing Low-Temperature Geothermal Resources to Condition Commercial Buildings,* ORNL/TM-2015/655, Oak Ridge National Laboratory.

Luo et al. 2010. "An Absorption Refrigeration System Used for Exploiting Mid-low Temperature Geothermal Resource." *Proceedings World Geothermal Congress 2010*, Bali, Indonesia, 25–29 April 2010.

McCabe, Kevin, M. Gleason, T. Reber, K. R. Young. 2016. "Characterizing U.S. Heat Demand for potential application of geothermal direct use," *GRC Transactions* **40**.

Mossman, Melville. 2010. *RSMeans Mechanical Cost Data 2011,* R.S. Means Company, Kingston, MA.

Mullane, Michelle, M. Gleason, K. McCabe, M. Mooney, T. Reber, K. R. Young. 2016. Database of Low-Temperature Hydrothermal Resource. https://gdr.openei.org/submissions/842 (*Accessed* on 11/11/2016)

National Research Council (US). 2010. Committee to Assess Fuel Economy Technologies for Medium- and Heavy-Duty Vehicles, *Technologies and Approaches to Reducing the Fuel Consumption of Medium-and Heavy-Duty Vehicles,* National Academies Press.

Rafferty, Kevin. 2001. "Well pumps and piping," *GHC Bulletin,* September.

SMU Geothermal Laboratory. 2016. Aggregated Well Data. http://geothermal.smu.edu/static/DownloadFilesButtonPage.htm (*Accessed* on 11/11/2016)

Wang et al. 2013. "Application of geothermal absorption air-conditioning system: a case study." Applied Thermal Engineering 50, 71–80.

Wang, R., L. Wang, J. Wu. 2014. *Adsorption Refrigeration Technology: Theory and Application,* John Wiley & Sons.

Wang, Yu, M. Douglas LeVan. 2009. "Adsorption equilibrium of carbon dioxide and water vapor on zeolites 5A and 13X and silica gel: pure components," *Journal of Chemical & Engineering Data* **54**(10): 2839–2844.

Welch, Robert A., Dwight F. Rychel. 2004. *Produced Water from Oil and Gas Operations in the Onshore Lower 48 States,* Northrop Grumman Mission Systems, Information & Technical Services Division, Tulsa, Oklahoma.

Yang, Z., X. Tang, M. Qu, O. Abdelaziz, K. R. Gluesenkamp. 2014. *Development of Updated ABsorption SIMulation Software (ABSIM)*. Oak Ridge National Laboratory (ORNL); Building Technologies Research and Integration Center (BTRIC).

Yu, N., Wang, R. Z., & Wang, L. W. (2013). Sorption thermal storage for solar energy. Progress in Energy and Combustion Science, 39(5), 489-514.

Yu, N., Wang, R. Z., Lu, Z. S., Wang, L. W., & Ishugah, T. F. (2014). Evaluation of a three-phase sorption cycle for thermal energy storage. Energy, 67, 468-478.

APPENDIX A. LOADING FACTORS OF VARIOUS SOLID DESICCANTS

The assumed operating conditions of the solid desiccants used in the ADS systems for space cooling in summer, space heating in winter, and simultaneous heating and cooling (H&C) in shoulder seasons are listed in Table A.1.

Table A.1. Operation conditions for different seasons and applications

	Summer cooling	Winter heating	Shoulder-season H&C
Desiccant adsorbing temperature, °C	36.4	55	55
Evaporation temperature, °C	5.2	0	5.2
Condensation temperature, °C	36.4	20	25

Tables A.2 and A.3 list the water loadings of different solid desiccant materials under various conditions. The loadings are calculated based on the source temperature and operating temperatures listed in Table A.1. The highlighted loading differences are the highest loading difference (thus highest system energy density) among all four materials in the same scenario.

Table A.2. loading of solid desiccants at 100°C source temperature

Material	Silica Gel	Zeolite 13X	Zeolite 5A	AQSOA Z02
Cooling loading	0.1119	0.2254	0.2166	0.2928
Summer regeneration loading	0.03596	0.1919	0.1742	0.04484
Cooling loading difference	0.07594	0.0335	0.0424	0.24796
Heating loading	0.03884	0.1891	0.1711	0.0543
Winter regeneration loading	0.02124	0.1684	0.1471	0.01876
Heating loading difference	0.0176	0.0207	0.024	0.03554
Heating and cooling loading	0.05146	0.1997	0.1839	0.0842
Shoulder season regeneration loading	0.0355	0.1914	0.1736	0.04484
Heating and cooling loading difference	0.01596	0.00083	0.0103	0.03936

Table A.3. Loadings of solid desiccants at 150°C source temperature

Material	Silica Gel	Zeolite 13X	Zeolite 5A	AQSOA Z02
Cooling loading	0.1119	0.2254	0.2166	0.2928
Summer regeneration loading	0.0059	0.1293	0.101	0.005116
Cooling loading difference	0.106	0.0961	0.1156	0.287684
Heating loading	0.03884	0.1891	0.1711	0.0543
Winter regeneration loading	0.0035	0.1003	0.0769	0.002094
Heating loading difference	0.03534	0.0888	0.0942	0.0522
Heating and cooling loading	0.05146	0.1997	0.1839	0.0842
Shoulder season regeneration loading	0.005826	0.1285	0.1004	0.005
Heating and cooling loading difference	0.045634	0.0712	0.0835	0.0792

APPENDIX B. ASSUMPTIONS USED IN THE MODELS

The nominal operating conditions

Absorption cooling technology is used in TSGA, CTSGA, and Ice systems, and adsorption cooling technology is used in ADS systems. According to AHRI standard 560-2000, the rating condition for absorption chillers is 100°C hot water and 29.4°C cooling water. This rating condition is assumed as the nominal operating condition for the TSGA system. Higher hot water temperatures are used in this study as the nominal operating conditions for the CTSGA and Ice systems. There is not standard rating condition for adsorption chillers yet, it is assumed that the nominal operating condition of an ADS system is 150°C hot water and 29.4°C cooling water. All these systems produce 7.2°C chilled water. The nominal (rating) operating conditions of TSGA, CTSGA, Ice and ADS systems are listed in Table B.1.

Table B.1. Nominal operating conditions of absorption/adsorption systems

System	Heat source temperature (°C)	Cooling water temperature (°C)	Chilled water temperature (°C)
TSGA (single-effect LiBr/H_2O absorption)	100	29.4	7.2
CTSGA (single-effect LiBr/H_2O absorption)	110	29.4	7.2
Ice (single-effect ammonia/water absorption)	150	29.4	7.2
ADS (single-effect AQSOA Z02 adsorption)	150	29.4	7.2

Approach temperatures in heat exchangers and cooling towers

- The difference between cooling water supply temperature and the wet-bulb temperature of the ambient air is 5.6°C
- The difference between the hot water supply temperature and the geothermal resource temperature is 5°C

Evaporating and condensing temperature of ADS system

While the evaporating and condensing temperatures of TSGA, CTSGA, and Ice systems are determined with computer simulations of a single-effect absorption cooling system, these temperatures of an ADS system are approximated in this study based on following assumptions:

- a temperature difference of 2°C between the 45°F (7.2°C) chilled water and the evaporating refrigerant (i.e., the evaporating temperature is 5.2°C).
- a temperature difference of 1.4°C between the cooling water and the water vapor condensation (in the desorber) or the solid desiccant (in the absorber).

APPENDIX C. SORPSIM SIMULATION OF TSGA AND CTSGA

TSGA system is modeled with ORNL's SorpSim program. SorpSim, a modular computer program for simulation of absorption systems, is developed based on the original ABSIM program (Grossman 2001) by Yang et al. (2014). From the thermodynamic point of view, the two-step absorption cooling is basically a single-effect absorption cycle operated with heat from the low temperature geothermal resources. The system diagram of the computer model is shown in Fig. C.1.

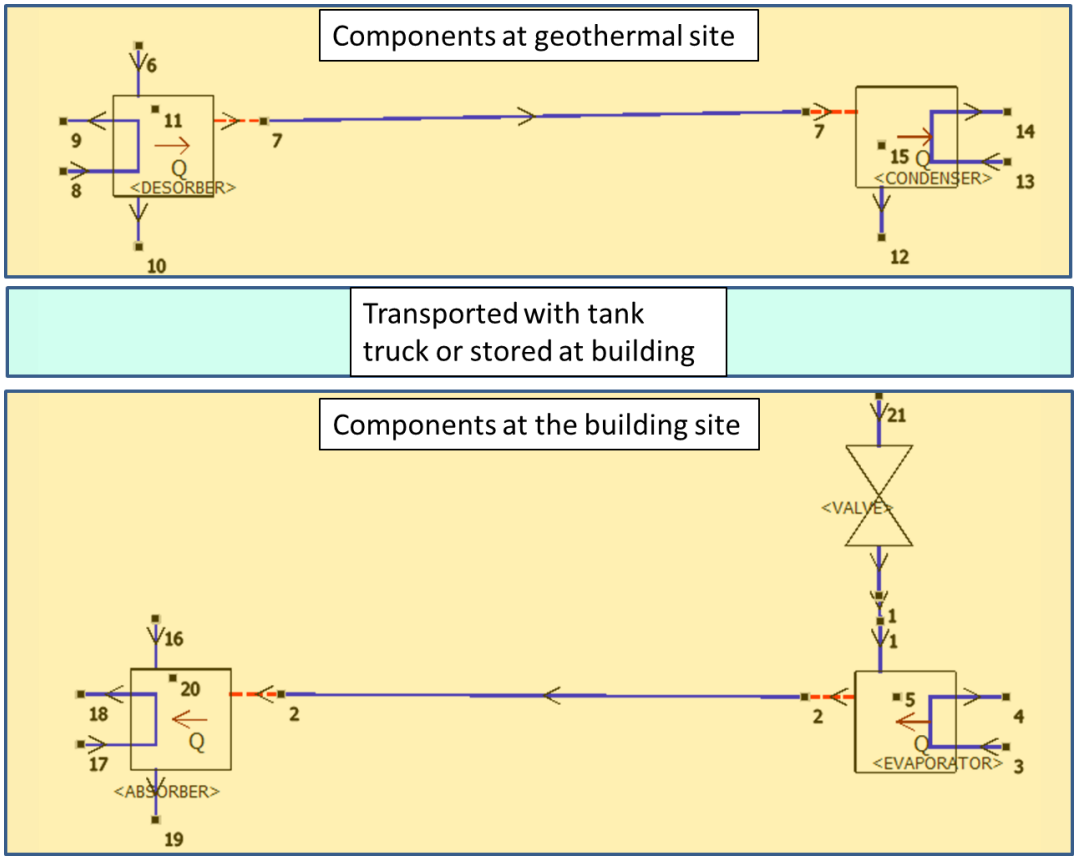

Fig. C.1. A SorpSim diagram showing the simulation of the two-step absorption cooling.

The modeled TSGA system uses LiBr/H_2O solution as the working fluid and it has a cooling capacity of 3,861 kW at the standard rating condition (Table B.1). Key design parameters listed in Table C.1 are determined with SorpSim simulations. Based on these parameters, the thermal COP of the TSGA system is 0.7 at rating condition.

Table C.1. Design parameters for the baseline TSGA system

Type	UA value (kW/°C)	NTU (-)	Effectiveness (-)	Closest approach (°C)	LMTD (°C)	Heat load (kW)
Evaporator	600	1.2	0.712	3.239	6.433	3861
Desorber	350	1.6	0.736	9.033	15.92	5571
Condenser	1000	1.5	0.776	1.761	4.072	4073
Absorber	700	3	0.915	1.706	6.228	4359

For the TSGA system, since there is no crystallization, the concentration of the solution leaving the desorber at state point #10 is the same as the solution inlet in the absorber at state point #16; similarly, the weak solution leaving the absorber at state point #19 has the same concentration as the desorber inlet at state point #6. The mass flow rate of state points on the same stream of solution (#10-#16, #19-#6) and water (#12-#21) are the same, assuming the regeneration rate is the same as the consumption rate.

For the CTSGA system, the solution and water flow rates at the geothermal site and the building site are different. The water condensation rate at the geothermal site (flow rate of #12) is higher than the water evaporation rate at the building side (flow rate of #21). The strong solution produced in the desorber at the geothermal site has a higher concentration than the crystallization concentration at the ambient temperature (around 63% at 30°C). However, the strong solution leaving from the tank at the building site is kept at the crystallization concentration as long as there still is any crystal left in the tank. Since the strong solution has a higher concentration than that of the TSGA system, its flow rate in the absorber is reduced to keep the evaporator's cooling output is about the same as that in the TSGA system under the same operating condition.

The capacity of the CTSGA system is only affected by the wet-bulb temperature of the ambient air because crystallization in the tank makes the strong solution concentration independent from the heat source temperature. The thermal COP of the simulated CTSGA system (COP_{Th_CTSGA}) at the rating condition is 0.72, which accounts for the difference between the heat input rate at the geothermal site ($power_{heat\ input}$) and the cooling output rate at the building site ($power_{cooling}$) with following equation:

$$COP_{Th\_CTSGA} = \frac{power_{cooling}}{power_{heat\ input}} * \frac{flowrate_{condensed}}{flowrate_{evaporated}}$$

where $flowrate_{condensed}$ and $flowrate_{evaporated}$ are the flow rate of the water being condensed at the geothermal site and the water being evaporated at the building site, respectively.

APPENDIX D. MODELING ALGORITHM FOR LDD

The LDD system utilizes crystal of the liquid desiccant solution (i.e., LiCl-H_2O crystal) to store and transport geothermal energy to the building and provide dehumidification. As shown in Fig. D.1, at the geothermal site, the weak solution leaving the transported container is first heated by the hot geothermal fluid, and then distributed onto the open surface of the regenerator. Ambient air is blown across the solution, and the water content in the solution evaporates into the ambient air to concentrate the solution. Once the solution releases enough water and becomes strong in the regenerator, it flows back to the container to be cooled to generate crystal salt hydrate. The remaining solution is recirculated to the heater and regenerator for further concentration. At the building site, strong solution is first cooled using water from the cooling tower, and then distributed onto the open surface of the dehumidifier. Since the cool, strong solution maintains very low water vapor pressure above its surface, vapor in the process air condensates into the solution while the air is blown across the solution. After absorbing the water vapor in the process air, the solution becomes warm and diluted. It is then circulated back to the container to dissolve crystal and become strong again. Unlike the conventional absorption cooling systems, where desiccant solution absorbs water vapor in a near-vacuum chamber to enable water evaporation and chilled water production, the LDD system exposes the desiccant solution to the process air at ambient pressure to remove water vapor from the process air and thus reduce the latent cooling load of an air conditioning system.

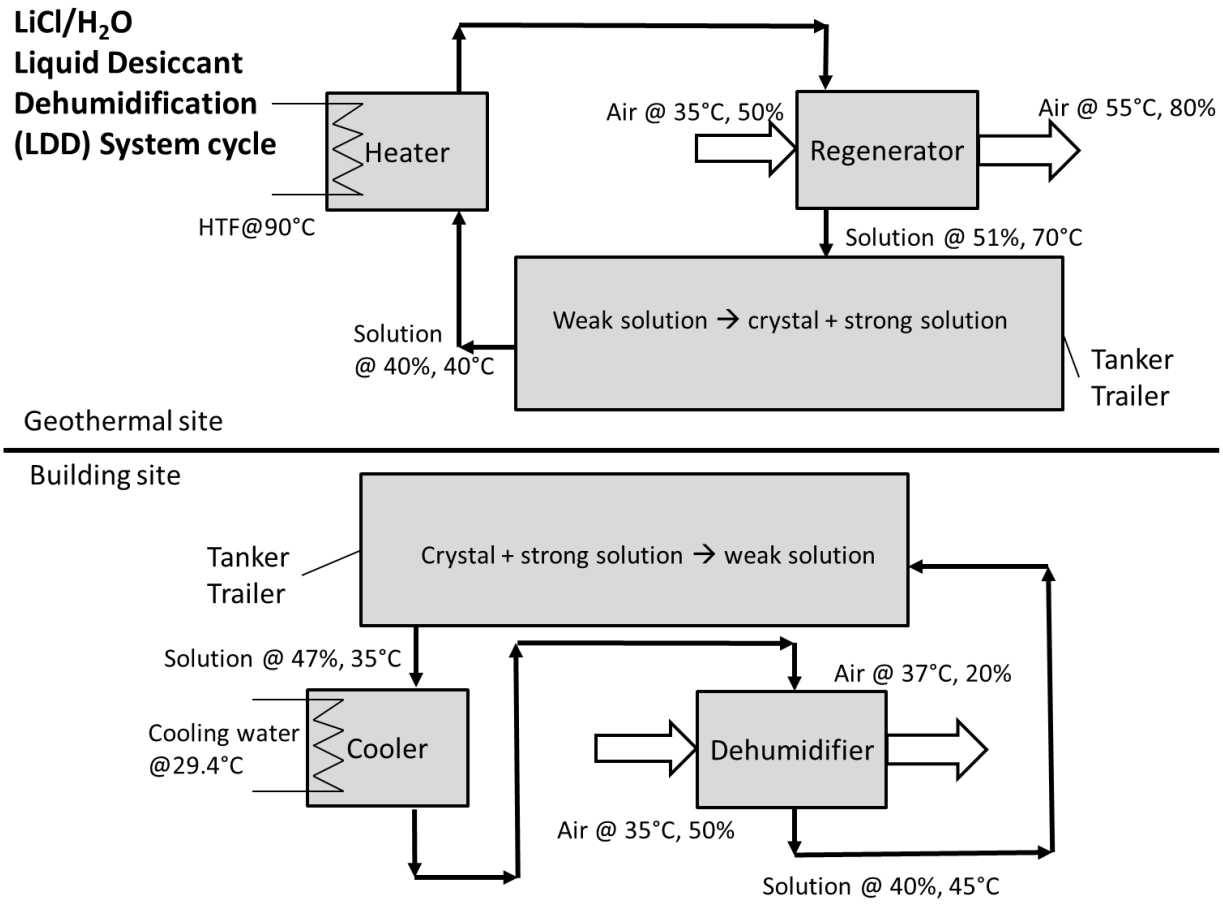

Fig. D.1. Liquid desiccant dehumidification (LDD) system cycle.

Unlike other technologies that handle the entire cooling load of the building and thus can directly replace the entire conventional electric chiller system, the LDD system can only deal with the latent cooling load that is otherwise met with the electric chiller by mechanically cooling the processed air to below the dew point to condensate the excess moisture. Therefore, instead of replacing the electric chiller, the LDD system operates in conjunction with the electric chiller. Meanwhile, the humidity of the outdoor air varies significantly by months, and sometimes the LDD system is not able to handle the entire latent cooling load. Since the LDD system uses LiCl-H_2O crystal (70% salt mass fraction) to store energy and dissolve into solution for dehumidification, it can only use tractor-trailer transportation. Changes in air humidity affect the energy density that the LDD system can achieve, making the transportation operating cost vary significantly as well. Therefore, performance calculation of the LDD system and the associated tractor-trailer transportation system is carried out on a monthly basis. The baseline energy consumption to which the LDD system is compared with is the power consumption of the electric chiller that is proportional to the latent cooling load. The electricity savings resulting from the LDD system is also calculated on a monthly basis.

The calculation of LDD system performance begins with evaluating the dehumidified air humidity by:

$$\varepsilon_{deh} = \frac{w_{ai}(T_{db}, T_{wb}) - w_{ao}}{w_{ai}(T_{db}, T_{wb}) - w_{si_{deh}}(T_{wb}, c_{ws})}$$

In the above equation, ε_{deh} is the humidity effectiveness of the dehumidifier, which is a device-specific constant. The *w* refers to the humidity ratio of the air, and subscript *ai* means the air inlet, namely the outdoor air to be dehumidified; subscript *ao* means the air outlet, namely the processed air; and si_{deh} means the solution inlet, which determines the driest state of the process air that can be dehumidified in the dehumidifier. $w_{si_{deh}}$ is calculated based on the solution temperature (assuming being cooled to wet-bulb temperature) and concentration of the solution (determined by the crystallization concentration at the ambient temperature) using correlations of LiCl-H_2O solution physical properties given by Conde (2004).

The supply air from air-conditioning systems is usually at 12.8°C and 95% relative humidity, and the corresponding humidity ratio is 0.006 kg vapor/kg dry air. The LDD system is designed to dehumidify the outdoor air to close to 0.06, but not below. If the original calculation result of w_{ao} is below 0.06 (in which case the LDD system would over-dehumidify the air with the strongest solution possible), the equation would be used reversely, setting $w_{ao} = 0.06$ and calculating the minimum solution concentration c_{ws} that is able to process the entire latent load. If the original calculation result of w_{ao} is above 0.06, it means the LDD system is not able to process the entire latent load with even the strongest solution.

Either way, the final w_{ao} is used to calculate the moisture removal rate (MRR) given the outdoor air mass flow rate (FR_{oa}) required to satisfy the ventilation requirement of the building:

$$MRR = FR_{oa} * (w_{ai} - w_{ao})$$

The final solution concentration x is used to estimate the crystallization in the regeneration process at the geothermal site:

$$\varepsilon_{reg} = \frac{w_{si_{reg}}(T_{src}, c_{ws}) - w_{so_{reg}}(T_{src}, c_{ss})}{w_{si_{reg}}(T_{src}, c_{ws}) - w_{ai}(T_{db}, T_{wb})}$$

In the above equation, ε_{reg} is the humidity effectiveness of the regenerator, which is a device-specific constant. It refers to the ratio of the actually evaporated moisture against the ideally maximum evaporated moisture. The $w_{si_{reg}}$ is calculated using the weak solution concentration and the heat source temperature. After moisture evaporation, the solution concentration becomes higher and the solution outlet surface air humidity ratio is lower. Once the strong solution concentration exceeds the crystallization concentration at the wet-bulb temperature, the strong solution can be crystallized in the tanker. With this function, for a given ε_{reg}, air temperatures, crystallization concentration, and weak solution temperature, the minimum source temperature for crystallization (T_{src}) can be calculated. Comparing this T_{src} with the given geothermal source temperature, we can determine whether the LDD system can operate under the given conditions of the month.

Once the crystallization is confirmed, the peak load and total load of the LDD system can be calculated with following equation:

$$totalLoad = MRR * h_{fg} * OptHour$$

$$peakLoad = MRR * h_{fg}$$

In the above equation, $OptHour$ is the monthly operation hours of the building.

Two solution pumps circulate the solution at the dehumidifier and the regenerator, and their flow rates are set at twice the mass flow rate of the outdoor air. At the building site, the strong solution entering the dehumidifier is pre-cooled by the cooling tower of the electric chiller system, thus the heat rejection of the LDD system requires no additional equipment or operating cost. At the geothermal site, the concentrated solution can be cooled to crystallize by heat loss to the ambient by controlling the regeneration circulation flow rate, and no additional heat rejection equipment is needed either.

The peak load and solution circulation flow rate are used to calculate the initial cost of the LDD system equipment:

$$IC_{LDD_{equip}} = IC_{LDD_{equip}}(peakload) + 2 * IC_{pump}(FR)$$

According to Dieckmann et al. (2008), the normalized cost of the liquid desiccant dehumidification device is about $385/ton.

The LDD system operating cost includes only the pumping electricity cost, which is calculated as

$$OPC_{LDD_{electricity}} = 2 * ElePrice * \frac{FR * \Delta P * density}{\eta}$$

The density of $LiCl/H_2O$ solution is around 1300kg/m^3, the pressure drop of the circulation pump is assumed at 10 psi, and the pump efficiency is 0.7.

Like the CTSGA system that also uses crystal as the energy storage media, the energy density of the LDD system is calculated given the high/low solution concentration, as well as the crystal ratio in the tanker, as expressed with Eq. (9).

APPENDIX E. USER MANUAL OF THE ENERGY ANALYSIS TOOL

Navigating the Interface

Navigation through the interface is performed by clicking on the buttons at the bottom of each page or by clicking on the hyperlinks in the progress bar. Each page has a "Save and Continue" button that will store the form field values supplied by the user and continue to the next page if all required fields have been completed. If a required field is incomplete, the interface will display an alert message and will not allow the user to continue to the next page until the field has been completed. If present, the "Previous" button will allow the user to return to the previous page while retaining all saved values, and the "Start Over" button will return to the beginning page while clearing all saved values. As pages are completed, their titles in the progress bar will become hyperlinked, allowing the user to return directly to a completed page if desired.

If a user returns to a previously completed page and alters a form field value, the change will not be saved unless the "Save and Continue" button is pressed. If the user presses the "Save and Continue" button on a previously completed page, the following pages will no longer be accessible to the user without proceeding through them in order and saving the values again in order to prevent potential conflicts from occurring.

Other Interface Features

Each page has a "Use Default Values" button, which will automatically fill in the fields on the page with general values. In some cases, a button or checkbox must be pressed before all default values can be filled in. After the button is pressed, the user may still alter the values of any field if desired before or after clicking the "Save and Continue" button.

The  icon next to a form field can be clicked to open a glossary page linked to that particular field's entry.

Some fields allow units to be selected (e.g., miles vs. kilometers). In these cases, the user should be careful to select the desired unit along with the value filled into the field, as mismatched units will cause the user-supplied values to be converted by the interface. In other words, if the user types "5 miles" but selects kilometers as the unit by mistake, the interface will read the field as 5 kilometers or 3.11 miles.

The "Results" page has two buttons that appear only on that page: "Printable Version" and "Select data." The "Printable Version" button will open a printing dialog box for the currently displayed tab (i.e., "Calculation Results," "Charts," or "Input Values") with simple style formatting. The "Select data" button will automatically select the cells in a displayed data table for copying to the clipboard.

Operation Procedure

The interface starts with a welcome page as in Fig. E.1.

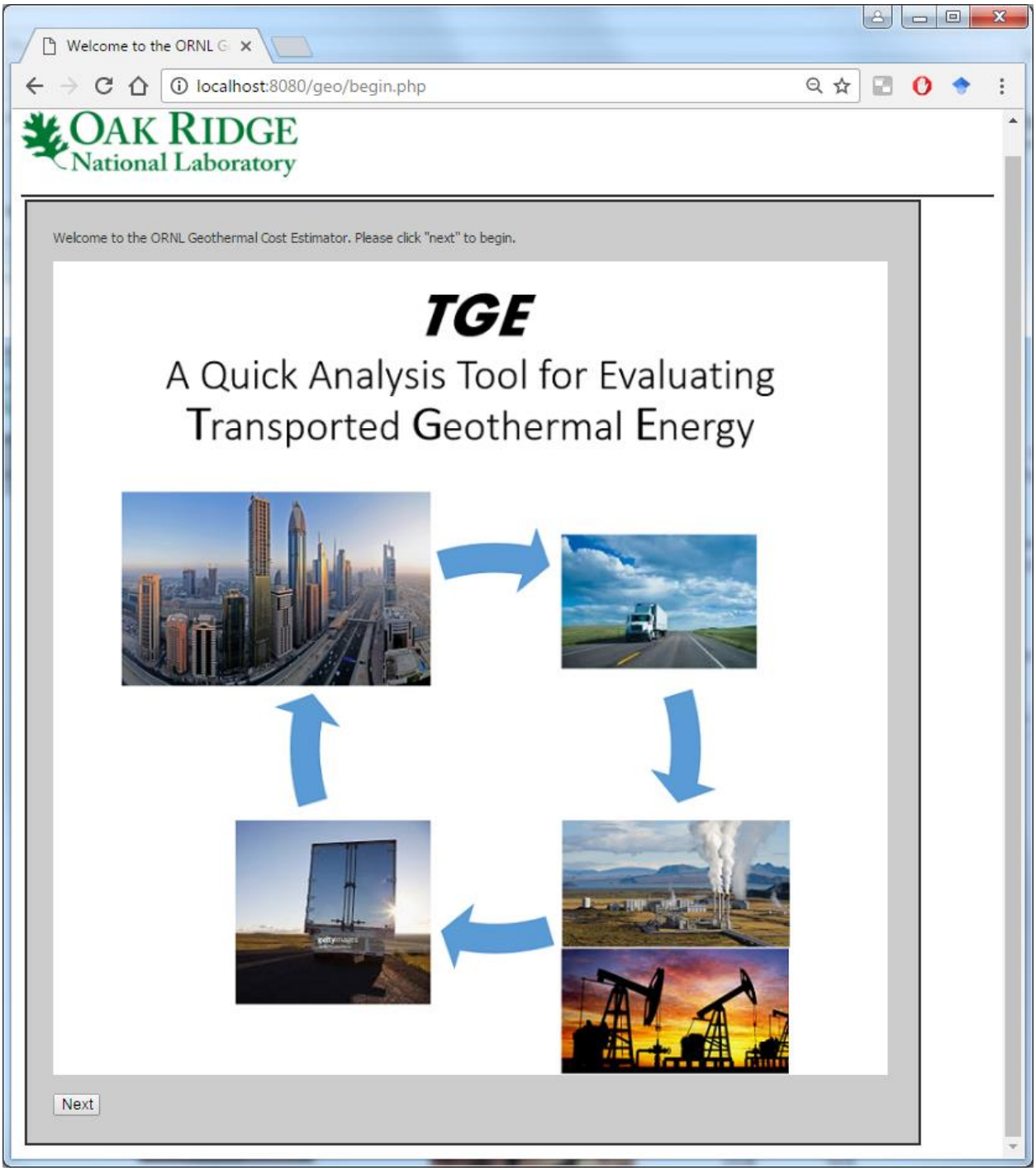

Fig. E.1. Welcome page of the interface.

The first input page (Fig. E.2) is for geothermal site information, where the user is asked to provide the temperature and flow rate of the geothermal fluid, as well as the initial and operating cost for using the geothermal fluid.

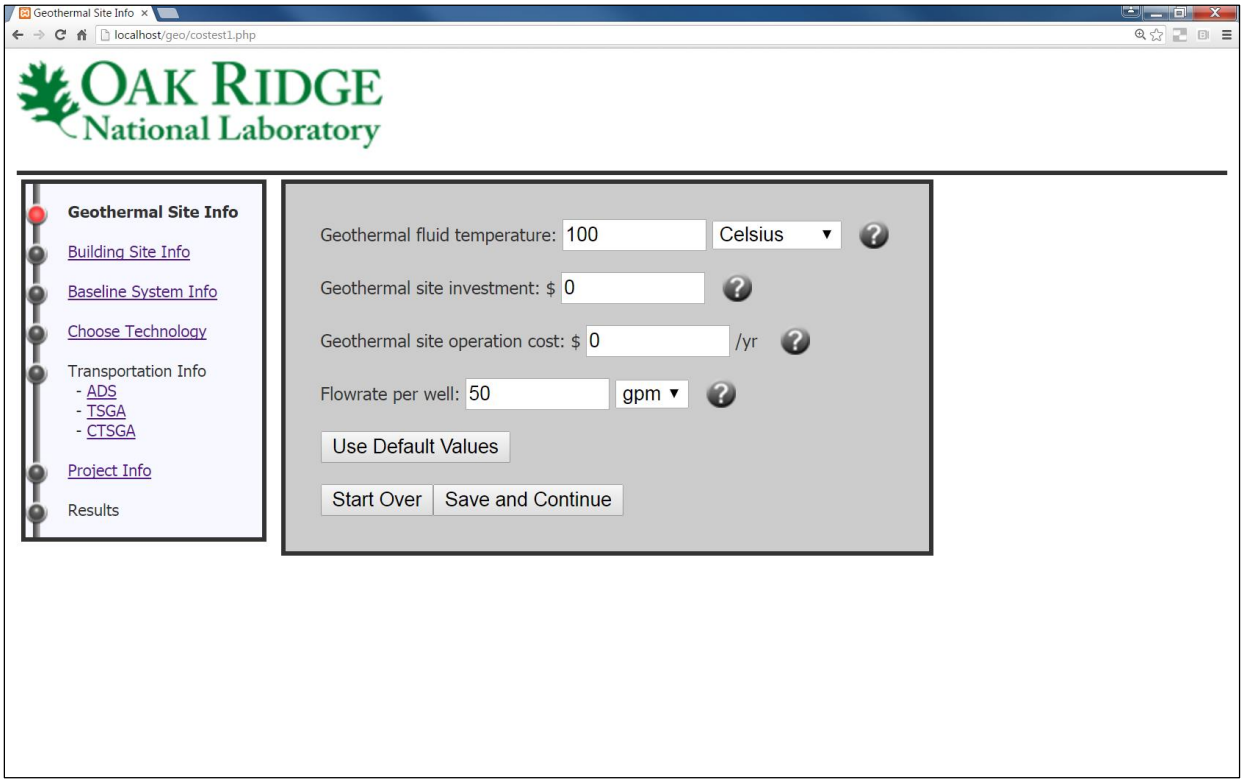

Fig. E.2. Geothermal site information page.

The second input page (Fig. E.3) is for building site information. The building location specified in this page is linked to weather data files to automatically pull out the dry- and wet-bulb temperature data of the selected location. Either heating or cooling applications can be selected, and the peak load and annual total load are required for the selected application. Finally, the local price of natural gas or electricity is either input by the user or it can be obtained from a built-in database[22] by clicking "Get Electricity Price for State" or "Get Natural Gas Price for State".

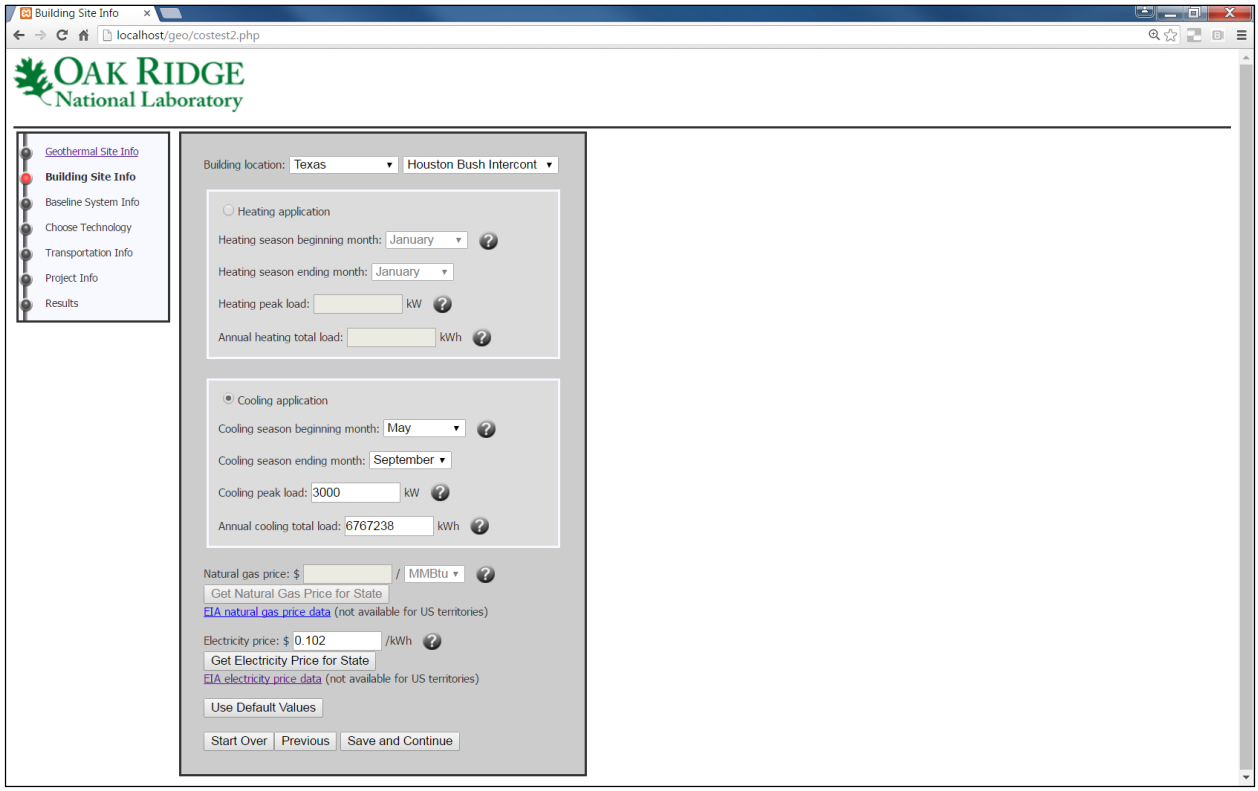

Fig. E.3. Building site information page.

[22] https://www.eia.gov/electricity/monthly/epm_table_grapher.cfm?t=epmt_5_6_a

The third input page (Fig. E.4) is for baseline system information. If heating application is selected on the building site information page, the user needs to provide boiler efficiency. In the case that cooling application is selected, as shown in Fig. E.4, the COP at design condition and the seasonal average COP of the baseline chiller, against which the transportable geothermal energy is compared, as well as the power consumption of pumping system and heat rejection (i.e., cooling tower) needs to be provided. On top of this page is the average dry-bulb and wet-bulb temperature in the cooling (or heating) season at the location specified in the previous page.

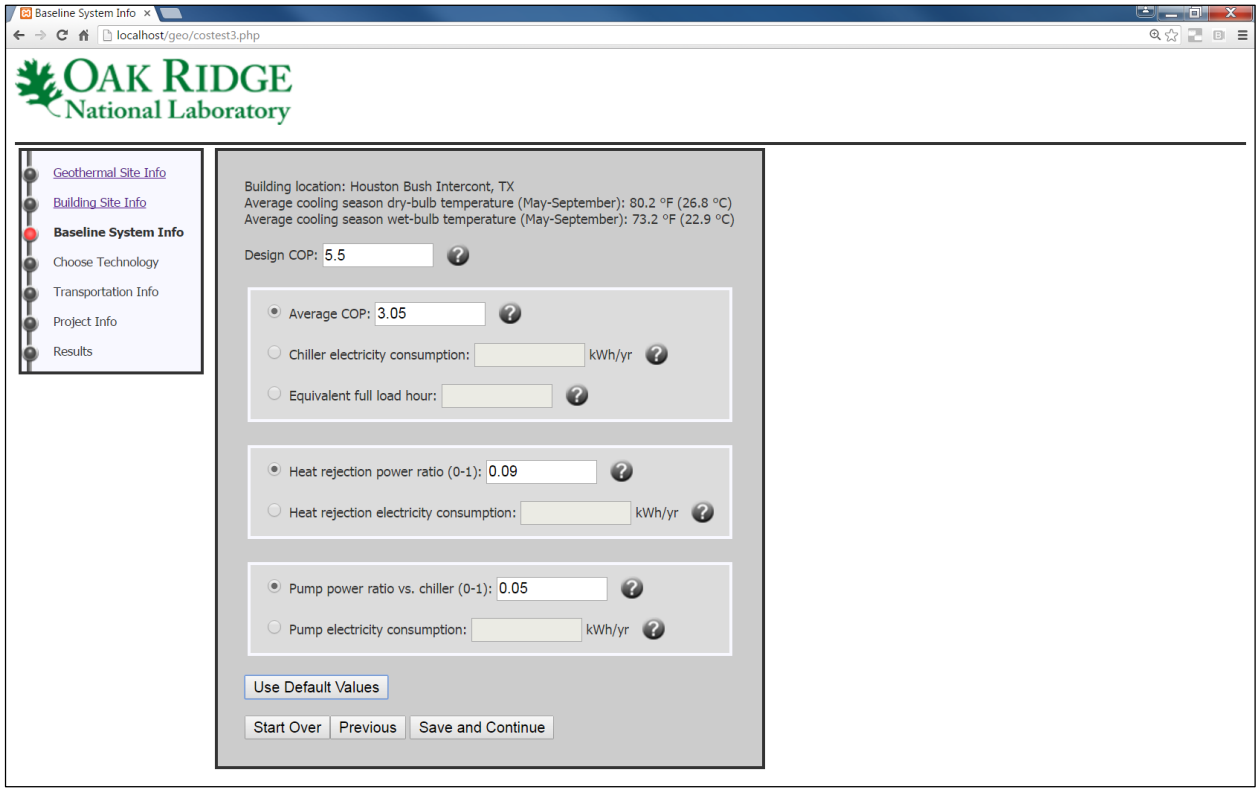

Fig. E.4. Baseline system information page.

The fourth input page is for transported geothermal technology (Fig. E.5). Based on the user-specified geothermal source temperature, operating conditions (e.g., weather conditions), and expected end-use application (e.g., heating or cooling), the interface will show the available technologies that can meet those user-defined constraints. A brief description including a diagram of each technology is provided, and the user can use the checkbox to select the technologies to compare. Figure E.6 shows an example of the description.

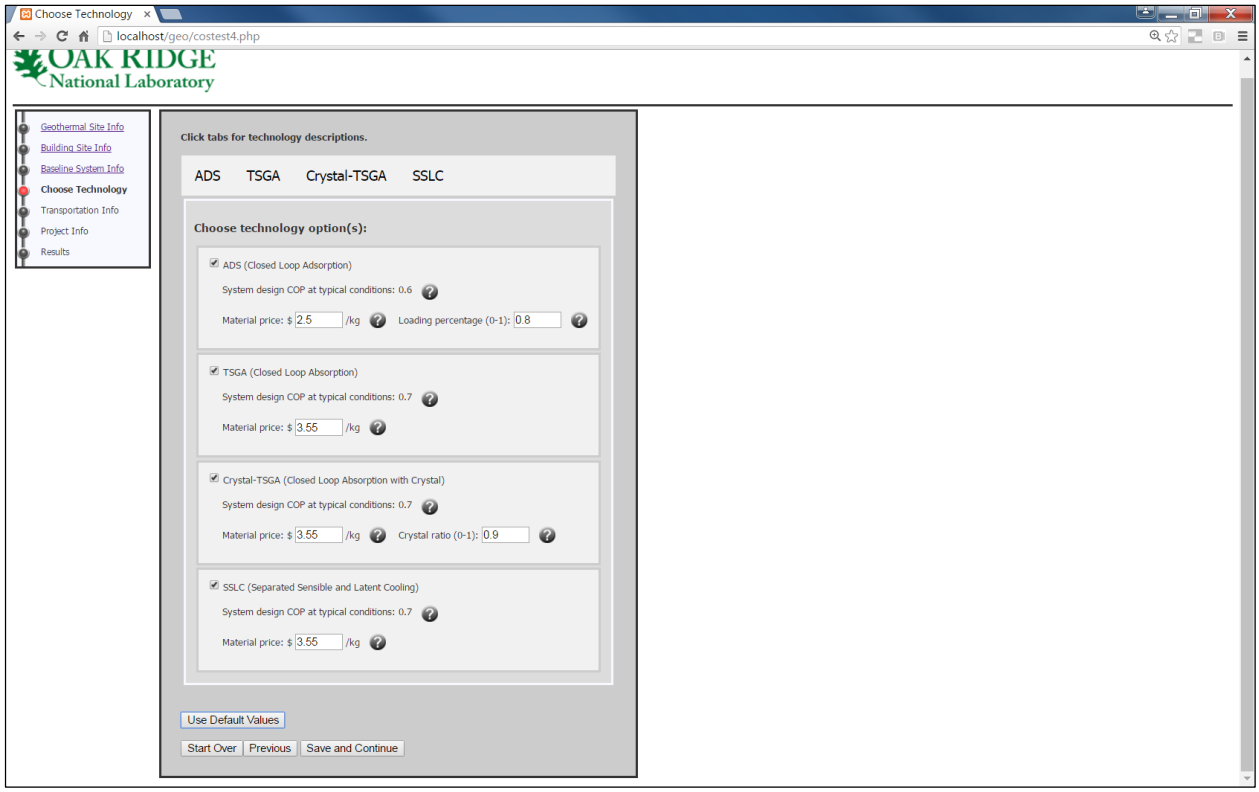

Fig. E.5. Technology selection page.

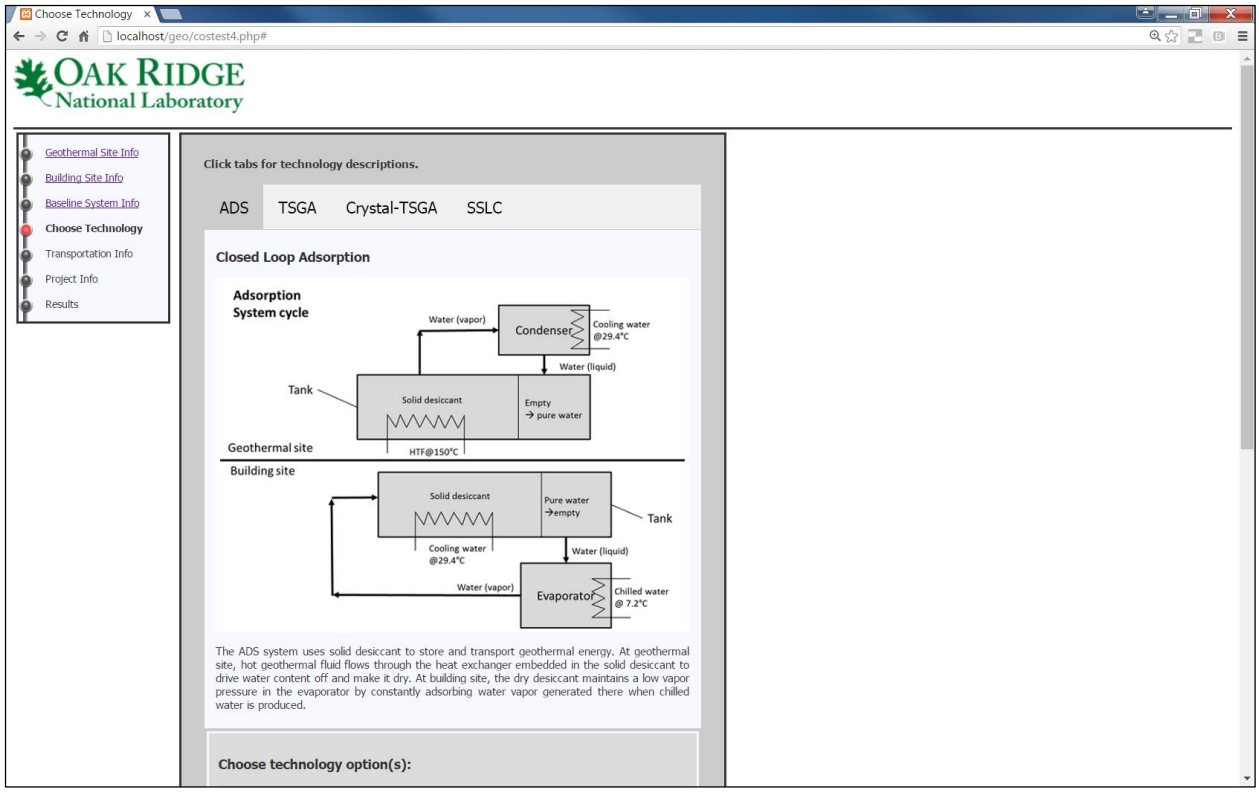

Fig. E.6. Technology selection page showing a brief description of a selected technology.

The fifth input page is for transportation options (Fig. E.7). Based on the technology selection in the previous page, the interface lists the available means of transportation. Currently, trucking transportation has been implemented and is available for all technologies. As shown in Fig. E.7, the user needs to (1) provide the distance between the geothermal site and the building site; (2) either select to use the maximum weight for trailer under federal law, or provide the custom net weight for the transported media on board; (3) provide the initial cost of transportation related equipment; and (4) specify the fuel type for transportation. For a particular technology, two-step geothermal absorption (TSGA), either or both of the "tractor-trailer" and "pipeline" options can be selected. For the "pipeline" option, an additional input for "Right-of-way cost" is needed, as shown in the bottom of Fig. 8.

If multiple technologies are selected on the previous page, there will be a series of pages for the transportation information for each of the selected technologies.

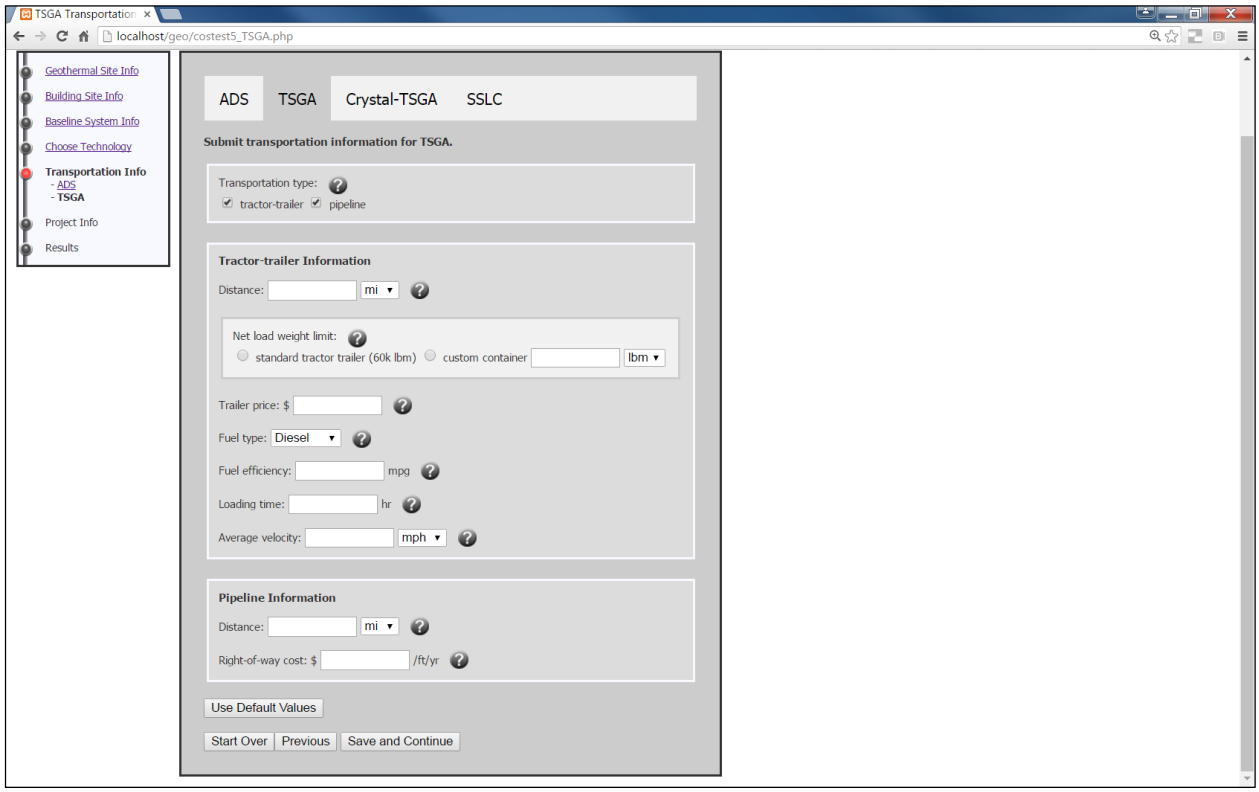

Fig. E.7. Transportation information page (showing two transportation options for the TSGA technology).

The final input page (Fig. E.8) is for project information including project lifetime and discount rate for calculation of levelized cost of saved electricity. Finally, the user can click the "calculate" button and evoke the calculation engine with all the input information collected through the previous pages.

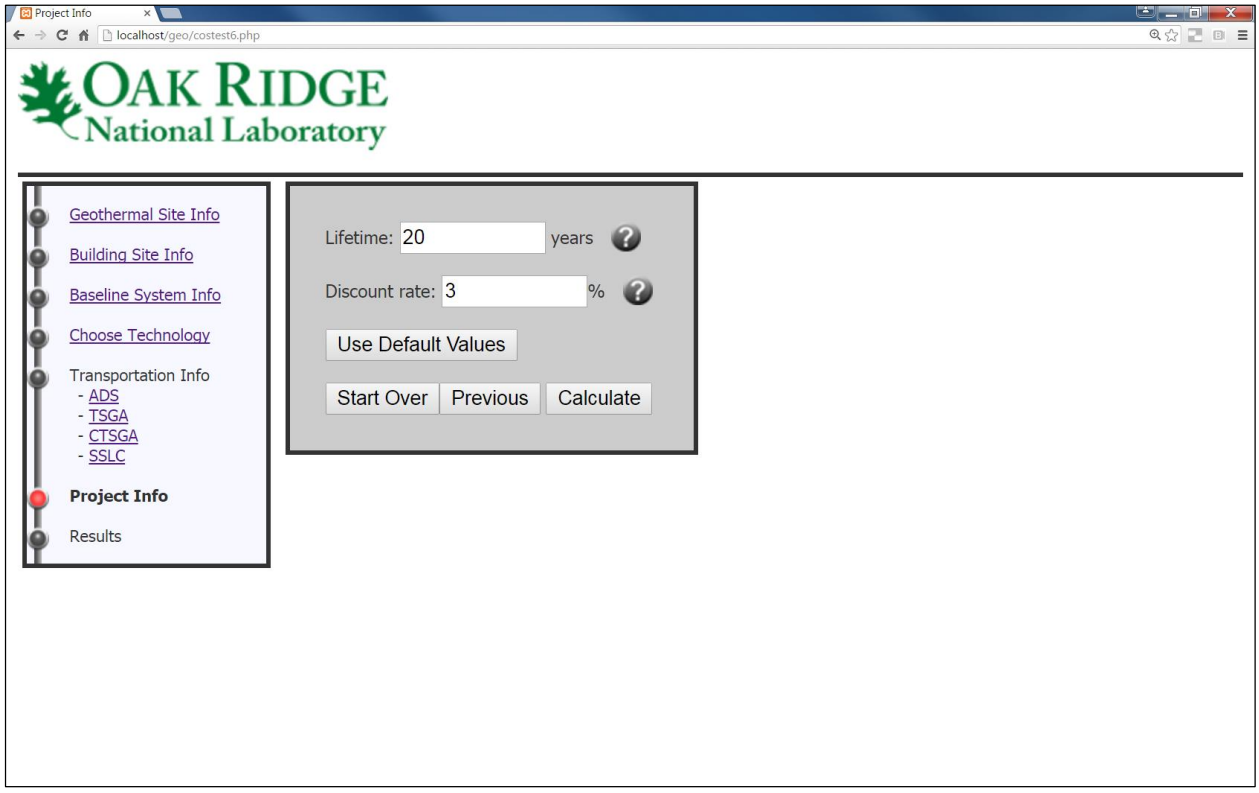

Fig. E.8. Project information page.

Once the calculation engine finishes the calculation, the results are sent back via an output data file, and the results are displayed in tables and charts on the interface as shown in Fig. E.9. The results include the economics, including payback period, levelized cost of saved electricity (LCOSE) for each cost component, and energy/environment impact (i.e., the primary energy consumption and carbon emission compared with a baseline system). These results are listed in a table (as shown in Fig. E.9). In addition, the LCOSE breakdown is also shown in a pie chart. The cost and performance of both the selected technology and a baseline technology are compared through a series of bar charts (as shown in Fig. E.10). Finally, the results of all the selected technologies and the baseline system are compared in tabular and graphical formats, as shown in Fig. E.11.

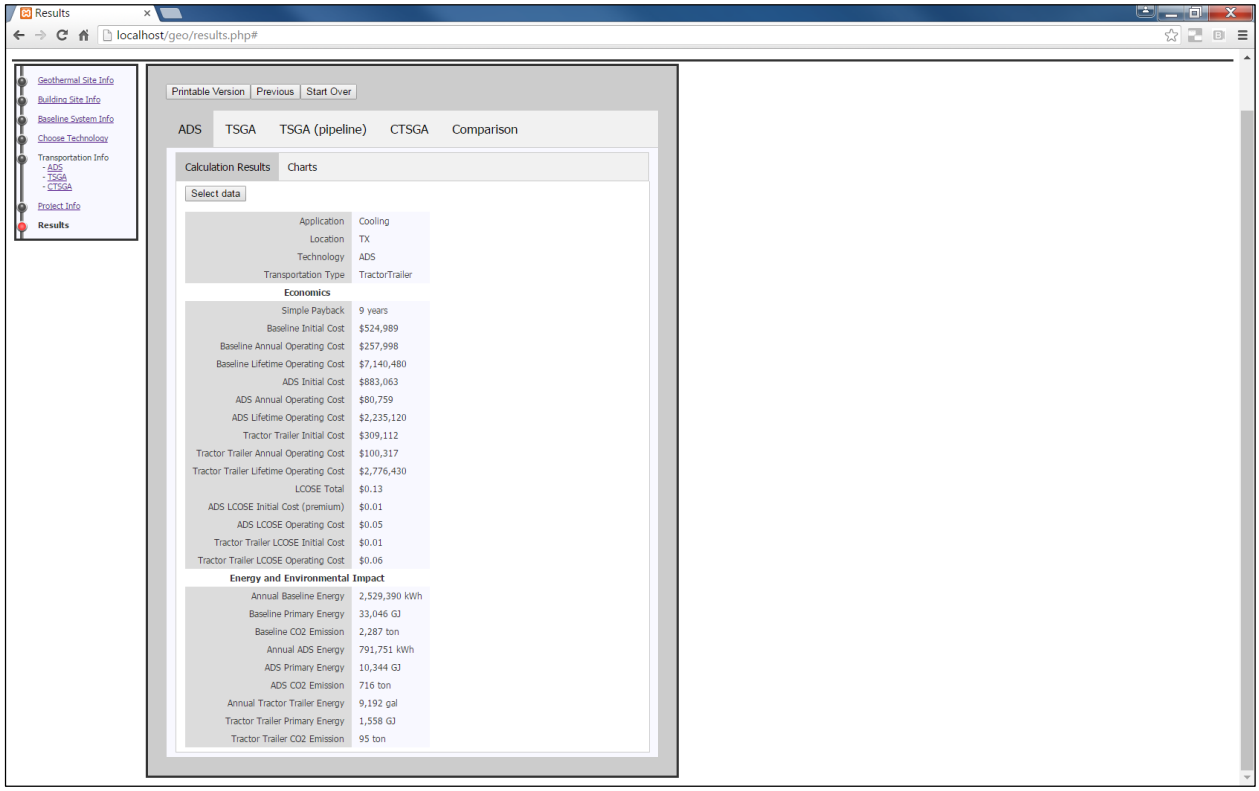

Fig. E.9. Result page (showing tabulated results of one of the selected technologies).

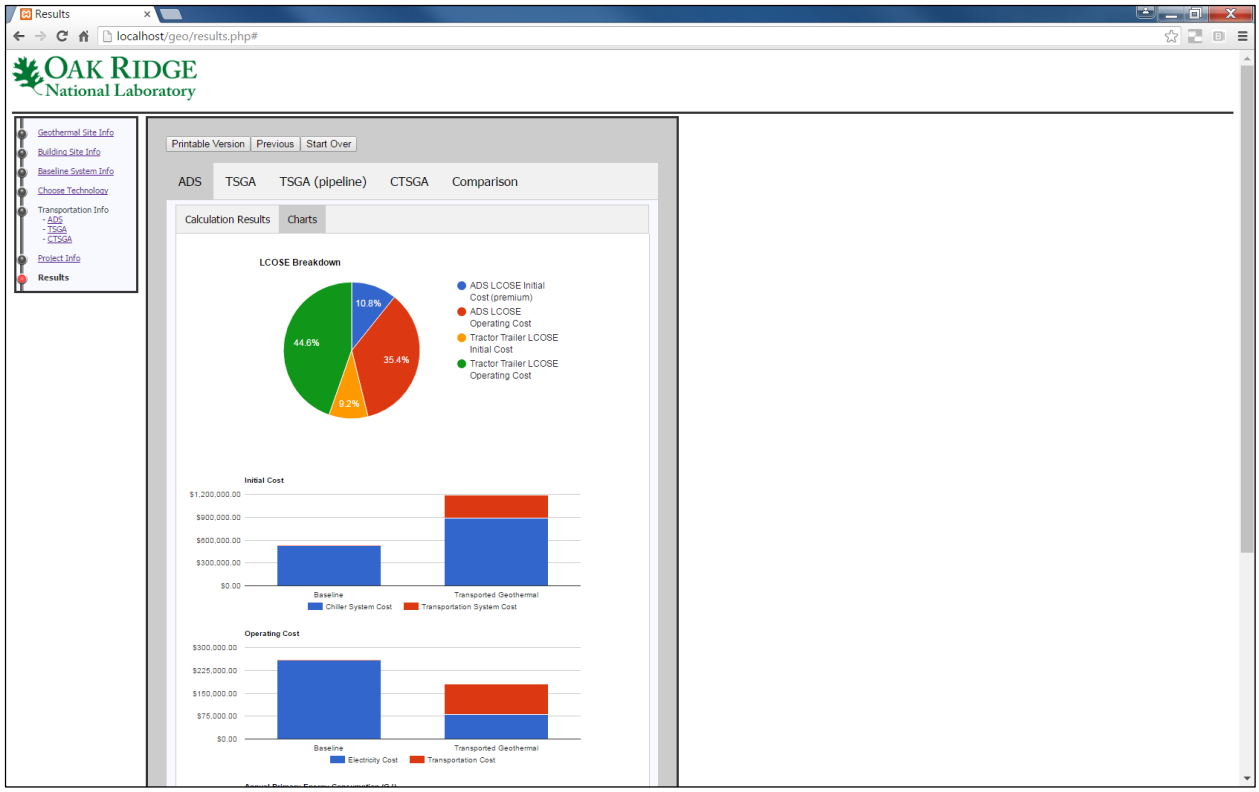

Fig. E.10. Result page (showing graphical results of one of the selected technologies along with the results of a baseline technology).

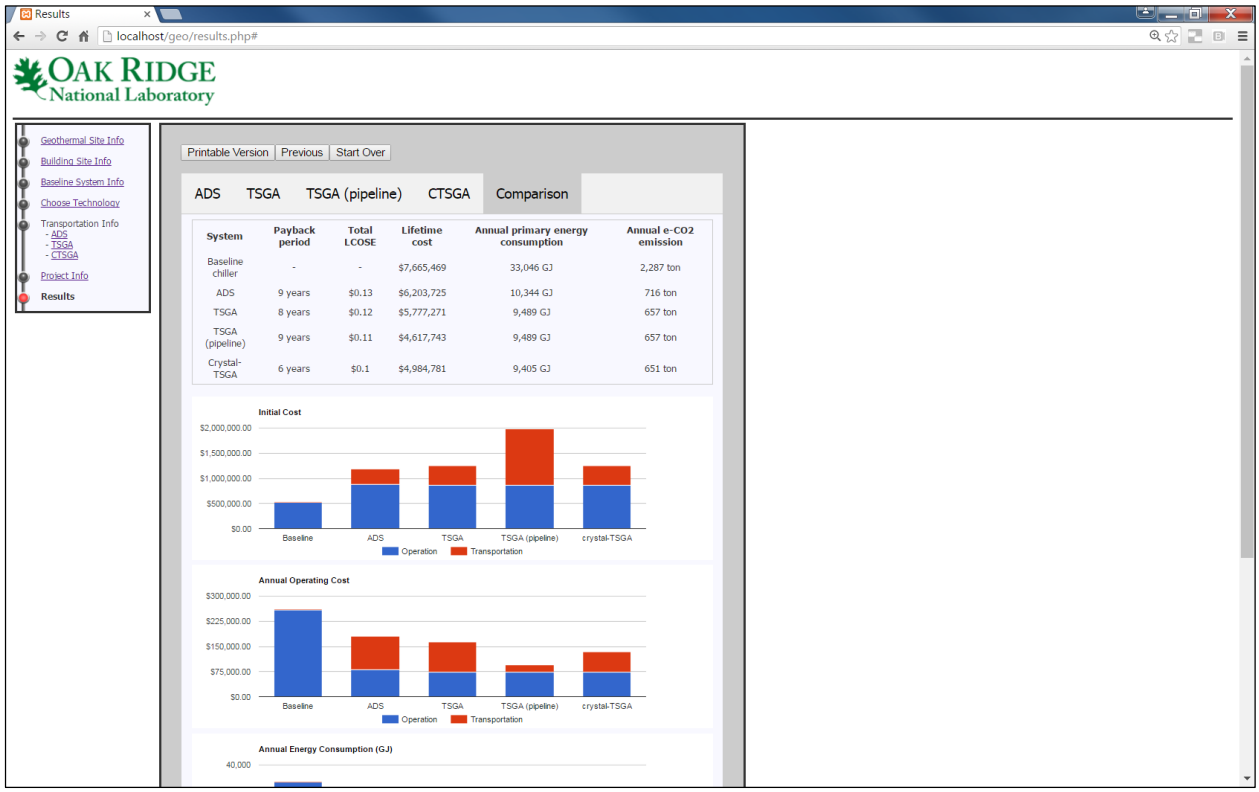

Fig. E.11. Result page (showing tables and charts to compare various technologies).